GAMMA RADIATION FROM THE ALPHA PARTICLE BOMBARDMENT OF C^{12}

Thesis by
James Daniel Larson

In Partial Fulfillment of the Requirements
For the Degree of
Doctor of Philosophy

California Institute of Technology
Pasadena, California
1965
(Submitted May 14, 1965)

ACKNOWLEDGEMENTS

This research project was instigated at the suggestion of Professor W. A. Fowler and continued under his direction with able assistance from Professors T. Lauritsen, W. Whaling, C. A. Barnes and R. W. Kavanagh. The major portion of the work presented was shared with Dr. R. H. Spear who thereby earned not only very sincere gratitude but condolences as well. Portions of the text will be found to have been extracted in paraphrase or verbatim from a paper co-authored with Dr. Spear and, therefore, do not necessarily represent an original contribution by the present author. Dr. J. D. Pearson must belatedly be thanked for his ever congenial share in the design, construction and use of the laboratory apparatus. Helpful discussions with Drs. T. A. Tombrello and F. C. Barker have been an influence on the final form of this thesis. The contributions of so many others, faculty, staff, students and visitors of the Kellogg Radiation Laboratory, remain unheralded but not forgotten.

This research was supported in part by the Office of Naval Research [Nonr - 220(47)].

ABSTRACT

The excitation function of the reaction $C^{12}(\alpha, \gamma)O^{16}$ has been studied over the region E_α = 2.8 to 8.3 MeV using a NaI(T1) detector and enriched C^{12} targets. Resonances were observed at E_α = 3.24, 3.58, 4.26, 5.81, 7.05, 7.88 and 8.13 MeV, corresponding to O^{16} states at E_x = 9.59, 9.85, 10.36, 11.52, 12.45, 13.07 and 13.26 MeV. Radiative widths Γ_γ for ground state radiation from the states at 9.59, 9.85, 11.52 and 12.45 MeV were measured to be 0.022 $\pm$ 0.005, 0.0059 $\pm$ 0.0006, 0.66 $\pm$ 0.09 and 7 $\pm$ 1 eV, respectively. Radiative widths for cascade radiation from the 9.85 and 10.36 MeV states through intermediate states of O^{16} were measured to be 0.0012 $\pm$ 0.0004 and 0.046 $\pm$ 0.006 eV, respectively. Interference effects in ground state radiation from the 13.07 MeV (1^-) state support evidence for an underlying 2^+ state at nearly the same energy. Other information on excited states of O^{16} is presented.

TABLE OF CONTENTS

Table of Contents cont'd.

I. INTRODUCTION

A. Excitation of O^{16}

In the language of contemporary nuclear physics, O^{16} is an even-even, self-conjugate, doubly-magic, spherical nucleus of the alpha particle series He^4, Be^8, C^{12}, O^{16}, Ne^{20}, etc. This host of symmetry properties makes O^{16} a frequent test case for theoretical analyses and emphasizes the need for detailed experimental knowledge of its excited states. An energy level diagram (Figure 1) selected from the compilation of Lauritsen and Ajzenberg-Selove (1962) serves to illustrate that despite its many symmetries, O^{16} does have the usual complex structure of excitation energies and that a great body of experimental information on these excited states already has been acquired. Such a wealth of information changes the role of experiment subtly from that of general exploration to one of minute scrutiny.

Observed excited states of O^{16} depicted in Figure 1 represent results from overlapping experiments by many workers (see Ajzenberg-Selove and Lauritsen 1959). For convenience, excitation energies indicated in Figure 1 are used throughout the present work in reference to particular states; exceptions occur whenever experimental results are being directly quoted or new states discussed. Besides the excitation structure, Figure 1 reveals schematically that O^{16*} becomes energetically unstable to break-up into $C^{12} + \alpha$ at $E_x = 7.162$ MeV and into $N^{15} + p$ at $E_x = 12.126$ MeV. Between these energies the interaction $C^{12} + \alpha$ alone leads to O^{16*} as a compound nucleus without the complexity of additional particle decay modes. (Decay into C^{12*}(4.43 MeV) + α beginning at $E_x = 11.595$

MeV is suppressed by the Coulomb barrier until $E_x \approx 13$ MeV.) Above $E_x = 12.126$ MeV particle decay into either protons or alpha particles must be taken into consideration and complications increase rapidly at higher excitation energies.

Bombardment of C^{12} by alpha particles leads selectively to states in the compound nucleus 0^{16*} which, because $J^{\pi} = 0^+$ for both target and projectile, are of the "natural" spin-parity sequence $J^{\pi} = 0^+, 1^-, 2^+, 3^-, 4^+$, etc. (Blatt and Weisskopf 1952). By discriminating against the remaining "unnatural" states this interaction automatically removes the parity ambiguity (for a given spin) from resonances both observed and unobserved (but identified by other techniques) and selects a somewhat less cluttered spectrum of energy levels. Most compound nuclei so excited decay by re-emission of an alpha particle or, when energetically possible, another heavy particle. In a very few cases (one in $\approx 10^6$) an alpha particle is "captured" by C^{12} with subsequent de-excitation of the 0^{16} excited state through gamma ray emission. Ground state radiation from the alpha capture reaction, $C^{12}(\alpha, \gamma)0^{16}$, is of pure electric multipole orders and especially simple to interpret (Blatt and Weisskopf 1952).

The intended purpose of the present experiment was: a) to measure the excitation function of ground state radiation from the reaction $C^{12}(\alpha, \gamma)0^{16}$ over the range of alpha particle bombarding energies made available with the advent of the tandem electrostatic accelerator, b) to supplement by improved measurements the existing knowledge of the radiative widths of several states in 0^{16} accessible with this range of energies and c) to provide where possible new measurements of radiative widths for states not yet

studied with this reaction. A less ambitious program was finally accomplished by truncating the available spectrum of alpha particle energies to exclude measurements below $E_\alpha = 2.8$ MeV and above $E_\alpha = 8.3$ MeV. Between these limits a fairly consistent program of experimental study could be conducted; whereas, it was felt that rather special techniques were becoming increasingly necessary at the extremes where problems of background are most severe. Independent measurements of resonance widths and energies proved a useful by-product of the investigation; limited information on cascade radiation and confirmation of certain spins and parities also were obtained.

B. Previous $C^{12}(\alpha, \gamma)O^{16}$ Results

Although for many years the low energy region of the $C^{12}(\alpha, \gamma)O^{16}$ reaction has been accessible with single state electrostatic accelerators, the alpha capture cross section is very small and only a limited amount of work has been done with these machines (see Ajzenberg-Selove and Lauritsen, 1959). Early results were as follows:

a) By bombarding thick carbon targets with low energy alpha particles Allan and Sarma (1955) were able to set an upper limit of $3 \times 10^{-29} cm^2$. MeV for the integrated $C^{12}(\alpha, \gamma)O^{16}$ cross section at $E_\alpha = 1600$ keV. Gamma radiation directly attributable to the de-excitation of O^{16} was not observed in this experiment and it is now reasonably certain that the true cross section is several orders of magnitude below this limit.

b) Bloom et al. (1957) studied ground state radiation from the broad 9.59 MeV, 1^- state of O^{16} which was excited by

bombarding an isotopically enriched C^{12} target with 3.45 MeV alpha particles. A gamma ray profile characteristic of the 5.1 cm x 5.1 cm NaI(T1) detector for 9.59 MeV radiation was observed and from the yield a radiative width, Γ_γ = 0.006 eV (within a factor of two), was determined. The stated purpose of this experiment was to investigate the isotopic spin impurities to be found in O^{16} levels. The El transition to the ground state from the 9.59 MeV, T = 0 state is forbidden by the isotopic spin selection rule and such radiation is expected to be considerably inhibited. The radiative width measured in this experiment was found to be smaller than had been anticipated for this region of O^{16} (Wilkinson 1956a).

c) The excitation function for ground state radiation from $C^{12}(\alpha, \gamma)O^{16}$ for E_α = 3.2 to 6.2 MeV was studied by Meads and McIldowie (1960) in an effort to obtain radiative widths for ground state E2 transitions from the 2^+ levels at 9.85 and 11.52 MeV in O^{16}. The widths obtained for these levels using a 10.2 cm x 10.2 cm NaI(T1) detector and an enriched C^{12} target were Γ_γ = 0.02 $\pm$ 0.01 and 0.9 $\pm$ 0.2 eV, respectively. No effort was made to observe El radiation from the 9.59 MeV state.

C. Astrophysical Implications

Interest in the $C^{12}(\alpha, \gamma)O^{16}$ reaction has been spurred by its application in the theory of stellar interiors and nucleosynthesis (see Burbidge et al. 1957). Following hydrogen burning by proton-proton

and CNO processes (schematically, $4H^1 \rightarrow He^4 + Q$), the helium-rich core of a typical star is expected to contract gravitationally until helium burning by the 3α process ($3He^4 \rightarrow C^{12} + Q$) ignites at temperatures near 10^8 °K (Salpeter 1957). Proceeding concurrently with the 3α process is the conversion of C^{12} to O^{16} by alpha capture. Although the resonant reaction rate of the 3α process (involving Be^8 and C^{12*}) is sufficiently well determined for detailed astrophysical interpretation (Seeger and Kavanagh 1963; Cox and Salpeter 1964), the experimental uncertainty in the corresponding rate for $C^{12}(\alpha, \gamma)O^{16}$ leads to an ambiguous lifetime for the evolving star as pointed out by Fowler and Hoyle (1964).

If $C^{12}(\alpha, \gamma)O^{16}$ proceeds slowly with respect to 3α burning, the residual core will contain a large fraction of C^{12} after all helium has been consumed. This leads to a stage of carbon burning (principally, $2C^{12} \rightarrow Mg^{24} + Q$) at temperatures near 6×10^8 °K which lasts some 10^6 years (Reeves and Salpeter 1959). Conversely, if $C^{12}(\alpha, \gamma)O^{16}$ proceeds rapidly compared to 3α, the overall effect of helium burning is to produce O^{16} ($4He^4 \rightarrow O^{16} + Q$). The central core depleted in C^{12} will contract until oxygen burning ($2O^{16} \rightarrow S^{32} + Q$) is initiated at temperatures near 2×10^9 °K (Reeves and Salpeter 1959); however, it has been hypothesized that at such temperatures the rate for the reaction $e^+ + e^- \rightarrow \nu_e + \bar{\nu}_e$ as predicted from the Conserved Vector Current Theory of Feynman and Gell-Mann (1958) will provide sufficient energy loss through neutrino emission to shorten the stellar life during this process to a few days (Chiu and Stabler 1961; Levine 1963; Fowler and Hoyle 1964). Thus the stellar lifetime and evolution subsequent to helium burning depends critically upon how rapidly $C^{12}(\alpha, \gamma)O^{16}$ proceeds relative to the 3α process.

Deinzer and Salpeter (1964) have calculated the residual C^{12} in the core of a helium burning star for various estimated values of the $C^{12}(\alpha, \gamma)O^{16}$ reaction rate since the true cross section is not known. Direct measurements of the alpha capture cross section at relevant stellar energies of a few hundred keV have not proved possible and accurate measurements do not extend below $E_\alpha = 3$ MeV. Under these circumstances it is customary to extrapolate higher energy data to the lower stellar energies; however, the bound state at $E_x = 7.12$ MeV in O^{16} which is expected to be the major contributor to the cross section at stellar energies remains completely unprobed by alpha capture experiments. Estimates of the $C^{12}(\alpha, \gamma)O^{16}$ reaction under stellar conditions have been limited to a consideration of the systematic properties of better known O^{16} states (Burbidge et al. 1957; Fowler and Hoyle 1964).

II. EXPERIMENTAL PROCEDURE

Alpha particle beams used in this experiment were obtained from the ONR-CIT tandem accelerator. The general properties of this accelerator including the production of alpha particle beams by neutral helium injection have been discussed in detail in the literature (Van de Graaff 1960; Rose 1961; Rose et al. 1961; Gove 1961). The remainder of the apparatus used in this experiment has been mentioned in the literature (Spear et al. 1963; Pearson and Spear 1964; Larson and Spear 1964) and detailed descriptions appear in the PhD Thesis of Pearson (1963). It is, then, with considerable redundancy that the following description is given of the apparatus used in this experiment. Attention will be centered on those features particularly applicable to the $C^{12}(\alpha, \gamma)O^{16}$ experiment.

A. Beam Energy and Intensity

Energetic charged particle beams from the tandem accelerator are deflected through 90^{o} by a momentum analyzing magnet. While the present experiment was being conducted, repeated tests by J. A. McNally, Pearson (1963) and Honsaker (1965) determined the equivalent energy calibration of this analyzer to within approximately 0.1% using nuclear reaction techniques (for examples, see Bromley et al. 1959a). Throughout this experiment beam trajectory defining slits at the entrance and exit of the analyzer were maintained with apertures from 0.25 to 0.51 cm. These settings permit charged particles with energy variations from $\pm$ 0.15% to $\pm$ 0.3%, respectively, to successfully traverse the analyzer (see Pearson 1963, p. 19); however, in normal operation the beam is always well centered

between the defining slits in order to achieve optimum transmission. For analysis of the present experiment it was assumed that at all times the energy of the alpha particle beam was determined to $\pm$ 0.3%; comparison of excitation energies listed in Table II with results by Browne and Michael (1964) and others indicates that energy errors reported in the present experiment have been quite conservatively estimated. (Other error sources from target thickness and resonance location also contribute to the entries in Table II.)

Beams of singly charged helium ions (He^+) were used for bombarding energies up to E_α = 6 MeV; for higher energies the doubly charged beam (He^{++}) was necessary. Available beam currents were typically 1 - 3 μA He^+ and 0.3 - 1 μA He^{++}. Individual bombardment "runs" were normalized by measuring the total charge transported by the incident beam to the target (integrated beam current) using an Eldorado model CI-110 current integrator. The accuracy of this device was tested repeatedly during the course of the experiment by measuring the time required for a source of constant current to produce the same charge reading recorded for the data. Errors detected in these tests were usually no more than 1% (Pearson 1963, p. 9). (Equipment repairs are initiated whenever such standard laboratory devices fail to achieve routine specifications.) Although there is evidence that the glass target chamber used allows reliable current integration without elaborate electron suppression, the usual precautions were taken by maintaining the target at +300 volts and an incident-electron suppressor ring (Figure 3) at -300 volts.

B. Target Chambers

Some preliminary work using natural carbon targets (Larson and Spear 1961; see Figure 9) was done with the T-shaped glass target chamber described in detail by Pearson (1963, his Figure 2). Demountable vacuum seals to this chamber were of conventional neoprene 0-rings lubricated with Dow Corning high vacuum grease. Pressures of typically 10^{-6} torr were obtained with a conventional oil diffusion pump assisted by liquid nitrogen cold traps. This target chamber allowed beam deposition of natural carbon from organic vapors in the vacuum system at a rate wholly unacceptable for the preservation of enriched C^{12} targets to be employed later in the experiment (see page 26).

Accretion of natural carbon on the targets was significantly reduced by using the target chamber shown in Figure 3. The principal features of this design are the following:

a) The target chamber communicates with the rest of the vacuum system only through a beam transmission tube, 1 cm diameter x 30 cm long, immersed in liquid nitrogen.

b) Auxiliary pumping of the target chamber is provided by a 9 ℓ/s ion pump which is inherently free of organic contamination.

c) Except for demountable vacuum seals of low vapor pressure Viton 0-rings (unlubricated), no organic materials are used in the target chamber construction.

d) The assembly may be baked to 100° C to outgas interior surfaces prior to use.

The restricted beam transmission tube helps to isolate the target chamber from the rest of the vacuum system by minimizing the migration of organic vapors and surface contaminants into the target chamber. With very little gas originating from within this "clean" vacuum system, the 9 ℓ/s ion pump is capable of maintaining more than a factor of 10 in pressure differential across the beam transmission tube and pressures as low as 2×10^{-8} torr have been measured at the ion pump. Under normal operating conditions, with several watts being dissipated by the beam striking the target, the pressure rises to about 10^{-7} torr indicating considerable outgassing by those components being heated. Most of the data for the present experiment were acquired using this target system.

Although the target system of Figure 3 admirably served its experimental purpose, a number of mechanical improvements were incorporated in a revised cold trap (Figure 4) designed by V. F. Ehrgott. Thermal radiation from surrounding walls is an important lifetime consideration for liquid nitrogen traps and the reservoir shown in Figure 4 is demountable so that its exterior surface may be kept clean and polished for high reflectivity. The cylinder surrounding this reservoir is an integral part of a 15 cm plumbing system (standard 6" pipe). By a more judicious choice of machined and welded joints, accurate alignment along the beam axis has been greatly facilitated. The ion pump and glass target chamber in Figure 3 were coupled to the cold trap in Figure 4 to provide the target system used in obtaining data shown in Figures 13 and 14.

The choice of a glass target chamber was made both for convenience and utility. An optically transparent target chamber allows visual inspection of the target geomctry and surface conditions during bombardment and permits the exact beam location to be ascertained with fluorescent quartz viewers. Electrical insulation of the target is necessary for accurate charge measurement by the standard beam current integration technique (page 8) and glass provides ideal insulation properties. Glass is eminently suitable for high vacuum work but its mechanical properties limit structural applications. When struck by stray beam or scattered particles, the variety of constituent elements found in common forms of glass can produce highly undesirable sources of background.

Enriched C^{12} targets used in this system where supplied by the Isotopes Division, Oak Ridge National Laboratory. They were prepared by polymerizing C^{12} enriched acetylene (isotopically 99.94% C^{12}) onto 0.025 cm thick tantalum backings. Comparison of background yields from C^{13} + α reactions (see Figures 9 and 10) indicate that these targets do contain significantly less than the natural abundance of C^{13} (normally 1.1%). Measurements of target thickness are described on pages 25 and 36.

C. Gamma Ray Detection System

The low reaction cross sections measured in this experiment made imperative the use of a radiation detector of high efficiency. The detection system consisted of a 10.2 cm x 10.2 cm right circular, cylindrical NaI(T1) crystal coupled to a 12.7 cm CBS 7819 photomultiplier. Signals from the photomultiplier were amplified by

a conventional integrating pre-amplifier followed by a double delay-line clipped Hamner model N328 amplifier and processed by a Radiation Instruments Development Laboratory model 34-12, 400 channel pulse height analyzer. Data were stored in 200 channel segments allowing the remaining half of the analyzer memory to retain a comparison spectrum.

Very high count rates from reactions such as $C^{12}(\alpha, \alpha'\gamma_{4.43})C^{12}$ (Figure 15) caused observable gain increases in the CBS 7819 photomultiplier. Gain variations were monitored by frequently recording between experimental runs the pulse height produced by 2.615 MeV gamma rays from ThC''. When rapid gain changes were encountered, these monitoring checks were made before and after each run; except for such occasions, monitoring checks could be made every few runs with gain variations between checks typically less than 1%. All analyzed spectra had energy scales adjusted to these monitor readings even though the correction in yield due to 1% gain changes is negligibly small. High counting rates also caused severe overloading of the electronics resulting in pulse pile-up and appreciable dead-time for the multichannel analyzer; consequently, whenever high counting rates threatened to become detrimental to the experiment, beam intensities were reduced.

During most of this experiment the 10.2 cm x 10.2 cm NaI(T1) crystal was encased in a 30.5 cm diameter lead cylinder, as sketched in Figure 5, which provided 8 cm or more of lead shielding radially from the detector. As shown, the face of the crystal was completely exposed. The detector and shielding, weighing some 300 kilograms, were supported by a movable platform which allowed complete freedom of motion of the detector in radius and angle (in one plane)

about the target. The center of rotation of the detector at a fixed radius was adjusted to intersect the beam axis. Pearson (1963) has described the calibration of this equipment for more detailed angular studies.

Interference effects involving odd terms in the Legendre polynomial series (page 48) made it very desirable to measure radiation at angles greater than 90^{o}. Use of the existing 30.5 cm lead shield would have forced the detector to be at least 20 cm from the target at 135^{o}. Before undertaking possible alternatives, a measurement was made with the bare NaI(T1) crystal which could then be placed 7.6 cm from the target at this backward angle (Figure 5). An attendant rise of 55% in room background over the energy region of interest was acceptable, allowing this simple solution of the problem.

D. NaI(T1) Detection Efficiency

Detection response of the 10.2 cm x 10.2 cm NaI(T1) crystal as a function of energy and geometry was determined by performing numerical integrals of the following form (Lazar et al. 1956):

$$J_n = \frac{1}{2\pi} \int_{\text{Crystal}} P_n e^{-\mu_1 \ell_1} (1 - e^{-\mu_2 \ell_2}) \, d\Omega' .$$

For a system with axial symmetry this becomes

$$J_n = \int_{\text{Crystal}} P_n(\cos\theta') \, e^{-\mu_1(E)\ell_1(\theta')} (1 - e^{-\mu_2(E)\ell_2(\theta')}) \sin\theta' \, d\theta'$$

where $P_n(\cos\theta')$ = Legendre polynomial of order n

$\ell_1(\theta')$ = gamma ray path length in absorbing material preceeding the NaI(T1) crystal

$\mu_1(E)$ = linear attenuation coefficient for a gamma ray in the absorbing material

$\ell_2(\theta')$ = gamma ray path length in NaI(T1)

$\mu_2(E)$ = linear attenuation coefficient for a gamma ray in NaI(T1)

$E = E_\gamma$ = gamma ray energy

θ' = angle of the gamma ray with respect to the symmetry axis of the detector (the source is assumed to lie on the symmetry axis of the detector, defined as $\theta' = 0$).

The linear attenuation coefficients $\mu(E)$ are available in tabulated form for a variety of materials (Grodstein 1957). The detection efficiency, defined as that fraction of gamma rays emitted by an isotropic point source which interact with the detector, is given by the integral $J_0/2$.

By a suitable coordinate transformation, Rose (1953) has demonstrated that the integrals J_n form a simple relationship between the axial coordinate system of the detector (designated here by primes) and the coordinate system defined by the incident alpha particle and emerging gamma ray. For an emitted gamma ray angular distribution of the form

$$W(\theta) = \sum_n a_n P_n(\cos\theta),$$

where θ = angle of the gamma ray relative to the direction of the incident alpha particle beam (Figure 5),

a detector subtending a finite solid angle will measure the distribution $(J_0/2)W(\theta)_{obs}$, where (see Pearson 1963, Appendix A)

$$W(\theta)_{obs} = \sum_n a_n (J_n/J_0) P_n(\cos\theta), \quad |J_n/J_0| \leq 1 .$$

The quantities (J_n/J_0) are Rose's attenuation factors; in effect they describe the detector response to higher order polynomial terms in the angular distribution. These factors tend generally to decrease with increasing n, producing a less rapidly varying angular dependence, or "smoothing", of the observed angular distribution. For the two geometries used most extensively in this experiment (Figure 5), the values of (J_n/J_0) for the 10.2 cm x 10.2 cm NaI(T1) detector are:

Distance (source to detector)	Efficiency	Calculated attenuation factors (E_γ = 10 MeV)			
	$J_0/2$	J_1/J_0	J_2/J_0	J_3/J_0	J_4/J_0
2.7 cm	0.110	0.82	0.53	0.25	0.04
7.6 cm	0.037	0.94	0.84	0.70	0.54

It is obvious that placing the detector close to the target makes it quite insensitive to the higher order polynomial terms.

E. Standard Spectra

The calculated NaI(T1) detection efficiency includes all processes through which the incident gamma ray may interact with the crystal and suffer a loss of energy. It is assumed that these processes will result in some subsequent manifestation of the energy in the form of a light pulse. The various energy transfer mechanisms of the scintillation process, photo-electric effect, Compton effect and pair production, combine to produce the familiar NaI(T1) pulse spectrum (Bell 1955). In most practical experiments only a fraction of the total pulse spectrum is discernable from a general background of other signals which may arise from thermal noise, cosmic rays, neutrons and competing gamma ray processes. For this reason it is necessary not only to establish the total efficiency of the detector but in addition to select some measureable portion of the observed spectrum and determine the relative efficiency of this spectrum fraction to the total efficiency.

Three "standard" gamma rays, obtained from well known (p, γ) reactions, were used to calibrate the 10.2 cm x 10.2 cm NaI(T1) detector over the desired energy region:

E_γ(MeV)	E_p(MeV)	Reaction	Spectrum Fraction (0.8 - 1.1 E_γ)
7.447	0.991	$Be^9(p,\gamma)B^{10}$	56%
9.17	1.747	$C^{13}(p,\gamma)N^{14}$	53%
12.15	0.675	$B^{11}(p,\gamma)C^{12}$	52%

While these reactions show a strong monoenergetic gamma ray of the energy indicated, competing reactions produce some background in every case. For example, the 9.17 MeV spectrum, shown in Figure 6, contains a contamination from 6.44 MeV cascade radiation. In addition, the low energy (small pulse height) portion of each of these spectra is completely obscured by background pulses. To establish the complete profile of monoenergetic radiation it is necessary to make some estimate for the shape of this obscured portion of the standard spectra. Produced primarily by Compton scattering, this portion of a NaI(T1) spectrum does not change rapidly as a function of pulse height for gamma rays of several MeV (Heath 1957, 1962) and is frequently approximated (Kavanagh 1956; Parker 1963; Pearson 1963) by a linear extrapolation to the zero energy (zero pulse height) axis. In the present case, the approximation was made by projecting a straight line tangentially from the more reliable portion of the spectrum at higher energies to the zero energy axis. The location of this "zero intercept" for the linear extrapolation is subject to considerable uncertainty; for this experiment the analytic intercept proposed by Zerby and Moran (1961) has been employed.

Zerby and Moran (1961) argue that the first channel of a spectrum is occupied by events which resulted from gamma rays scattered only in the forward direction. Such events are described by the integral

$$f_0 = J_0^{-1} \Delta E \int_{\text{Crystal}} (2\pi r_0^2 \, m_0 c^2 \, E^{-2}) \, D \ell_2(\theta') \, e^{-\mu_2(E) \ell_2(\theta')} \sin \theta' \, d\theta'$$

where f_0 = fraction of total spectrum in the first channel

ΔE = energy width of the first channel

E = gamma ray energy

r_0 = classical electron radius

m_0c^2 = electron rest energy

D = electron density in NaI(T1)

$\ell_2(\theta')$ = gamma ray path length in NaI(T1)

$\mu_2(E)$ = linear attenuation coefficient for a gamma ray in NaI(T1)

$J_0/2$ = detector efficiency (pages 13 and 14)

$(2\pi r_0^2 m_0c^2 E^{-2})$ = Compton scattering cross section for an energy loss ΔE (Davisson 1955).

Beyond the first channel, Zerby and Moran generate the remainder of the spectrum through Monte Carlo calculations which follow the life history within the detector of individual photons and their interaction products. The probability function $(1 - e^{-\mu_2(E)\,\ell_2(\theta')})$ is used to determine whether an incident gamma ray interacts with the crystal; once interaction is assumed, the Monte Carlo calculations serve only to locate this particular event within the spectrum. Uniform sampling over solid angle of an isotropic point source fills these spectra with exactly the number of counts predicted by the

efficiency integral $J_0/2$ (page 13). Thus the calculated spectra of Zerby and Moran, which fit very well to experimental results in the region of large pulse heights and negligible background, provide for the obscured region of low pulse height a profile which is intimately related to the calculations of total detection efficiency described in the previous section.

Contending that the results of Monte Carlo calculations (Miller and Snow 1960; Zerby and Moran 1961) are not representative of complete gamma ray spectra, Heath (1962) has shown that experimental NaI(T1) spectra may be better fitted by semi-empirical techniques, especially in the region of small pulse height. Heath's results return favor to the method of horizontal extrapolation which has in the past been used to link experimental spectra to the zero energy axis (Kavanagh 1956; Pearson 1963) in analogy with the known, rather flat energy-loss distribution of gamma rays which undergo Compton scattering (Davisson 1955). However, it must be observed that Heath's purpose is to reproduce accurately the true experimental profile whereas the present purpose of determining that fraction of the calculated detection efficiency contained in a particular portion of the spectrum would seem better served by using the analytic zero intercept. From this point of view, the calculated spectra of Zerby and Moran stipulate where pulses included in the efficiency integral $J_0/2$ are to be found in experimental spectra.

For comparison, both methods of extrapolation are shown in Figure 6. The 9.17 MeV spectrum has been continued smoothly under the 6.44 MeV cascade contamination where it joins to the linear extrapolations at about $E_\gamma/2$. (Linear extrapolation from near $E_\gamma/2$ to the zero energy axis is typical of all three standard

spectra.) The difference in total counts encompassed by these two extrapolations amounts to 9%, 14% and 17% for the 7.477, 9.17 and 12.15 MeV spectra, respectively; as a consequence, values of radiative width (or cross section) quoted later would have been increased by these same percentages had the horizontal extrapolation been employed. These differences may be considerably inflated since background in the spectra necessarily biases the arbitrarily chosen horizontal extrapolation toward high values. After allowance is made for the much poorer resolution of the 10.2 cm x 10.2 cm detector it may be concluded that the complete 9.17 MeV profile extrapolated to the analytic zero intercept (Figure 6) bears a reasonable (albeit crude) resemblance to the curves calculated by Zerby and Moran (1961) for radiation up to 7.5 MeV detected by a 7.6 cm x 7.6 cm NaI(T1) crystal.

The 10.2 cm x 10.2 cm NaI(T1) detector fails to resolve the series of lines associated with the photo peak and two escape peaks of gamma rays above 7 MeV; however, the resultant broad peak produced by these unresolved lines (Figure 6) contains typically about half the total counts of the entire spectrum. While a measure of the height of this peak is frequently convenient for gamma ray spectroscopy, the low gamma ray yields of this experiment dictated that integration over a sizeable portion of the spectrum be carried out in order to achieve adequate statistics. An arbitrary choice was made to sum counts over the interval 0.8 - 1.1 E_γ in each spectrum. This choice allows about 50% of the spectrum to be retained (see tabulation on page 16) while rejecting most of the background (for examples, see Figure 7).

F. Radiative Width Determination

The yield from a nuclear reaction may be described in the following manner (Fowler et al. 1948):

$$Y = \int_{E-\xi}^{E} (\sigma/\epsilon)\, dE$$

where Y = yield per incident particle

ξ = target thickness in energy units

σ = cross section

E = energy of incident particle

ϵ = stopping cross section of target material.

If for a resonant (α, γ) reaction the energy dependence of σ is assumed to correspond to the Breit-Wigner expression (Blatt and Weisskopf 1952, pp. 392, 437)

$$\sigma_R = \pi\lambda\!\!\!^{-2}\omega \frac{\Gamma_\gamma \Gamma_\alpha}{(E - E_R)^2 + \Gamma^2/4}$$

the integration may be performed analytically and the yield then becomes

$$Y = \frac{2\pi\lambda\!\!\!^{-2}\omega\Gamma_\alpha}{\epsilon\Gamma}\left[\tan^{-1}\frac{E - E_R}{\Gamma/2} - \tan^{-1}\frac{E - E_R - \xi}{\Gamma/2}\right]$$

where $\lambda\!\!\!^{-}$ $= \hbar(2ME)^{-1/2}$ = deBroglie wavelength of the interacting particles

Γ = total resonance width

Γ_α = alpha particle width

Γ_γ = radiative width

E_R = resonance energy

ω $= (2J + 1)(2s + 1)^{-1}(2I + 1)^{-1}$ = statistical factor

J = total angular momentum of system (spin of resonant state)

s = spin of incident particle

I = spin of target nucleus

For alpha particles bombarding C^{12}, the spins of the interacting particles are zero (ie. $s = I = 0$) and ω becomes simply $2J + 1$.

In this experiment measurements were made of the maximum yield from each resonance. A maximum occurs in the above expression when $E = E_R + \xi/2$ and is of the form

$$Y_{max} = \frac{4\pi\lambda\!\!\!^{-2}\omega\Gamma_\alpha\Gamma_\gamma}{\epsilon\,\Gamma} \tan^{-1}(\xi/\Gamma) .$$

In terms of observed and calculated quantities (pages 13, 14 and 15), the maximum yield is

$$Y_{max} = \frac{1}{k(J_0/2)} \times \frac{N_{max}(\theta)}{\sum_n (a_n/a_0)(J_n/J_0)P_n(\cos\theta)}$$

where $N_{max}(\theta)$ = maximum counts observed at angle θ within $0.8 - 1.1\ E_\gamma$

k = spectrum fraction within $0.8 - 1.1\ E_\gamma$

$k(J_0/2)$ = NaI(T1) net detection efficiency .

Substituting this expression for Y_{max} into the previous equation and solving for Γ_γ gives

$$\Gamma_\gamma = \frac{1}{k(J_0/2)} \times \frac{N_{max}(\theta)}{\sum_n (a_n/a_0)(J_n/J_0)P_n(\cos\theta)} \times \frac{\epsilon\Gamma}{4\pi\lambda^2\omega\Gamma_\alpha \tan^{-1}(\xi/\Gamma)} .$$

This formula was used to determine Γ_γ from measurements at discrete angles. In cases where angular distribution data were fitted by Legendre polynomials, the term

$$N_{max}(\theta)/\sum_n (a_n/a_0)(J_n/J_0)P_n(\cos\theta)$$

was replaced by the coefficient of the zero order term, a_0, in the observed polynomial expansion.

Errors in the radiative width measurements arise from three major sources: calculated detection efficiency, experimental yield and target thickness. Table IV lists the estimated percentage standard deviations which apply to the resonance transitions described in Part III. Separate contributions to the experimental yield are classified as current integration, background corrections, statistics, geometry and angular corrections. Error sources not specifically mentioned are either included with other contributions or presumed negligible.

Common to all determinations of radiative width is the net detection efficiency $k(J_0/2)$. The linear attenuation coefficients $\mu(E)$ used in the efficiency calculations differ from experiment by less than 5% (Grodstein 1957); the effect of this uncertainty upon the efficiency integrals $J_0/2$ is 3% for the 2.7 cm geometry and only 1.5% at 7.6 cm (see pages 13, 14 and 15). Integrals of this type have been found to agree well with experiment (Heath 1957), consequently the overall detection efficiency given by $J_0/2$ is probably accurate to better than 5%. Because of the obscured spectral region at low energies, the spectrum fraction k associated with the interval 0.8 - 1.1 E_γ is not easily determined. While the analytic zero intercept extrapolation (page 17) is expected to provide a reasonable estimate for the unobserved portion of the spectrum at low energies, the lack of experimental verification near 10 MeV (Zerby and Moran 1961) makes it difficult to properly assign an error to this calculation; however, a value somewhat greater than 5% may be anticipated. With these limitations and the rather poor quality of the typical standard spectra under consideration (for example, Figure 6), a somewhat arbitrary choice of 10% has been universally applied as

the standard deviation of the net absolute detection efficiency calculated for gamma ray energies near 10 MeV.

Data permitting, the total gamma ray yield for each resonance was obtained from a weighted average of an angular distribution measurement at the resonance peak with data from excitation runs over the resonance at several fixed angles. The standard deviation of these several measurements at each resonance should provide a good estimate for the errors involved in this technique and is included in Table IV. The estimated errors for those measurements which were limited to a fixed angle are listed individually as counting statistics, geometry (uncertainty in location and confinement of the beam spot relative to the detector) and angular distribution correction factors (page 15).

The thickness of the enriched C^{12} target used most extensively in this experiment was measured to within 7% at the narrow 9.85 MeV resonance (Figure 12 and page 36). An additional small error, depending on uncertainties in the published stopping cross sections (Whaling 1958), results when this measured thickness is extrapolated to other energies. Also, the stopping cross section ϵ occurs independently in the expression for the radiative width (page 23). These three sources are combined in the value of 8% quoted in Table IV as the thickness error for this target. The target used for the 9.59 MeV resonance could not conveniently be measured by the same method because of the greater background from $C^{13}(\alpha, n)O^{16}$ produced by its increased thickness. A measurement with this target of the apparent width of the 11.52 MeV resonance, compared to a measurement of the same resonance with the thinner target, resulted in a 15% uncertainty for the thicker target.

G. Background

The characteristically low yield from the $C^{12}(\alpha, \gamma)O^{16}$ reaction allows relatively weak sources of radiation to become competitive as background. The present experiment was performed in an underground room surrounded by earth and concrete. In this location the otherwise unshielded 10.2 cm x 10.2 cm NaI(T1) detector recorded 1/6 count/second within the energy interval 10 - 15 MeV; this reduced to about 1/10 count/second with the detector housed in the 30.5 cm lead shield (page 12). Although nearly constant over this energy range, the "room background" (presumed to originate from cosmic ray sources) increases at lower energies becoming 60% larger for the interval 5 - 10 MeV. While not sufficiently strong to cause serious problems, the room background was always observable in spectra and corrections were made to the data by subtracting this time dependent contribution. For the most sensitive measurement at E_α = 3.3 MeV (Figure 11a) the spectrum contained 16% room background in the 0.8 - 1.1 E_γ interval.

Sensitivity of the NaI(T1) crystal to neutrons (Shafroth et al. 1958; Thompson 1964) introduces the most persistent background problem for C^{12} + α experiments. The 1.1% isotopic abundance of C^{13} in natural carbon provides sufficient yield from $C^{13}(\alpha, n)O^{16}$ to severely compromise $C^{12}(\alpha, \gamma)O^{16}$ results. For this reason, preliminary experiments using natural carbon targets (see Figure 9) were repeated with targets enriched to 99.94% C^{12} (page 11). These targets produced a much improved excitation function relatively free of $C^{13}(\alpha, n)O^{16}$ contamination (Figure 10) but the neutron induced background retains a prominent role in the individual spectra as evidenced by the exponential character of the underlying background found in all the curves of Figure 7.

Above E_α = 5.1 MeV, gamma radiation of 6.13 MeV (and later 6.92 MeV and 7.12 MeV) from $C^{13}(\alpha, n\gamma)O^{16}$ (Spear et al. 1963) begins to burden already overloaded spectra (Figure 7). The excitation function for this reaction, shown in Figure 8, fluctuates rapidly with energy revealing some 22 resonances in the interval E_α = 5 - 10 MeV. This rich source of background is especially detrimental to observations of gamma ray cascades which proceed via these same 6 and 7 MeV levels from the higher excited states of O^{16}.

The most difficult source of background to combat in any nuclear experiment arises from competing reactions generated by the same target and projectile. Above E_α = 7.7 MeV the 4.43 MeV radiation from $C^{12}(\alpha, \alpha'\gamma)O^{16}$ (Figure 15) begins to dominate the C^{12} + α spectra. As may be seen from Figures 7c and 7d, 4.43 MeV radiation is readily distinguished from the 13 MeV ground state radiation of this region but the intense yield from inelastic scattering, about 10^4 times the capture radiation, tends to overload the detection system and as a consequence limits the rate of data accumulation for the $C^{12}(\alpha, \gamma)O^{16}$ experiment.

III. RESULTS

A. Excitation Function

The excitation function for ground state gamma radiation from $C^{12}(\alpha, \gamma)O^{16}$ for E_α = 2.8 to 8.3 MeV is shown in Figure 10. The lower scale represents the energy of the bombarding alpha particles E_α; the upper scale gives the corresponding energy of excitation E_x in O^{16} determined from the relationship $C^{12} + He^4 - O^{16} = 7.162$ MeV (Everling et al. 1961). The He^+ beam was used from 2.8 to 6.1 MeV and He^{++} from 5.6 to 8.3 MeV. Above 3.1 MeV the beam energy was varied in steps of 20 keV or less. Beam currents were typically 1 - 2 μA He^+ and 0.5 - 1 μA He^{++} although in the region near E_α = 8 MeV the beam current was reduced to as little as 0.02 μA to overcome pile-up problems caused by prolific 4.43 MeV gamma radiation from $C^{12}(\alpha, \alpha'\gamma)C^{12}$ (Figure 15). Charge accumulation per data point varied from 900 μC He^+ in the low energy region to 150 μC He^{++} near E_α = 8 MeV.

For this excitation function the NaI(T1) detector was set at 45° to the beam axis with its face parallel to the target surface and approximately 2.7 cm from the beam spot. The ordinate N in Figure 10 represents the number of counts per microcoulomb of He^+ ions detected within the spectral region 0.8 E_x - 1.1 E_x. As described on pages 16 and 20, this portion of the spectrum contains about 50% of the pulses emitted by the detector for gamma rays of energy E_x. The data shown have been corrected for dead-time losses (less than 7%) and the time dependent room background has been subtracted. Statistical error bars are shown for a few sample points. In the region of overlap, the yields from singly and doubly

charged helium beams for the resonance at E_α = 5.8 MeV differ by only 6%, a value slightly larger than the sum of the statistical errors associated with these measurements.

Resonances in Figure 10 attributable to the $C^{12}(\alpha, \gamma)O^{16}$ reaction have been outlined by solid curves; the excitation energies at resonance are indicated by arrows. Other structure in the data is presumed to arise from $C^{13}(\alpha, n)O^{16}$ and $C^{13}(\alpha, n\gamma)O^{16}$ and the gross characteristics of this background can be associated with the known behavior of these reactions (Bonner et al. 1956; Walton et al. 1957; Spear et al. 1963). Background in the region E_α = 5 - 8 MeV may be compared with the detailed structure of the $C^{13}(\alpha, n\gamma)O^{16}$ reaction shown in Figure 8. The slight step in the background at 6.1 MeV in Figure 10 may be associated with resonance #5 in Figure 8. From the height of this step at 6.1 MeV and the observable character of the background from 6 to 6.8 MeV it is clear that above 5 MeV the underlying background due to $C^{13}(\alpha, n\gamma)O^{16}$ in Figure 10 is of negligible proportions. The reduction in background achieved with enriched C^{12} targets may be realized by comparing Figure 10 to results obtained with a natural carbon target of comparable thickness shown in Figure 9.

Both target and projectile are 0^+ states and only resonances of spin 1^- or 2^+ are expected to give appreciable radiation to the ground state through E1 or E2 electromagnetic transitions, respectively (Blatt and Weisskopf 1952). Known states which would be expected to provide such ground state radiation are (Ajzenberg-Selove and Lauritsen 1959):

E_x(MeV)	J^π	Transition
9.59	1^-	E1
9.85	2^+	E2
11.52	2^+	E2
12.44	1^-	E1
13.10	1^-	E1

As indicated, ground state radiation from the states at 9.85, 11.52, 12.44 and 13.10 MeV is readily identified in Figure 10. Although the broad resonance at 9.59 MeV is known to yield ground state radiation (Bloom et al. 1957), the structure in Figure 10 between E_α = 3.0 and 3.5 MeV cannot be attributed to radiation from this state and must result almost entirely from the broad resonant structure known to occur in the reaction $C^{13}(\alpha, n)O^{16}$ in this energy region (Bonner et al. 1956; Walton et al. 1957).

Two other resonances which appear to give "ground state" radiation are found at excitation energies of 10.36 MeV (4^+) and 13.26 MeV (3^-) in Figure 10. In both these cases the apparent yield of radiation is far greater than might be expected for true ground state transitions and it is apparent that the close proximity of the detector to the target has resulted in substantial summing within the detector of gamma rays cascading through intermediate states of O^{16} at about 6 and 7 MeV excitation. A background of intense 6 and 7 MeV radiation from $C^{13}(\alpha, n\gamma)O^{16}$ (Spear et al. 1963) prevents detection of cascade radiation from the 13.26 MeV state but in the case of the 10.36 MeV state a strong cascade member has been observed and the excitation function for radiation arising from

a cascade through the 6.92 MeV, 2^+ level of O^{16} is displayed on the graph inset in Figure 10.

B. The 9.59 MeV State

Gamma ray spectra from which were acquired the data shown in Figure 10 failed to indicate the presence of ground state radiation from the broad 1^- state at 9.59 MeV in O^{16}. Although variations in yield for alpha particle energies from 3.0 to 3.5 MeV indicate some structure, this is almost entirely due to fluctuations in the $C^{13}(\alpha, n)O^{16}$ cross section which undergoes a broad resonance structure in this region (Bonner et al. 1956; Walton et al. 1957). Bloom et al. (1957) have demonstrated that it is very difficult to observe the ground state radiation from this level in the presence of the $C^{13}(\alpha, n)O^{16}$ background. A special effort was made, therefore, to explore this region using a thicker C^{12} target (96 $\mu g/cm^2$, corresponding to 145 keV for 3.3 MeV alpha particles incident at 45^o to the surface) which would permit more rapid data accumulation.

A gamma ray spectrum showing ground state radiation from the 9.59 MeV level is presented in Figure 11a; no corrections have been made to this data. For this spectrum the detector was placed 2.7 cm from the target and at 90^o to the beam axis. Data were accumulated over a period of about 10 hours with a total integrated charge of 45,000 μC He^+. The adjacent spectrum, Figure 11b, taken with an enriched (54%) C^{13} target at the same bombarding energy, 3.30 MeV, shows the neutron induced background from $C^{13}(\alpha, n)O^{16}$ (page 26) to decrease nearly exponentially with energy under the peak of the 9.59 MeV radiation. This exponential shape has been found characteristic of neutron spectra from NaI(Tl)

detectors (Thompson 1964). Energy calibration of the 9.59 MeV spectrum, indicated by arrows in Figure 11a, was obtained by comparison with spectra from the nearby 9.85 MeV resonance (page 35). A number of additional spectra of 5,000 μC, taken at various angles and energies, qualitatively confirm that the radiation under observation came from a broad 1^- state.

The amount of 9.59 MeV radiation was determined by subtracting from the spectrum in Figure 11a varying amounts of the "standard" 9.17 MeV gamma ray spectrum (see Figure 6) and comparing with the $C^{13}(\alpha, n)O^{16}$ background in Figure 11b. This process, facilitated by the use of semi-log spectrum plots, indicated that the spectrum in Figure 11a contains approximately 4800 counts from 9.59 MeV radiation in the energy interval from 0.8 to 1.1 E_γ (page 20). Combined with the center of mass width Γ_{CM} = 645 keV measured previously by Hill (1953) this yield implies a radiative width $\Gamma_\gamma = 0.022 \pm 0.005$ eV (see page 21). The sources of error listed in Table IV for this measurement indicate that although good statistics were achieved a 10% uncertainty resulted from the process of extracting the resonant yield from the background. Additional geometrical and angular errors (Table IV) are attached to this single angle measurement for which the radiation pattern was assumed to be characteristically E1, "smoothed" by the close proximity of the detector to the target. The value Γ_γ = 0.022 eV corresponds to $|M|^2 = \Gamma_\gamma/\Gamma_{\gamma W} = 5.8 \times 10^{-5}$, where $\Gamma_{\gamma W}$ (Weisskopf limit, see page 62) is the radiative width calculated from an extreme single-particle model assuming a nuclear radius $R = 1.2\ A^{1/3} \times 10^{-13}$ cm (Wilkinson 1960).

Although the prominent feature found in channels 70 - 80 of Figure 11a is suggestive of possible cascade radiation from the

9.59 MeV state, this same feature is also to be found in the background spectrum, Figure 11b. The background in this lower energy region is several times that where the 9.59 MeV ground state radiation peak is observed making the identification of lower energy cascade radiation very difficult. There is no direct evidence for any cascade radiation but the greater background found at lower energies limits the experimental resolving power to perhaps 1/10 that for 9.59 MeV radiation and it can only be concluded that any ≈ 7 MeV radiation is probably in less quantity than the direct ground state radiation. A search for possible cascade radiation using time coincidence techniques is rendered very difficult in low yield gamma ray experiments by the reduction of counting rates concomitant to the introduction of an additional detector; no attempt was made in this experiment to find cascade radiation through coincidence methods.

The previous measurement of radiative width for the 9.59 MeV state was made by Bloom, Toppel and Wilkinson (1957) who obtained $\Gamma_\gamma = 0.006$ eV ("--- probably accurate to a factor of two or better."). Using a 450 $\mu g/cm^2$ enriched C^{12} target they determined the amount of 9.59 MeV radiation by subtracting from results at $E_\alpha = 3.45$ MeV a background spectrum obtained at $E_\alpha = 3.00$ MeV. The resulting subtracted distribution still contained some "small" $C^{13}(\alpha, n)O^{16}$ background contribution which was removed by subtracting an additional, unspecified fractional amount of the 3.00 MeV yield. The residual spectrum was found, within rather poor statistics, to fit the spectral curve expected of 9.59 MeV radiation for their 5.1 cm x 5.1 cm NaI(Tl) detector.

In addition to the hazard that the shape of the background spectra may differ for these two bombarding energies, this pro-

cedure of Bloom et al. (1957) is certain to produce a result which is too small because the subtracted spectrum taken at E_α = 3.00 MeV must still contain some yield from the broad 9.59 MeV resonance. An estimate of this yield assuming single-level resonance parameters (Tombrello, private communication) indicates that a spectrum taken at E_α = 3.00 MeV with a 450 $\mu g/cm^2$ C^{12} target should contain about 28% of the 9.59 MeV yield found at E_α = 3.45 MeV. Since no mention of this effect is made by Bloom et al. (1957), it must be assumed that their results should be multiplied by a factor of 1.4 to correct for the subtraction error. The second "small" background correction will make this factor somewhat larger. These adjustments are not sufficient to produce satisfactory agreement with the result $\Gamma_\gamma = 0.022 \pm 0.005$ eV found in the present experiment.

The expressed motivation for the experiment by Bloom et al. (1957) was to determine the isotopic spin impurity in this region of O^{16} excitation for which Wilkinson (1956a) had predicted $\alpha_0^2(1) \approx 10^{-3}$ to 10^{-2}, where $\alpha_0^2(1)$ represents the admixture by intensity of T = 1 impurity into the predominantly T = 0 state. The present value of Γ_γ = 0.022 eV corresponds to $\alpha_0^2(1) = 1.1 \times 10^{-3}$, in somewhat better agreement with the prediction of Wilkinson, thus strengthening the conclusion of Bloom et al. (1957) that the 9.59 MeV state can be described to a significant extent in terms of single-particle excitation from the ground state.

A recent study of the 9.59 MeV resonance has been made by Black and Treacy (1964). Using a 12.7 cm x 15.2 cm NaI(T1) detector located at 90° to the He^+ beam and 8.9 cm from a 70 $\mu g/cm^2$ enrichcd C^{12} target, they found little radiation present in a run of

122,000 μC He^+ and concluded from the data that $\Gamma_\gamma = 0.008\ ^{+0.016}_{-0.008}$ eV. This value is close to that obtained by Bloom et al. (1957) but the large error overlaps the result found in the present experiment. Black and Treacy (1964) observed 9.4 MeV background radiation from $C^{12}(d, \gamma)N^{14*}$ attributable to residual deuterium in the ion source of their single stage accelerator. This was not a problem in the present experiment since deuterium gas is not introduced into the helium ion source of the tandem accelerator (see pages 73 and 74).

C. The 9.85 MeV State

The first clearly discernable $C^{12}(\alpha, \gamma)O^{16}$ resonance appearing in Figure 10 occurs at $E_\alpha = 3.585 \pm 0.013$ MeV, corresponding to a level in O^{16} at $E_x = 9.851 \pm 0.010$ MeV. This level has been observed through a variety of reactions:

Reaction	E_x(MeV)	Γ_{CM}(keV)	Reference†
$C^{12}(\alpha, \alpha)C^{12}$	9.849 ± 0.010[a]	0.75	Hill (1953)
$C^{12}(\alpha, \alpha)C^{12}$	9.829 ± 0.020[a]	0.75	Jones (1962)
$C^{12}(\alpha, \gamma)O^{16}$	9.8[a]	---	Meads (1960)
$N^{14}(He^3, p)O^{16}$	9.847 ± 0.003	< 20	Browne (1964)
$O^{16}(p, p')O^{16*}$	9.85 ± 0.03	---	Hornyak (1955)
$F^{19}(p, \alpha)O^{16}$	9.852 ± 0.012	---	Squires (1956)
$C^{12}(\alpha, \gamma)O^{16}$	9.851 ± 0.010[a]	---	Larson (1964)

a - Assuming $C^{12} + He^4 - O^{16} = 7.162$ MeV (Everling 1961)

† - For this and similar tabulations which follow, references have been contracted to include the first author's name only.

The excitation energies listed are as quoted in the original papers with the exceptions, as indicated, where revised Q-values may introduce a small correction. The overall agreement of these excitation energies, within the quoted errors, is excellent and it may be observed that the recent, very accurate results of Browne and Michael (1964) establish this resonance as a convenient energy calibration for $C^{12}(\alpha, \gamma)O^{16}$ experiments.

Both Hill (1953) and Jones et al. (1962) find this level to be 2^+ with a center of mass width $\Gamma_{CM} = 0.75$ keV. This very narrow resonance width has provided a convenient means for measuring target thickness. An expanded graph for this region of excitation is shown in Figure 12. The apparent width of the 9.85 MeV resonance in this figure indicates that the target is 31 ± 2 keV thick for alpha particles of 3.59 MeV incident at 45^o to the surface, corresponding to a surface density of 22 $\mu g/cm^2$. This target was used for all of the resonance data shown in Figure 10. Another target of 14 $\mu g/cm^2$ surface density was used in acquiring some of the non-resonant background data found between $E_\alpha = 2.8 - 4.7$ MeV in Figure 10.

Measurements of this excitation step at angles of 0^o, 45^o and 90^o combined with the shape of the angular distribution measured in 15^o increments from 0^o to 90^o give a radiative width $\Gamma_\gamma = 0.0059 \pm 0.0006$ eV for ground state radiation from the 9.85 MeV resonance. For this "thick target" yield the term $\tan^{-1}(\xi/\Gamma)$ in the radiative width expression (page 22) reduces to $\pi/2$ and target thickness does not contribute to the estimated error (Table IV). The value $\Gamma_\gamma = 0.0059$ eV corresponds to $|M|^2 = 0.032$ for the E2 transition (see pages 61-63). This result may be compared to $\Gamma_\gamma = 0.02 \pm 0.01$ eV obtained previously by Meads and McIldowie (1960).

Attempts to measure the thickness of the 96 $\mu g/cm^2$ target using the 9.85 MeV resonance (page 25) revealed a small amount of 7 MeV cascade radiation present along with the ground state yield. The amount of this cascade radiation was determined by directly subtracting a spectrum taken below the resonance (at E_α = 3.57 MeV) from one taken on the resonance and comparing the relative amounts of ground state and 7 MeV cascade radiation in the difference spectrum. The result, obtained only for one detector angle 90^o, was $\Gamma_{\gamma(\text{cascade})} = 0.0012 \pm 0.0004$ eV. Although fairly long runs of 5,000 μC were used, the error comes principally from the poor statistics attendant to the subtraction process (Table IV). Extraction of the 7 MeV radiation from a background which includes the low energy tail of the ground state spectrum results in another significant source of error included under background correction in Table IV. The identity of the intermediate level at 7 MeV (6.92 MeV, 2^+ or 7.12 MeV, 1^-) was not established, leaving the angular distribution of the cascade radiation in doubt. An isotropic distribution was assumed for the radiative width estimate; however, with the 10.2 cm x 10.2 cm detector only 2.7 cm from the target the error introduced by this assumption is at most 12%.

D. The 10.36 MeV State

The resonance at $E_\alpha = 4.260 \pm 0.015$ MeV in Figure 10 corresponds to a state in O^{16} at $E_x = 10.357 \pm 0.011$ MeV with a center of mass width $\Gamma_{CM} = 27 \pm 4$ keV. Measurements of this state have been the following:

Reaction	E_x(MeV)	Γ_{CM}(keV)	Reference
$C^{12}(\alpha, \alpha)C^{12}$	10.37 ± 0.02^a	27 ± 3	Bittner (1954)
$C^{12}(\alpha, \alpha)C^{12}$	10.343 ± 0.025^a	25	Jones (1962)
$N^{14}(He^3, p)O^{16}$	10.353 ± 0.004	28 ± 8	Browne (1964)
$O^{16}(p, p')O^{16*}$	10.34 ± 0.03	---	Hornyak (1955)
$F^{19}(p, \alpha)O^{16}$	10.363 ± 0.014	25 - 30	Squires (1956)
$C^{12}(\alpha, \gamma)O^{16}$	10.357 ± 0.011^a	27 ± 4	Larson (1964)

a - Assuming $C^{12} + He^4 - O^{16} = 7.162$ MeV (Everling 1961).

Again, the results are in good agreement to within the quoted errors.

This state has been assigned a spin-parity of 4^+ as a result of $C^{12}(\alpha, \alpha)C^{12}$ work by Bittner and Moffat (1954) and Jones et al. (1962). Ground state radiation from this level is expected to be weak in comparison with that from the neighboring 2^+ levels (Blatt and Weisskopf 1952) and the apparent yield of "ground state" radiation in Figure 10 is attributable to summing of cascade members in the detector. With the 10.2 cm x 10.2 cm crystal only 2.7 cm from the target the probability for simultaneous detection of two cascade members is about 5%.

Inset in Figure 10 is a graph displaying the excitation function for gamma rays of energy 6.9 ± 0.1 MeV observed in the spectra from the 10.36 MeV resonance. The ordinate of the inset represents the number of pulses obtained within a window corresponding to gamma ray energies from 5.5 to 7.6 MeV. Measurements of this yield at angles of 0^o, 45^o and 90^o combined with an angular distri-

bution measurement at the peak of the resonance indicate that the 10.36 MeV, 4^+ state decays through the intermediate 6.92 MeV, 2^+ level with a radiative width $\Gamma_{\gamma(10.36 \rightarrow 6.92)} = 0.046 \pm 0.006$ eV. This result compares favorably with the value $\Gamma_{\gamma(10.36 \rightarrow 6.92)} = 0.040 \pm 0.008$ eV obtained recently from $C^{12}(\alpha, \gamma)O^{16}$ cascade measurements by Gorodetzky et al. (1963).

The possibility of the 6.92 MeV state decaying appreciably through modes other than direct radiation to the ground state seems slight. Decay through the 6.13 MeV state (60% of any 6.13 MeV radiation is included in the summation from 5.5 to 7.6 MeV) was not observed to be appreciable in the spectra; furthermore, measurements made by Wilkinson and Toppel (quoted in Wilkinson 1956a) have shown that decay via the 6.13 MeV state is less than 2×10^{-3} times as probable as decay to the ground state. Decay through the 6.05 MeV state followed by pair emission has been shown to be negligible (Gorodetzky et al. 1962).

The value $\Gamma_{\gamma(10.36 \rightarrow 6.92)} = 0.046$ eV corresponds to $|M|^2 = 49$ (pages 61-63) for the E2 transition between the 10.36 MeV, 4^+ and 6.92 MeV, 2^+ states. This is in marked contrast with the value $|M|^2 = 0.032$ given earlier for the ground state E2 transition from the 9.85 MeV, 2^+ level and suggests some sort of generic relationship between the 6.92 MeV and 10.36 MeV states of O^{16}. A theoretical basis for this result may be found in the recent articles on rotational band structure by Brink and Nash (1963) and Borysowicz and Sheline (1964) who have successfully described nearly all of the low lying even parity states of O^{16} in terms of rotational bands. In their analyses the lowest prolate deformation band includes the states at 6.05 (0^+), 6.92 (2^+), 10.36 (4^+) and 16.2 MeV (6^+) (see Figure 2).

E. The 11.52 MeV State

The resonance at $E_\alpha = 5.809 \pm 0.018$ MeV in Figure 10 corresponds to a state in O^{16} at $E_x = 11.519 \pm 0.014$ MeV with a width $\Gamma_{CM} = 73 \pm 5$ keV. This state has been observed through several of the reactions previously mentioned:

Reaction	E_x(MeV)	Γ_{CM}(keV)	Reference
$C^{12}(\alpha, \alpha)C^{12}$	11.53 ± 0.02^a	80 ± 8	Bittner (1954)
$C^{12}(\alpha, \gamma)O^{16}$	11.53^a	---	Meads (1960)
$N^{14}(He^3, p)O^{16}$	11.521 ± 0.004	78 ± 8	Browne (1964)
$O^{16}(p, p')O^{16*}$	11.51 ± 0.03	---	Hornyak (1955)
$C^{12}(\alpha, \gamma)O^{16}$	11.519 ± 0.014^a	73 ± 5	Larson (1964)

a - Assuming $C^{12} + He^3 - O^{16} = 7.162$ MeV (Everling 1961).

Again, agreement of the measured quantities is quite satisfactory.

Measurements of the 11.52 MeV resonant yield at angles of 0^o and 45^o combined with an angular distribution measurement in 15^o increments from 0^o to 90^o give a width $\Gamma_\gamma = 0.66 \pm 0.09$ eV for ground state radiation corresponding to $|M|^{2\gamma} = 1.6$ (pages 61-63) for the E2 transition. This is smaller than the value $\Gamma_\gamma = 0.9 \pm 0.2$ eV obtained for this resonance by Meads and McIldowie (1960) but not necessarily inconsistent since Meads and McIldowie had considerably more background apparent in their excitation function. A recent electron scattering experiment by Bishop et al. (1964) gave $\Gamma_\gamma = 0.86$ eV which tends to confirm the higher value. The total

level width Γ_{CM} = 73 keV used in determining the present result (page 23) is 9% less than the earlier published value (Bittner and Moffat 1954) and thus may account for some of the discrepancy.

This resonance at E_α = 5.8 MeV occurs near the upper limit in energy for beams of singly charged alpha particles accelerated by the ONR-CIT tandem accelerator. Although the region above E_α = 6 MeV was, of necessity, covered exclusively by the He^{++} beam, there is a region from about 4 to 6 MeV which is readily accessible using either of the available ion beams. In order to achieve greater beam intensity (the He^+ beam contains typically about five times the particle density of the He^{++} beam), the He^+ beam was used throughout this region of overlap; however, the 11.52 MeV resonance provided a convenient opportunity to compare directly the results obtained from each beam. At 45^o the yields from the two charge states differed by only 6% (page 28), a result not inconsistent with the possible errors involved and adequately satisfactory for the desired accuracy of the experiment.

F. The Region of Excitation From 12.3 to 13.3 MeV

The region of excitation in O^{16} above the N^{15} + p threshold at 12.126 MeV has long been available to low energy proton experiments (Fowler and Lauritsen 1940; see also Ajzenberg-Selove and Lauritsen 1959). Despite this accessibility, however, some considerable confusion about this region has persisted (see, for example, Hagedorn 1957). A general review of the N^{15} + p experiments has been provided by Hebbard (1960) who in his analysis of the existing data verified that resonances at E_p = 0.338, 1.010 and 1.210 MeV correspond to O^{16} states at excitation energies of 12.44

MeV (1^-), 13.10 MeV (1^-) and 13.26 MeV (3^-). (Only states of natural spin-parity are being considered in this discussion.) Hebbard finds that the two 1^- states interfere constructively in the case of $N^{15}(p, \alpha)C^{12}$ and destructively for $N^{15}(p, \gamma)O^{16}$; he concludes that both states are of mixed isobaric spin, the 12.44 MeV state being predominantly T = 0 and the 13.10 MeV state predominantly T = 1, with a 15% admixture of the minor component in each case. Although a consensus of spin and parity for each level has been reached, the data frequently have led to conflicting and contradictory results for these states.

The fact that these observed resonances proved tenaciously intractable to single-level analysis and unambiguous spin-parity assignments has led to speculation on the existence of unobserved levels in this region (Wilkinson 1953; Hebbard 1960). Hebbard's analysis of angular distribution data from $N^{15}(p, \alpha)C^{12}$ suggested the presence of unobserved states at proton energies of approximately 500 keV (0^+) and 1000 keV (2^+) corresponding to O^{16} excitation energies of 12.60 and 13.06 MeV. In their study of $C^{12}(\alpha, \alpha)C^{12}$, Bittner and Moffat (1954) found that the behavior of the $\ell = 0$ and $\ell = 2$ phase shifts near the upper energy limit of their experiment (E_x approximately 12.9 MeV) suggested the presence of broad 0^+ and 2^+ states in this region. The $C^{12} + \alpha$ data of both Ferguson and McCallum (1961) and G. Mitchell et al. (1961, 1964) suggested the presence of more than one state in the region of $E_x = 13$ MeV, possibly a mixture of 1^- and 2^+. Recently, evidence for the existence of a broad 2^+ state at $E_x = 13$ MeV was claimed by Tanner and I. Mitchell (1962, private communication) who observed asymmetries about 90° in angular distribution measurements of radiation from $C^{12}(\alpha, \gamma)O^{16}$ at $E_\alpha = 7.9$ MeV.

Asymmetries of the type reported by Tanner and Mitchell are relatively rare in gamma ray spectroscopy. Transitions from an isolated state with well defined spin and parity produce angular distributions symmetric about 90^{o}. Only terms which arise from the interference of opposite parity nuclear states contain the odd powers of cos θ necessary to produce an asymmetric angular distribution (Blatt and Weisskopf 1952). Adequate resolution of possible odd powers in cos θ requires that measurements be made to angles as much greater than 90^{o} as is practicable. The dictates of low yield from the alpha capture reaction and a necessarily bulky detector made 135^{o} a practical limit for this experiment. At this angle the detector can still be located at a distance less than its own diameter from the target (see Figure 5) while the measurements conveniently complement data taken at 45^{o} in emphasizing any asymmetries.

Striking confirmation of the asymmetries reported by Tanner and Mitchell is given by the 135^{o} excitation function shown in Figure 13 and angular distributions from 0^{o} to 135^{o} at energies E_{α} = 7.06, 7.42, 7.88 and 8.00 MeV shown in Figure 14. The data for both Figures 13 and 14 were taken with the unshielded NaI(T1) crystal (page 12) placed 7.6 cm from the target spot; this distance corresponds to the closest practical approach of the detector to the target at the most extreme backward angle measured, 135^{o} (Figure 5). The 22 $\mu g/cm^{2}$ target was perpendicular to the beam axis. In each figure the ordinate N represents the number of counts per 450 μC of He^{++} ions observed within the spectrum interval 0.8 - 1.1 E_{x}. Corrections to the data have been made for room background and dead-time. In addition, the data in Figure 14 have been corrected

for anisotropic absorption of radiation in the target backing (2.54 cm x 2.54 cm x 0.025 cm tantalum). Error bars in Figures 13 and 14 represent statistical errors only.

The dashed curve in Figure 13, showing the 45^{o} excitation function where it differs from that of 135^{o}, is based on data (some of which also appears in Figure 14) taken with this same geometrical configuration and a knowledge of the general shape of the 45^{o} excitation function in this energy region (Figure 10). The 45^{o} excitation functions shown in Figures 10 and 13 must be expected to differ slightly as the radiation patterns change because of the different solid angles subtended by the detector in each case. Failure of the 45^{o} and 135^{o} curves to coincide (Figure 13) is indicative of the presence of odd powers of cos θ, hence interference between opposite parity states, in the radiation pattern.

The solid curves in Figure 14 represent least squares fits to the corrected data by the expression $W(\theta) = a_0 + a_1 P_1(\cos\theta) + a_2 P_2(\cos\theta) + a_3 P_3(\cos\theta) + a_4 P_4(\cos\theta)$. Meaningful higher order terms cannot be obtained from this data (page 15) but, as yet, no significance has been attached to terms higher than $P_4(\cos\theta)$. Corrections for the finite solid angle subtended by the detector were made after the method of Rose (1953), giving the values of the Legendre coefficients for a point detector listed in Table I. Errors listed in Table I are from statistical sources only.

G. The 12.44 MeV State

The resonance appearing at $E_\alpha = 7.05 \pm 0.02$ MeV in Figures 10 and 13 corresponds to a state in O^{16} at $E_x = 12.45 \pm 0.02$ MeV with $\Gamma_{CM} = 100 \pm 10$ keV. A variety of reactions confirm this state:

Reaction	E_x(MeV)	Γ_{CM}(keV)	Reference
$C^{12}(\alpha, \alpha)C^{12}$	12.44 $\pm$ 0.02[a]	173 $\pm$ 17	Bittner (1954)
$C^{12}(\alpha, \alpha)C^{12}$	12.45 $\pm$ 0.02[a]	---	Ferguson (1961)
$C^{12}(\alpha, \gamma)O^{16}$	12.44[a]	80	I. Mitchell (1964)
$N^{14}(He^3, p)O^{16}$	12.437 $\pm$ 0.007	94 $\pm$ 15	Browne (1964)
$N^{15}(p, \alpha)C^{12}$	12.443[b]	88	Schardt (1952)
$N^{15}(p, \gamma)O^{16}$	12.443[b]	88	Hebbard (1960)
$C^{12}(\alpha, \gamma)O^{16}$	12.45 $\pm$ 0.02[a]	100 $\pm$ 10	Larson (1964)

a - Assuming $C^{12} + He^4 - O^{16} = 7.162$ MeV (Everling 1961).

b - Assuming $N^{15} + H^1 - O^{16} = 12.126$ MeV (Everling 1961).

The early discrepancy in total width between experiments in $N^{15} + p$ (Schardt *et al.* 1952) and $C^{12} + \alpha$ (Bittner and Moffat 1954) created some doubt about the unique identity of this state (Hebbard 1960); recent evidence preponderantly favors a single 1^- level at $E_x = 12.44$ MeV. The data are otherwise in good agreement.

The results from $N^{15}(p, \alpha)C^{12}$ (isotropic angular distribution of long range alpha particles) and $N^{15}(p, \gamma)O^{16}$ (presence of ground state radiation) uniquely associate this resonance with a 1^- state in O^{16} (Hebbard 1960). The angular distribution from $C^{12}(\alpha, \gamma)O^{16}$ at $E_\alpha = 7.06$ MeV is of the form (Table I)

$$W(\theta) = a_0 [1.00 - (1.04 \pm 0.07)P_2(\cos\theta)]$$

$$+ [\text{negligible terms in } P_1, P_3 \text{ and } P_4]$$

in good agreement with the theoretical angular distribution,

$$W(\theta) = a_0 [1 - P_2(\cos \theta)] ,$$

expected for an E1 transition between 1^- and 0^+ states. Additional evidence is supplied by I. Mitchell and Ophel (1964) who find the $C^{12}(\alpha, \gamma)O^{16}$ yield at angles of 45^o, 90^o and 135^o to be consistent with an E1 transition.

The radiative width of the 12.44 MeV state was determined from the excitation function at 45^o (Figure 10) and an angular distribution from 0^o to 135^o (Figure 14) with the result $\Gamma_\gamma = 7 \pm 1$ eV, corresponding to $|M|^2 = 0.008$ (pages 61-63)for the E1 transition. This result is in good agreement with the value $\Gamma_\gamma = 8$ eV obtained by Hebbard (1960) from a single-level analysis of $N^{15}(p, \gamma)O^{16}$.

H. The States at 13.1 MeV

Resonances corresponding to an excitation energy near 13.1 MeV in O^{16} have been observed in a variety of reactions:

Reaction	E_x(MeV)	Γ_{CM}(keV)	Reference
$C^{12}(\alpha, \alpha)C^{12}$	13.10 ± 0.02^a	---	Ferguson (1961)
$C^{12}(\alpha, \alpha'\gamma)C^{12}$	13.12^a	90	G. Mitchell (1964)
$C^{12}(\alpha, \gamma)O^{16}$	13.09^a	135	I. Mitchell (1964)
$N^{14}(He^3, p)O^{16}$	13.105 ± 0.015	160 ± 30	Browne (1964)
$N^{15}(p, \alpha)C^{12}$	13.1^b	130	Schardt (1952)
$N^{15}(p, \alpha'\gamma)C^{12}$	13.11^b	117 ± 24	Bashkin (1957)

continued

Reaction	E_x(MeV)	Γ_{CM}(keV)	Reference
$N^{15}(p, p)N^{15}$	13.09[b]	---	Hagedorn (1957)
$N^{15}(p, \gamma)O^{16}$	13.090 ± 0.010[b]	131 ± 10	Hagedorn (1957)
$O^{16}(p, p')O^{16*}$	13.06 ± 0.03	---	Hornyak (1955)
$C^{12}(\alpha, \gamma)O^{16}$	13.07 ± 0.02[a]	135 ± 20	Larson (1964)
$C^{12}(\alpha, \alpha'\gamma)C^{12}$	13.13[a]		Larson (1964)

a - Assuming $C^{12} + He^4 - O^{16} = 7.162$ MeV (Everling 1961).

b - Assuming $N^{15} + H^1 - O^{16} = 12.126$ MeV (Everling 1961).

This tabulation is representative of the published data, but not exhaustive. The wide distribution of resonance energies from the various reactions is well verified as part of the anomalous behavior in this region. Although precise determination of the many N^{15} + p results is subject to individual interpretation and analysis, detailed studies have demonstrated that the (p, p), (p, α), (p, α'γ) and (p, γ) reactions do not coincide in energy at this resonance (Hagedorn 1957; Bashkin et al. 1959; Hebbard 1960). Discussion of the $C^{12}(\alpha, \alpha'\gamma)C^{12}$ reaction is deferred to a later section (page 54) where it is treated in more detail.

The angular distribution measured at $E_\alpha = 7.88$ MeV (Figure 14) provides unmistakable evidence for interference between opposite parity states. Since a 1^- state has already been associated with this resonance to explain numerous N^{15} + p results, the interfering even

parity state almost certainly must be 2^+; a 0^+ state could give no ground state radiation and states of spin 4 or higher should be exceedingly weak. A comparison of the 45^o and 135^o excitation functions (Figures 10 and 13) suggests that the 2^+ state has approximately the same energy and width as the 1^- state.

Quantitative confirmation of this conclusion can be obtained by considering the theoretical distribution expected of interfering gamma ray spectra. For an interference between 1^- and 2^+ states the angular distribution should be of the form (see Sharp et al. 1959)

$$W(\theta) = (3A_1^2 + 5A_2^2)P_0 + (-3A_1^2 + (25/7)A_2^2)P_2 - (60/7)A_2^2 P_4$$

$$+ 6\sqrt{3}\, A_1 A_2 \cos\theta_{12}(P_1 - P_2)$$

where A_1 = amplitude coefficient of the 1^- state

A_2 = amplitude coefficient of the 2^+ state

θ_{12} = phase difference between amplitudes

P_n = $P_n(\cos\theta)$ = Legendre polynomial of order n.

It is apparent that two restrictions are imposed on the radiation pattern governed by this expression. First, the even order polynomial coefficients, representing superposition of the normal E1 and E2 radiation patterns, sum to zero while, second, the terms in the odd polynomials, representing interference between these transitions, must have equal magnitude coefficients, but of opposite sign. A comparison with experimental results at E_α = 7.88 MeV

(Table I) shows that these conditions are approximately met by the data.

Other possible combinations of opposite parity states produce improbable restrictive conditions on the odd order polynomial coefficients:

Interfering states	a_1/a_3
1^-, 2^+	-1.00
1^-, 4^+	0
2^+, 3^-	+2.57
Observation	
Larson and Spear (1964)	-1.31 ± 0.46
I. Mitchell and Ophel (1964)	-1.12 ± 0.21

With this comparison it is obvious that the observations strongly favor the 1^-, 2^+ interference, as had been expected from qualitative arguments. As implied, very similar coefficients for the angular distribution at $E_\alpha = 7.9$ MeV have been obtained concurrently by I. Mitchell and Ophel. Their results,

$$W(\theta) \propto P_0 + (0.38 \pm 0.05)P_1 - (0.93 \pm 0.05)P_2 - (0.34 \pm 0.06)P_3 - (0.13 \pm 0.05)P_4 \text{ at } E_\alpha = 7.90 \text{ MeV},$$

obtained from detailed observations in this region are, as shown, somewhat more accurate (compare with Table I).

The $C^{12}(\alpha, \gamma)O^{16}$ experiments have now verified the existence of an underlying 2^+ state at 13.1 MeV but information on the precise properties of this level has yet to be obtained. I. Mitchell and Ophel (1964, 1965) conclude that the 2^+ resonance is centered about 50 keV higher than the 1^- state at $E_\alpha = 7.98$ MeV corresponding to $E_x = 13.15 \pm 0.10$ MeV with $\Gamma_{CM} \approx 250$ keV, $(A_2/A_1)^2 \approx 0.03$ and $\Gamma_\gamma \approx 0.6$ eV. The results of the present experiment in no way contradict the conclusions of I. Mitchell and Ophel and, depending on interpretation of Figures 10 and 13, lend qualitative support. The procedures of the two experiments are sufficiently similar to allow some combination of results. Subject to the restriction that $(a_2/a_0) + (a_4/a_0) = -1$ (page 48), the following averages, weighted by percentage errors, may be obtained:

Averaged experimental parameters for interfering states at 13.1 MeV (I. Mitchell and Ophel 1964; Larson and Spear 1964)

$$a_2 = 0.90 \pm 0.03$$

$$a_4 = 0.10 \pm 0.03$$

$$(A_2/A_1)^2_{7.9\ \mathrm{MeV}} \approx (1/3)(a_4/a_2) = 0.037 \pm 0.01$$

Since the resonant energies of the 1^- and 2^+ states apparently are not coincident, the ratio $(A_2/A_1)^2_E$ taken at a fixed energy is not truly representative of the relative cross section maxima; however, at the present level of experimental uncertainty, this omission probably is not significant. The value $(A_2/A_1)^2 \approx 0.03 \pm 0.015$ quoted by I. Mitchell and Ophel does take into account the dis-

placement of the resonances. The approximation $(A_2/A_1)_E^2 \approx (1/3)(a_4/a_2)$ is excellent for ratios of (a_4/a_2) near (1/10).

This small value for $(A_2/A_1)^2$ indicates that, despite considerable distortion of the angular distribution from symmetry about 90° (Figure 14, E_α = 7.88 MeV), E1 radiation from the 1^- state represents about 94% of the total ground state yield observed at this resonance. A single-level determination (page 21) using the ratio $(\Gamma_\alpha/\Gamma) = (40/140)$ given by Hebbard (1960) produces a radiative width $\Gamma_\gamma(1^-) = 32 \pm 5$ eV corresponding to $|M|^2 = 0.033$ (pages 61-63) for the E1 transition from the 1^- state at 13.10 MeV. The $N^{15}(p, \gamma)O^{16}$ cross section revised to 700 μb (Hebbard 1960) corresponds to Γ_γ = 62 eV for this transition. However, Hebbard (1965, private communication) points out that his analysis of $N^{15}(p, \alpha)C^{12}$ data indicated the (p, α) cross section could contain a contribution from an underlying 2^+ state amounting to approximately 20% of the total yield (Hebbard 1960, p. 308). If the (p, α) cross section for the 1^- resonance is correspondingly reduced by 20%, values of Γ_α/Γ and Γ_p/Γ become $\Gamma_\alpha/\Gamma = (29/140) = 0.21$ and $\Gamma_p/\Gamma = (111/140) = 0.79$. Then $\Gamma_\gamma(\alpha, \gamma) = 32(40/29)$ eV = 44 eV, $\Gamma_\gamma(p, \gamma) = 62(100/111)$ eV = 56 eV and the discrepancy is within experimental error. Further adjustment of the data is not warranted without improved experimental values of $\sigma(p, \alpha)$ and $\sigma(p, \gamma)$; but assuming the total width $(\Gamma = \Gamma_p + \Gamma_\alpha + \Gamma_{\alpha'} + \Gamma_\gamma \approx \Gamma_p + \Gamma_\alpha)$ of this resonance to be 135 keV, the radiative widths may conveniently be written as $\Gamma_\gamma(\alpha, \gamma) = (9 \pm 1.5)(\Gamma/\Gamma_\alpha)$ eV and $\Gamma_\gamma(p, \gamma) = 44\ (\Gamma/\Gamma_p)$ eV. With the present values $\Gamma/\Gamma_\alpha \approx 5$ and $\Gamma/\Gamma_p \approx (5/4)$, it is apparent that a single-level value of $\Gamma_\gamma(1^-) \approx 50 \pm 10$ eV is consistent with the

available data. A small amount of cascade radiation, presumably from the 1^- state, with $\Gamma_{\gamma(13.10 \rightarrow 6.05)} = 0.7 \pm 0.2$ eV, has been found in this region of excitation by Gorodetzky et al. (1963).

The presence of substantial ground state radiation between the resonances at 12.44 and 13.10 MeV (Figures 7c, 10, 13, 14) suggests that constructive interference between the two 1^- states occurs in $C^{12}(\alpha, \gamma)O^{16}$. Hebbard (1960) has performed a two-level analysis of these resonances, including destructive interference between resonances to fit $N^{15}(p, \gamma)O^{16}$ and constructive interference for $N^{15}(p, \alpha)C^{12}$. Barker (private communication) believes these interference effects are compatible with a simple model of isotopic spin mixing between the levels. The implication clearly is that final values of the level parameters must come through multi-level analysis of all the data.

The radiative width of the 2^+ state at 13.15 MeV may be written, for thin target yields, as

$$\Gamma_\gamma(2^+) = \Gamma_\gamma(1^-)(A_2/A_1)^2(\Gamma_2/\Gamma_1)(\Gamma_{\alpha 1}/\Gamma_1)(\Gamma_2/\Gamma_{\alpha 2}) .$$

Introducing (see above) $\Gamma_\gamma(1^-) = (9 \pm 1.5)(\Gamma_1/\Gamma_{\alpha 1})$ eV, $(A_2/A_1)^2 = (0.037 \pm 0.01)$, $\Gamma_1 = 135$ keV and $\Gamma_2 = 250$ keV into this expression gives the tentative result

$$\Gamma_\gamma(2^+) = (0.6 \pm 0.2)(\Gamma_2/\Gamma_{\alpha 2}) \text{ eV},$$

corresponding to $|M|^2 = 0.8\ (\Gamma_2/\Gamma_{\alpha 2})$, (pages 61-63). Final evaluation awaits improved measurements of the 2^+ state including a determination of $\Gamma_{\alpha 2}$.

I. The 13.26 MeV State

The resonance observed in Figure 10 at $E_\alpha = 8.13 \pm 0.03$ MeV corresponds to a state in O^{16} at $E_x = 13.26 \pm 0.02$ MeV with $\Gamma_{CM} = 26 \pm 10$ keV. The following is a representative sample of the reactions through which this resonance has been observed:

Reaction	E_x(MeV)	Γ_{CM}(keV)	Reference
$C^{12}(\alpha, \alpha)C^{12}$	13.27 ± 0.02[a]	---	Ferguson (1961)
$C^{12}(\alpha, \alpha'\gamma)C^{12}$	13.27[a]	40	G. Mitchell (1964)
$N^{14}(He^3, p)O^{16}$	13.253 ± 0.005	25 ± 8	Browne (1964)
$N^{15}(p, \alpha'\gamma)C^{12}$	13.260 ± 0.003[b]	21 ± 1	Schardt (1952)
$N^{15}(p, p)N^{15}$	13.26[b]	---	Hagedorn (1957)
$C^{12}(\alpha, \gamma)O^{16}$	13.26 ± 0.02[a]	26 ± 10	Larson (1964)
$C^{12}(\alpha, \alpha'\gamma)C^{12}$	13.27[a]		Larson (1964)

a - Assuming $C^{12} + He^4 - O^{16} = 7.162$ MeV (Everling 1961).

b - Assuming $N^{15} + H^1 - O^{16} = 12.126$ MeV (Everling 1961).

The spin and parity of this state have in the past suffered a vacillatory existence between 3^- and 4^+ (Hagedorn 1957); the less ambiguous of the N^{15} + p experiments indicate 3^-. The results of $C^{12}(\alpha, \alpha)C^{12}$, $C^{12}(\alpha, \alpha')C^{12*}$ and $C^{12}(\alpha, \alpha'\gamma)C^{12}$ (Ferguson and McCallum 1961; G. Mitchell et al. 1961, 1964; I. Mitchell and Ophel 1964, 1965) also favor the 3^- assignment. Very little ground state radiation is to be expected from a 3^-

state and the resonant yield at this energy in Figure 10 is presumably due largely to summing in the detector of gamma rays cascading through O^{16} states at 6 and 7 MeV excitation; this has been verified by I. Mitchell and Ophel (1964). The intense yield of 6 and 7 MeV radiation from $C^{13}(\alpha, n\gamma)O^{16}$ (Spear et al. 1963) forestalled direct observation of cascade radiation from this state.

J. Inelastic Scattering

In Figure 15 is data obtained by R. H. Spear with the assistance of J. D. Pearson showing the excitation function for $C^{12}(\alpha, \alpha'\gamma_{4.43})C^{12}$ for E_α = 7.5 to 10.5 MeV (Larson and Spear 1961, 1964). Resonances appear at E_α = 7.96, 8.14, 8.98, 10.08 (broad) and 10.20 MeV, corresponding to states in O^{16} at E_x = 13.13, 13.27, 13.90, 14.72 and 14.81 MeV, respectively. Similar results have been obtained by G. Mitchell et al. (1961, 1964) and, in part, by I. Mitchell and Ophel (1964, 1965). These levels have also been observed through $C^{12}(\alpha, \alpha)C^{12}$ and $C^{12}(\alpha, \alpha')C^{12*}$ by Ferguson and McCallum (1961); to within experimental error there is general agreement on the resonance energies.

The first two $C^{12}(\alpha, \alpha'\gamma)C^{12}$ resonances should be expected to relate directly to resonances observed and already described for $C^{12}(\alpha, \gamma)O^{16}$ (pages 46-54). At E_α = 8.14 MeV there is satisfactory agreement in energy between these resonant reactions while experiments mentioned in the previous paragraph conclude a spin-parity of 3^-, linking this resonance to the 3^- state found in N^{15} + p reactions. In contrast, the first $C^{12}(\alpha, \alpha'\gamma)C^{12}$ resonance at E_α = 7.96 MeV (Figure 15) appears shifted in energy by some 50 keV (I. Mitchell and Ophel 1964) above the corresponding resonance

in $C^{12}(\alpha, \gamma)O^{16}$. Angular studies of the $C^{12}(\alpha, \alpha'\gamma)C^{12}$ reaction by G. Mitchell et al. (1964) and I. Mitchell and Ophel (1964) indicate that the 13.13 MeV resonance conforms to the same distribution pattern as the nearby 13.26 MeV (3^-) state and is fully consistent with a 3^- assignment. This choice may be avoided by postulating an overlap of angular distributions from the 1^- and 2^+ states now known to exist in this region (see G. Mitchell et al. 1964); however, recent studies of the inelastic alpha particles by I. Mitchell and Ophel (1965) preclude this possibility and definitely establish a new 3^- state at $E_x = 13.13 \pm 0.01$ MeV, $\Gamma_{CM} = 100$ keV.

K. Summary

Graphs of the excitation function for the reaction $C^{12}(\alpha, \gamma)O^{16}$, displaying ground state radiation from states of O^{16} at 9.85 (2^+), 11.52 (2^+), 12.44 (1^-), 13.10 (1^-) and 13.15 MeV (2^+), are shown in Figures 10 and 13. Through the interaction of cascade members with the NaI(T1) detector, radiation from states at 10.36 (4^+) and 13.26 MeV (3^-) also is observed (Figure 10). A single spectrum of ground state radiation from the 9.59 MeV (1^-) state is shown in Figure 11a. These ground state and cascade transitions observed in the present experiment are indicated schematically in an energy level diagram of O^{16} shown in Figure 2a.

Summarized in Table II is information on excitation energies and total widths for the resonances observed in this experiment. Omitted entries could not reliably be measured by the methods used. To within experimental errors, these results are in good agreement with the recent survey by Browne and Michael (1964) and earlier measurements (see Ajzenberg-Selove and Lauritsen 1959).

Except where otherwise indicated in the text, the total widths Γ_{CM} listed in Table II have been employed in the radiative width calculations.

The radiative widths determined by this experiment are listed in Table III. Spins and parities of the initial and final states are from other sources (Ajzenberg-Selove and Lauritsen 1959). The indicated multipolarities of transitions to the 0^+ ground state are unique in every case; the E2 transition from the 4^+ state at 10.36 MeV to the 2^+ state at 6.92 MeV is parity favored and almost certainly dominant (Blatt and Weisskopf 1952). Either of the O^{16} levels at 7 MeV (6.92 MeV, 2^+ and 7.12 MeV, 1^-) may be participating in the cascade from the 2^+ state at 9.59 MeV. In the last column transition rates have been compared with the predictions of an extreme single-particle model through the ratio $\Gamma_\gamma/\Gamma_{\gamma W} = |M|^2$, assuming a nuclear radius $R = 1.2\ A^{1/3} \times 10^{-13}$ (Wilkinson 1960; see page 62). Contributions to the experimental errors quoted for the radiative widths have been individually listed in Table IV.

Table V contains a comparison of the present results with other radiative width measurements. Within experimental errors there is agreement on transition strengths from the states at 10.36, 11.52 and 12.44 MeV; however, significant discrepancies exist between measurements of the transitions from states at 9.59 and 9.85 MeV. All measurements at the 9.59 MeV state have been plagued by the problem of extracting a very low yield from the large background; Figure 11a contains the most clearly defined spectrum of ground state radiation that has yet been observed from this resonance. The excitation measurements at 9.85 and 11.52 MeV by Meads and McIldowie (1960) contained considerably more background than is to be found in Figure 10, perhaps explaining

their larger values for the respective radiative widths. A more precise $N^{15}(p, \gamma)O^{16}$ experiment should improve comparisons of the 1^- resonance at 13.10 MeV (page 51).

Angular distributions taken in the region of the 12.44 and 13.1 MeV resonances (E_α = 7.06 and 7.88 MeV in Table I and Figure 14) confirm the existence of previously detected 1^- states at these energies and also provide conclusive evidence for a new 2^+ state near 13.15 MeV. These same results have been obtained concurrently by I. Mitchell and Ophel (1964, 1965) who also are able to identify the first resonance in $C^{12}(\alpha, \alpha'\gamma_{4.43})C^{12}$ as a new 3^- state in O^{16} at 13.13 MeV. Positive identification of a 2^+ state near 13 MeV, as predicted by Bittner and Moffat (1954) and Hebbard (1960) on the basis of inconclusive phase shift analyses, now leads to enhanced speculation about the existence of the broad 0^+ state predicted by these same authors to lie somewhere near 12.5 MeV (page 42).

IV. DISCUSSION

A. Radiative Selection Rules

Radiative transitions from states in 0^{16} excited by the alpha capture reaction are especially interesting because of the direct involvement of several well known electromagnetic selection rules. These rules derive from the conservation of angular momentum and parity and (less stringently) the charge independence of nuclear forces (Blatt and Weisskopf 1952).

Conservation of angular momentum and parity requires that radiative transitions to the 0^+ ground state of 0^{16} necessarily must carry off the total spin and parity ($J^\pi \rightarrow 0^+$) from the excited state. Thus the multipolarity of such transitions is uniquely specified as 2^J-pole, being pure electric if the parity changes by $(-1)^J$ and pure magnetic if by $(-1)^{J+1}$. With target and projectile contributing neither intrinsic spin nor parity (both 0^+), the $C^{12} + \alpha$ interaction excites only states in 0^{16} which correspond to the "natural" spin-parity sequence, $J^\pi = 0^+, 1^-, 2^+, 3^-, 4^+$, etc., arising from the relative angular momentum (with associated parity) of the interacting nuclei. As a consequence, the required parity change $(-1)^J$ restricts ground state radiation from $C^{12}(\alpha, \gamma)0^{16}$ to the electric multipole orders E1, E2, E3, E4, etc. (Conservation of angular momentum strictly forbids the $0^+ \rightarrow 0^+$ monopole transition by single photon emission; for example, the 0^+ first excited state of 0^{16} at 6.05 MeV decays by pair emission.) Since each multipole order gives rise to a distinct radiation pattern the spins and parities of 0^{16} states excited by this reaction may be determined uniquely by angular distribution measurements of ground state radiation.

The isotopic spin formalism provides a convenient method for expressing the concept of charge independence of nuclear forces. That is, in addition to space and spin coordinates a nucleon may be described by a vector (isotopic spin) whose two permitted projections ($\pm$) on the z-axis in charge space represent either neutron or proton states. A system of nucleons is then described by a total isotopic spin vector $\vec{T}$ whose projection $T_z = 1/2(N-Z)$ specifies the neutron-proton balance (or neutron excess). For a fixed number of nucleons, conservation of T_z is equivalent to charge conservation. If nuclear forces are assumed entirely charge independent, ie. (n-n) = (n-p) = (p-p), then in expressions for the energy of systems with the same $\vec{T}$ nucleons are equivalent and interchangeable. By its construction, however, the total isotopic spin must also remain unaltered with the interchange of equivalent nucleons (although the projection T_z records changes in charge); thus conservation of isotopic spin expresses charge independence of nuclear forces.

For symmetric members of nuclear multiplets (N' = Z, Z' = N) energy equivalence may be assured by the less restrictive condition of charge symmetry (charge parity). This simpler requirement is that (n-n) = (p-p). Since for these symmetric systems the balance of (n-p) forces is unaltered by the complete interchange of neutrons and protons, the (n-p) force need not be specified.

If the isotopic spin is to be a serviceable description for a system of nucleons, effects attributable to the characteristics distinguishing neutrons and protons (mass, magnetic moment, charge) must be small perturbations on the otherwise charge independent nuclear forces. In particular, electromagnetic inter-

actions obviously are charge dependent and can change the isotopic spin (but not T_z); however, certain restrictions are applicable. The perturbation Hamiltonian, H, for a radiating (or absorbing) nucleon system describes the electromagnetic interaction with Z protons of charge +e, magnetic moment μ_p and N neutrons of charge 0, moment μ_n. This Hamiltonian may be separated into two parts (Radicati 1952; Gell-Mann and Telegdi 1953), the first, H_0, containing a sum of interactions with (Z + N) identical particles of charge +e/2, moment $(\mu_p + \mu_n)/2$, the second, H_1, involving Z particles of charge +e/2, moment $(\mu_p - \mu_n)/2$ and N particles of charge -e/2, moment $(\mu_n - \mu_p)/2$. With this separation the total Hamiltonian $H = H_0 + H_1$ remains unchanged.

The system of identical particles acted upon by H_0 has a fixed isotopic spin which cannot be changed without altering the total number of nucleons present. Therefore $\Delta T = 0$ for electromagnetic transitions induced by H_0. If the proton-neutron mass difference is ignored, this system of uniform charges also does not permit the creation of an electric dipole moment (involving separation of centers of charge and mass); hence, to first order, H_0 does not contribute to electric dipole radiation. While it is apparent that H_1 operating on a system of both positive and negative charges can induce electric dipole transitions, it has been shown (Gell-Mann and Telegdi 1953) that a change of isotopic spin, $\Delta T = \pm 1$, must accompany H_1 whenever $T_z = 0$. Thus for self-conjugate nuclei (N = Z, $T_z = 0$) such as O^{16}, a selection rule which arises from the assumption of charge independence (or charge symmetry) of nuclear forces forbids to first order electric dipole transitions between states of the same isotopic spin. Higher order effects permit the violation of this isotopic spin selection rule; however, inhibition of electric dipole

radiation between states of the same isotopic spin assignment is observed in self-conjugate nuclei (Wilkinson 1960). A more general selection rule, $|\Delta T| \leq 1$ (Radicati 1952), limiting electromagnetic transitions to a single nucleon, is now subject to possible experimental test with the recent identification of nuclear excited states having $T = 2$, $T_z = 0$ (Garvey et al. 1964, 1964a).

As indicated, the electric dipole selection rule is derivable from charge symmetry (Kroll and Foldy 1952) and does not require the more stringent assumption of charge independence. An examination of charge independence is being conducted through the study of nuclear isobaric multiplets (Wilkinson 1964, 1964a). Available evidence favors the charge independent form of nuclear forces when known deviations such as the Coulomb interaction are treated as perturbation effects.

B. Systematics of Radiative Transitions

Some considerable insight into the relative strengths of radiative transitions has been acquired by systematically relating experimental observations to transition rates calculated on the basis of a simple nuclear model (Wilkinson 1953a, 1956, 1960). For this purpose electromagnetic transition probabilities are estimated using an extreme single-particle model in which a single proton moving within a featureless central potential transfers its entire orbital angular momentum L to an emitted photon. Proton radial wave functions for the initial and final configurations are taken to be constant out to a nuclear radius $R = r_0 A^{1/3}$ where they drop to zero. The resulting single-particle radiative transition probabilities are (Weisskopf 1951):

$$\tau^{-1}(EL) = \frac{2(L+1)}{L[(2L+1)!!]^2} \left(\frac{3}{L+3}\right)^2 \left(\frac{e^2}{\hbar c}\right) \left(\frac{\omega R}{c}\right)^{2L} \omega \text{ sec}^{-1}$$

$$\tau^{-1}(ML) = 10(\hbar/McR)^2 \tau^{-1}(EL).$$

Adopting $R = 1.2A^{1/3} \times 10^{-13}$ cm, the electric dipole (E1) and quadrupole (E2) radiative widths, in Weisskopf units, are estimated to be (Wilkinson 1960):

$$\Gamma_{\gamma W}(E1) = 6.8 \times 10^{-2} A^{2/3} E_\gamma^3 \text{ eV}$$

$$\Gamma_{\gamma W}(E2) = 4.9 \times 10^{-8} A^{4/3} E_\gamma^5 \text{ eV}.$$

Numerical coefficients are given for E_γ in MeV. Applied to 0^{16} (A = 16), these equations reduce to:

$$\Gamma_{\gamma W}(E1,\ A = 16) = 0.43\ E_\gamma^3 \text{ eV}$$

$$\Gamma_{\gamma W}(E2,\ A = 16) = 1.98 \times 10^{-6} E_\gamma^5 \text{ eV}.$$

This simple model predicts for 0^{16} that E1 transitions of 10 - 15 MeV should be stronger by a factor of 10^3 over E2 transitions of the same energy. In fact, experiment has shown them to be nearly equal (Figure 10 and Table III) indicating the operation of strong effects not included in the model.

Histograms in Figure 16, taken from Wilkinson (1960), display identified electric dipole (E1) and quadrupole (E2) transitions observed in light nuclei (A < 20) as a function of $|M|^2 = \Gamma_\gamma/\Gamma_{\gamma W}$. The E1 transitions show a distinct concentration about

$|M|^2 = 0.05$; however, dipole transitions inhibited by the isotopic spin selection rule, indicated by shading, are distinctly weaker than average by an order of magnitude or more in $|M|^2$. The E2 events show enhancement over the extreme single-particle estimates, typically to $|M|^2 \approx 5$. This is a contradiction to the Weisskopf model which is expected generally to overestimate transition strengths. For comparison, dashed curves in Figure 16 outline the results of a large number of transitions calculated with an intermediate coupling shell model (Wilkinson 1956, 1960). The detailed model calculations agree quite well with the E1 histogram indicating the favorable nature of a single-particle approach to dipole transitions. Disagreement between E2 events and the shell model calculations suggests the need for some mechanism more powerful than the single-particle concept, such as the collective motion of many charged particles (Bohr and Mottelson 1953), to explain electric quadrupole transitions.

Values of $|M|^2$ for E1 and E2 transitions observed in the present work are also indicated in Figure 16. These do not necessarily correspond to new additions to the appropriate histograms since experimental values for some of these transitions were known to Wilkinson in 1960 (see Table V). The E1 ground state transition from the 13.10 MeV (1^-), T = 1 state is isotopic spin allowed and has a radiative width typical for such transitions. The remaining E1 transitions violate the isotopic spin selection rule and are correspondingly weaker; however, the 12.44 MeV, E1 transition appears to be only slightly inhibited reflecting the strong T = 1 mixing in this state (Hebbard 1960). The 9.59 MeV, E1 transition is remarkable for its great inhibition. The E2 ground

state transitions from 2^+ states at 11.52 and 13.15 MeV show typical quadrupole enhancement. (The position in Figure 16 of the 13.15 MeV, E2 transition corresponds to $\Gamma/\Gamma_\alpha \approx 1$; see page 52.) In contrast, the ground state transition from the 2^+ state at 9.85 MeV is exceptionally weak whereas the E2 transition from the 4^+ state at 10.36 MeV to the 2^+ state at 6.92 MeV ($|M|^2 = 49$) may be the most enhanced in the light nuclei. (The E2 transition corresponding to $|M|^2 = 700$ is assumed by Wilkinson to be spurious.)

The cascade transition of undetermined multipolarity from the 9.85 MeV, 2^+ state to a state at 7 MeV (page 37) cannot yet be included in Figure 16. Possible transitions are:

Initial state		Final state		Multipolarity	$\lvert M\rvert^2$
9.85	2^+	6.92	2^+	E2	4
9.85	2^+	6.92	2^+	M1	3×10^{-3}
9.85	2^+	7.12	1^-	E1	2×10^{-4}

Inspection of Figure 16 confirms that the above values of $|M|^2$ for E2 and E1 (isotopic spin inhibited) transitions are rather typical of $C^{12}(\alpha, \gamma)O^{16}$ while reference to Wilkinson (1960) reveals the M1 transition to be one of uncommon inhibition. Thus none of these possibilities may be excluded on the basis of $|M|^2$ systematics; more than one type of radiation may actually have been observed.

The $C^{12}(\alpha, \gamma)O^{16}$ reaction failed to reveal ground state radiation from the narrow resonances of unknown spin and parity at E_x = 11.1 and 12.02 MeV (Γ < 12 keV, Browne and Michael 1964). The data of Figure 10 place the following approximate limits on ground state radiation from these levels:

Limits on ground state radiation

E_x(MeV)	11.1	12.02
$\omega\Gamma_\gamma$(eV)	$\leq 8 \times 10^{-3}$	$\leq 12 \times 10^{-3}$
$\|M\|^2$(E1)	$\leq 5 \times 10^{-6}$	$\leq 5 \times 10^{-6}$
$\|M\|^2$(E2)	$\leq 5 \times 10^{-3}$	$\leq 5 \times 10^{-3}$

Comparison with Figure 16 indicates that these are exceptionally small values of $|M|^2$ for E1 (isotopic spin inhibited) or E2 transitions; therefore, it is very probable that $J^\pi \neq 1^-$ or 2^+ for either of these states. Although one member of the "doublet" at 11.1 MeV (Browne and Michael 1964) is identified as 3^+ (Kuehner et al. 1959) the other member is expected to have natural spin-parity (Bittner and Moffat 1954); this state is probably 0^+, 3^-, 4^+, or 5^-. The 12.02 state may not be a member of the natural spin-parity sequence. Limits on possible cascade radiation from these states are not definitive because of $C^{13}(\alpha, n\gamma)O^{16}$ background (Figure 8).

C. Nuclear models of 0^{16}

The first T = 1 levels near 13 MeV in 0^{16} form a rather natural demarcation between the region of higher excitation with many states still to be thoroughly explored and the lower energy region of isolated levels which has already undergone extensive study. A recent survey of the 0^{16} spectrum by Browne and Michael (1964) using $N^{14}(He^3, p)0^{16}$ disclosed all of the known resonances below 13 MeV, with the exception of two very broad states ($\Gamma > 1$ MeV), and discovered only one new state from a previously unresolved pair. An appealing implication is that at most a few very broad or unresolved states remain to be discovered below 13 MeV in 0^{16}. This raises a question as to how well nuclear models of 0^{16} (shell, alpha particle and cluster) can predict the spectrum of presently known levels, including spins and parities of unassigned states, and whether undetected levels are predicted.

C1. Shell model

The nearly complete listing of even parity 0^{16} states up to 14.8 MeV in the recent shell model calculations of Borysowicz and Sheline (1964) makes it interesting to note those low-lying states not presently encompassed by shell model calculations. The only known even parity state below 14.8 MeV not included by Borysowicz and Sheline is the 2^+ state at 13.15 MeV (see Figure 2). Conceivably, this could be the second member of another K = 0 rotational band based on the proposed broad 0^+ state near 12.5 MeV (Bittner and Moffat 1954; Hebbard 1960). Shell model calculations of odd parity states resulting from single particle excitations predict the initial quartet of T = 1 states (near 13 MeV) as well as most of the

intermediate T = 0 states (Elliott and Flowers 1957; Gillet and Mau 1964). If the second calculated 3^- state is now associated with the newly found 3^- state at 13.13 MeV (I. Mitchell and Ophel 1964, 1965; see pages 54 and 55), the remaining uncommitted, known negative parity states are the broad resonances at 9.59 MeV, 1^- and 11.63 MeV, 3^-. Thus the following states (below 14 MeV) are not yet predicted by single particle, particle-hole or two particle-two hole calculations:

States not predicted by shell model calculations

E_x(MeV)	J^π	Γ_{CM}(keV)
9.59	1^-	650
11.08	?	<12
11.63	3^-	1200
12.02	?	<12
(12.5)	(0^+)	(Broad)
13.15	2^+	250

Defiance of the 9.59 MeV, 1^- state to single particle calculation has led to speculation that this state represents three particle excitation (Elliott and Flowers 1957; Bloom et al. 1957); the broad 3^- state at 11.63 MeV may share in the same mode of excitation. The comprehensiveness of the even parity calculations by Borysowicz and Sheline makes it tempting to speculate that the unassigned levels at 11.08 and 12.02 MeV also are not even parity states, adding grist to the three particle mill. (As a matter of clerical convenience in model discussions, the 11.096 MeV state is being assumed 3^+

leaving the 11.080 MeV state unassigned; this is in agreement with suggestions by Browne and Michael (1964) but remains unproven.)

C2. Alpha particle model

The early alpha particle model of Dennison (1940) has been able to accommodate increasing knowledge of the 0^{16} level structure with some considerable success (Dennison 1954; Kameny 1956). If an additional slight alteration is made by evenly splitting the energy of the first predicted $2^{\pm}$ doublet between states at 8.88 and 9.85 MeV, rather than fixing the energy of the 2^+ member at 9.85 MeV as was done in the original identification (a) by Dennison (who did not have available the 8.88 MeV, 2^- assignment), the following identification (a') results (for detailed prescriptions see Kameny 1956):

Alpha particle model of 0^{16}, identification (a')

Predicted		Observed		Predicted		Observed	
E_x(MeV)	J^π	E_x(MeV)	J^π	E_x(MeV)	J^π	E_x(MeV)	J^π
(6.05)	0^+	6.05	0^+	10.23	2^+	11.52	2^+
(6.13)	3^-	6.13	3^-	11.62	3^+	11.10	3^+
(7.02)	2^+	6.92	2^+	11.78	1^+	12.02	?
(7.02)	1^-	7.12	1^-	11.78	1^-	12.44	1^-
(9.36)	2^-	8.88	2^-	12.10	0^+	11.26	0^+
(9.36)	2^+	9.85	2^+	12.18	3^-	11.63	3^-
9.44	0^+	11.08	?	12.59	0^+	(12.5)	(0^+)
9.57	3^-			13.07	2^+	13.15	2^+

Alpha particle model of O^{16}, identification (a') cont'd.

Predicted		Observed		Predicted		Observed	
E_x(MeV)	J^π	E_x(MeV)	J^π	E_x(MeV)	J^π	E_x(MeV)	J^π
10.21	1^-	9.59	1^-	13.27	2^-	12.53	2^-
10.22	4^+	10.36	4^+	16.50	0^-	10.95	0^-

Four energy parameters have been fitted to the first six levels (indicated by parentheses). After some pushing and pulling all of the observed T = 0 states below 13.13 MeV have been listed. States of unassigned spin and parity at 11.08 and 12.02 MeV may be included if they are 3^- (or 0^+) and 1^+ respectively (assignments in harmony with the conclusions on page 65). A place is even reserved for the suspected 0^+ state near 12.5 MeV (Bittner and Moffat 1954; Hebbard 1960; see page 42). Aside from these ambiguities, the model predicts only one low-lying level (either 0^+ or 3^-) which has not been observed.

While it has been argued that identification (a) of the alpha particle model is discredited by its failure to put a 0^- state near 10.95 MeV (Bromley et al. 1959), it must be observed that although identification (b) places a 0^- state at 11.5 MeV (Kameny 1956) it also predicts at least six presently unobserved states between 7 and 11 MeV and is strained to include the states at 8.88 MeV (2^-) and 11.10 MeV (3^+). With the level structure of O^{16} up to 13 MeV now (hopefully) nearly determined, the economy of identification (a) appears preferable to the prodigality of (b).

C3. Cluster model

The cluster model predictions for O^{16} by Roth and Wildermuth (1960) contain a number of vacancies which may in part be filled by recent additions to the O^{16} energy level structure. The following list contains all of the experimentally known O^{16} levels below 13 MeV, except the 0^- state at 10.95 MeV, as well as a few others which seem to adapt to this model:

Cluster model of O^{16}

$C^{12} + \alpha$				$C^{12*} + \alpha$				
Predicted	Observed			Predicted	Observed			
	E_x(MeV)	J^π	θ^2_α		E_x(MeV)	J^π	θ^2_α	$\theta^2_{\alpha'}$
$3s, 0^+$	0.00	0^+		$3p, 1^-$				
$3p, 1^-$	7.12	1^-		$3p, 2^-$	8.88	2^-		
$2f, 3^-$	6.13	3^-		$3p, 3^-$	11.08	?	≤ 0.01	
$1h, 5^-$				$2f, 1^-$	12.44	1^-	0.02	3
$4s, 0^+$	6.05	0^+		$4s, 2^+$	9.85	2^+	0.0015	
$3d, 2^+$	6.92	2^+		$3d, 0^+$	(12.5)	(0^+)		
$2g, 4^+$	10.36	4^+	0.26	$3d, 1^+$	12.02	?		
$1i, 6^+$	16.2	6^+	≤ 0.3	$3d, 2^+$	11.52	2^+	0.03	
$4p, 1^-$	9.59	1^-	0.85	$3d, 3^+$	11.10	3^+		
$3f, 3^-$	11.63	3^-	0.73	$3d, 4^+$	13.87	4^+	≤ 0.04	≤ 0.4
$5s, 0^+$	11.26	0^+	0.76	$4p, 1^-$				
				$4p, 2^-$	12.53	2^-		≤ 0.7
				$4p, 3^-$	13.13	3^-	≤ 0.03	≤ 1.5
				$5s, 2^+$	13.15	2^+	≤ 0.06	≤ 2

Included are a few unfulfilled predictions (see Sheline and Wildermuth 1960 for construction) for which energies below 13 MeV might reasonably be anticipated. With the exception of the unobserved 1h, 5^- state, the lowest energy predictions based on $C^{12} + \alpha$ excitation are filled up to some 11 MeV; the next predicted levels 2h, 5^- and 4d, 2^+ very likely lie higher by more than 1 MeV. Excitations based on $C^{12*} + \alpha$ are prolific and identifications somewhat arbitrary. The states of unassigned spin and parity at 11.08 and 12.02 MeV will fit into 3^- (or 0^+) and 1^+ predictions (in agreement with the alpha particle model) but other choices are available. At a sacrifice to compactness, the 1^- state at 12.44 MeV has been moved from the 4p, 1^- identification ($\theta^2_{\alpha'} = 0.06$) given by Roth and Wildermuth to 2f, 1^- in order to increase $\theta^2_{\alpha'}$; this choice may be tested by determining whether alpha particles from $N^{15}(p, \alpha')C^{12*}$ are p or f wave.

The above values of θ^2_α (or $\theta^2_{\alpha'}$) not determined by the work of Bittner and Moffat (1954) were estimated from the relation $\theta^2_\alpha = (\Gamma_\alpha/2P)(3\hbar^2/2\mu a^2)^{-1}$. The scattering radius preferred by Bittner and Moffat, $a = 5.43 \times 10^{-13}$ cm, was used in the expression for the Wigner limit $(3\hbar^2/2\mu a^2)$, where μ is the reduced mass of the alpha particle; penetrabilities P were obtained from CØØL, a Coulomb wave function subroutine written for the IBM 7094 computer by T. A. Tombrello. In cases where the partial widths Γ_α (or $\Gamma_{\alpha'}$) are unknown, values for θ^2_α (or $\theta^2_{\alpha'}$) are based on total widths and the resulting uncertainty indicated by inequalities.

In summary, the shell model includes most of the low-lying O^{16} states but as yet offers no predictions of new levels. The alpha model identification (b) and the cluster model of $C^{12*} + \alpha$ excitations

supply abundant predictions which seem unlikely to be experimentally confirmed; however, the C^{12} + α excitations of the cluster model lack only a 5^- identification to be complete to about 13 MeV excitation. The resilient identification (a) of the alpha particle model offers a limited choice of spins and parities (0^+, 1^-, 3^-) for the unassigned states at 11.08 and 12.02 MeV; if two of these are confirmed, the model predicts only the one remaining unobserved level and is otherwise remarkably complete.

D. Future $C^{12}(\alpha, \gamma)O^{16}$ Experiments

When the present experiment was begun, it was hoped that measurements of $C^{12}(\alpha, \gamma)O^{16}$ could be obtained at sufficiently low alpha particle energies to allow confident extrapolation to energies of astrophysical significance (see pages 4-6). Although measurements of the resonances at E_α = 3.2 and 3.58 MeV (E_x = 9.59 and 9.85 MeV) were improved (Table V), this experiment lacked the sensitivity necessary to detect a contribution from the 7.12 MeV bound state which is expected to be dominant at stellar energies of a few hundred keV (see Burbidge et al. 1957; Fowler and Hoyle 1964). Estimates of interference effects between the 1^- states at E_x = 7.12 and 9.59 MeV in O^{16} by Tombrello (private communication) indicate that if a large reduced width (θ^2_α = 1) is assumed for the lower state, constructive interference enhances the cross section (relative to an isolated 9.59 MeV resonance) by a factor of 2 at $E_\alpha \approx 2.25$ MeV, giving $\sigma_c(\alpha, \gamma) \approx 1.2 \times 10^{-3}$ μb (corresponding to 1/30 of the peak cross section at E_α = 3.2 MeV); at the same energy destructive interference depresses the cross section by a factor 2/3 to $\sigma_d(\alpha, \gamma) \approx 4 \times 10^{-4}$ μb. These effects

become larger with decreasing alpha particle energy but all quantitative comparisons depend ultimately on parameters chosen for the two-level calculations. A future $C^{12}(\alpha, \gamma)O^{16}$ experiment which can measure a cross section of about 10^{-3} μb to within better than a factor of 2 may successfully detect the contribution from the 7.12 MeV state if θ_α^2 is large and constructive interference occurs with the 9.59 MeV state. This appears experimentally feasible although an order of magnitude improvement in resolution over the present experiment is required. To detect destructive interference, comparable resolution will be required in measuring a cross section nearer 10^{-4} μb. Should θ_α^2 be much smaller than unity, interference effects are reduced and the experiment appears to be prohibitively difficult using present techniques.

A note of warning! Black and Treacy (1964) have observed spurious 9 MeV gamma radiation from the bombardment of C^{12} by a beam of 3.3 MeV alpha particles. Such radiation may easily be confused with the yield from $C^{12}(\alpha, \gamma)O^{16}$. The explanation given by Black and Treacy is that the target was also being bombarded by deuterons having half the alpha particle energy. Through the reaction $C^{12}(d, \gamma)N^{14*}$, 1.65 MeV deuteron bombardment of C^{12} produces 9.4 MeV cascade radiation to the 2.31 MeV first excited state in N^{14}. The deuterons presumably originate as molecular D_2^+ ions from deuterium contamination within the accelerator's ion source; once produced, D_2^+ ions experience nearly the same acceleration trajectories as $(He^4)^+$ ions. This problem was not encountered in the present experiment since deuterium gas has never been used in the helium ion source of the tandem accelerator; moreover, an absolute upper limit can be placed on the actual

deuteron component by examining radiation spectra for low energy gamma rays from $C^{12}(d, p\gamma)C^{13}$. If all the counts corresponding to a gamma ray energy of 3.1 MeV in Figure 11a are attributed to $C^{12}(d, p\gamma)C^{13}$, then from the known cross section at $E_d = E_\alpha/2 = 1.65$ MeV (Bonner et al. 1949; Kashy et al. 1960), the maximum D_2^+/He^+ contamination in the beam used was less than 10^{-4}, an amount too small to cause appreciable $C^{12}(d, \gamma)N^{14*}$ background (see Allan and Sarma 1955). Even this represents a gross overestimate of the actual contamination present; the nominal D_2/He ratio for naturally occurring helium used in the ion source is about 10^{-8}. Tuning of the tandem accelerator for optimum He^+ output probably further reduces this ratio in the emerging beam. However, ion sources in single stage accelerators are commonly used for all types of gas including deuterium; Black and Treacy warn that the alpha particle beams from these machines must be tested for deuterium contamination before sensitive experiments are performed.

Other extensions of the present experiment are implied earlier in the text. Cascade radiation from the 9.85 MeV state (page 37) was observed by accident and not thoroughly studied. A more complete experiment, probably requiring coincidence measurements, would determine the intermediate state and radiation multipolarity of this cascade. The unassigned states at 11.1 and 12.02 MeV apparently yield no ground state radiation from $C^{12}(\alpha, \gamma)O^{16}$ (see page 65) but a complete investigation should reveal cascade radiation if either state is of natural spin-parity. If a state at 11.1 MeV is observed in a precise $C^{12} + \alpha$ experiment, the energy of the 3^+ state (11.080 or 11.096 MeV, Browne and Michael 1964) will also have been determined by elimination. At

energies above E_α = 8 MeV (E_x > 13 MeV) the $C^{12}(\alpha, \gamma)O^{16}$ reaction should be useful both in confirming spin-parity assignments (see page 58) and in studying radiative transitions between even parity states of the same and different rotational bands (see Figure 2 and Borysowicz and Sheline 1964).

REFERENCES

Ajzenberg-Selove, F. and Lauritsen, T. 1959, Nuclear Physics 11, 1.

Allan, H. R. and Sarma, N. 1955, Proc. Phys. Soc. 68A, 535.

Barker, F. C. 1965, private communication.

Bashkin, S. and Carlson, R. R. 1957, Phys. Rev. 106, 261.

Bashkin, S., Carlson, R. R. and Douglas, R. A. 1959, Phys. Rev. 114, 1543.

Bell, P. R. 1955, Beta- and Gamma-Ray Spectroscopy, ed. by Siegbahn, North-Holland Publishing, Amsterdam, Ch V.

Bishop, G. R., Betourne, C. and Isabelle, D. B. 1964, Nuclear Physics 53, 366.

Bittner, J. W. and Moffat, R. D. 1954, Phys. Rev. 96, 374.

Black, J. L. and Treacy, P. B. 1964, private communication.

Blatt, J. M. and Weisskopf, V. F. 1952, Theoretical Nuclear Physics, Wiley and Sons, New York.

Bloom, S. D., Toppel, B. J. and Wilkinson, D. H. 1957, Phil. Mag. 2, 57.

Bohr, A. and Mottelson, B. R. 1953, Math.-Fys. Medd. 27(#16).

Bonner, T. W., Evans, J. E., Harris, J. C. and Phillips, G. C. 1949, Phys. Rev. 75, 1401.

Bonner, T. W., Kraus, A. A., Marion, J. B. and Schiffer, J. P. 1956, Phys. Rev. 102, 1348.

Borysowicz, J. and Sheline, R. K. 1964, Physics Letters 12, 219.

Brink, D. M. and Nash, G. F. 1963, Nuclear Physics 40, 608.

Bromley, D. A., Gove, H. E., Kuehner, J. A., Litherland, A. E. and Almqvist, E. 1959, Phys. Rev. 114, 759.

Bromley, D. A., Ferguson, A. J., Gove, H. E., Kuehner, J. H., Litherland, A. E., Almqvist, E. and Batchelor, R. 1959a, Can. J. Phys. 37, 1514.

Browne, C. P. and Michael, I. 1964, Phys. Rev. 134B, 133.

Burbidge, E. M., Burbidge, G. R., Fowler, W. A. and Hoyle, F. 1957, Revs. Mod. Phys. 29, 547.

Carter, E. B., Mitchell, G. E. and Davis, R. H. 1964, Phys. Rev. 133B, 1421.

Cartledge, W. A., Marchand, G. and Reevers, H. 1963, private communication.

Chiu, H.-Y. and Stabler, R. 1961, Phys. Rev. 122, 1317.

Cook, C. W., Fowler, W. A., Lauritsen, C. C. and Lauritsen, T. 1957, Phys. Rev. 107, 508.

Cox, J. P. and Salpeter, E. E. 1964, Ap. J. 140, 485.

Davisson, C. M. 1955, Beta- and Gamma-Ray Spectroscopy, ed. by Siegbahn, North-Holland Publishing, Amsterdam, Ch II.

Deinzer, W. and Salpeter, E. E. 1964, Ap. J. 140, 499.

Dennison, D. M. 1940, Phys. Rev. 57, 454.
1954, Phys. Rev. 96, 378.

Elliott, J. P. and Flowers, B. H. 1955, Proc. Roy. Soc. A229, 536.
1957, Proc. Roy. Soc. A242, 57.

Everling, F., Koenig, L. A., Mattauch, J. H. E. and Wapstra, A. H. 1961, Nuclear Data Tables, Part 1, National Academy of Sciences - National Research Council, Washington, D. C.

Ferguson, A. J. and McCallum, G. J. 1961, Bull. Am. Phys. Soc. 6, 235.

Feynman, R. P. and Gell-Mann, M. 1958, Phys. Rev. 109, 193.

Fowler, W. A. and Lauritsen, C. C. 1940, Phys. Rev. 58, 192.

Fowler, W. A., Lauritsen, T. and Lauritsen, C. C. 1948, Revs. Mod. Phys. 20, 236.

Fowler, W. A. and Hoyle, F. 1964, Ap. J. Supp. 91, 201.

Gallmann, A. 1964, Nuc. Instr. and Meth. 28, 33.

Garvey, G. T., Cerny, J. and Pehl, R. H. 1964, Phys. Rev. Ltrs. 12, 726. 1964a, Phys. Rev. Ltrs. 13, 548.

Gell-Mann, M. and Telegdi, V. L. 1953, Phys. Rev. 91, 169.

Gillet, V. and Mau, N. V. 1964, Nuclear Physics 54, 321.

Gorodetzky, S., Mennrath, P., Chevallier, P., Scheibling, F. and Sutter, G. 1962, Physics Letters 1, 14.

Gorodetzky, S., Mennrath, P., Benenson, W., Chevallier, P. and Scheibling, F. 1963, J. de Physique 24, 887.

Gorodetzky, S., Bennenson, W., Chevallier, P., Disdier, D. and Scheibling, F. 1963a, Physics Letters 6, 269.

Gove, H. E. 1961, Nuc. Instr. and Meth. 11, 63.

Grodstein, G. W. 1957, NBS Circular 583.

Hagedorn, F. B. 1957, Phys. Rev. 108, 735.
1957a, Ph. D. Thesis, California Institute of Technology.

Heath, R. L. 1957, AEC Research and Development Report, IDO-16408.
1962, IRE Trans. on Nuclear Science NS-9, 294.

Hebbard, D. F. 1960, Nuclear Physics 15, 289.
1965, private communication.

Hill, R. W. 1953, Phys. Rev. 90, 845.

Honsaker, J. L. 1965, Ph. D. Thesis, California Institute of Technology.

Hornyak, W. F. and Sherr, R. 1955, Phys. Rev. 100, 1409.

Jones, C. M., Phillips, G. C., Harris, R. W. and Beckner, E. H. 1962, Nuclear Physics 37, 1.

Kameny, S. L. 1956, Phys. Rev. 103, 358.

Kashy, E., Perry, R. R. and Risser, J. R. 1960, Phys. Rev. 117, 1289.

Kavanagh, R. W. 1956, Ph. D. Thesis, California Institute of Technology.

Kavanagh, R. W. and Goosman, D. R. 1964, Physics Letters 12, 229.

Kraus, A. A. 1954, Phys. Rev. 94, 975.

Kroll, N. M. and Foldy, L. L. 1952, Phys. Rev. 88, 1177.

Kuehner, J. A., Litherland, A. E., Almqvist, E., Bromley, D. A. and Gove, H. E. 1959, Phys. Rev. 114, 775.

Larson, J. D. and Spear, R. H. 1961, Bull. Am. Phys. Soc. 6, 505.
1964, Nuclear Physics 54, 497.

Lauritsen, T. and Ajzenberg-Selove, F. 1962, Nuclear Data Sheets, National Academy of Sciences - National Research Council, Washington, D. C.

Lazar, N. H., Davis, R. C. and Bell, P. R. 1956, Nucleonics 14(#4), 52.

Lazar, N. H. 1958, IRE Trans. on Nuclear Science NS-5, 138.

Levine, M. 1963, Ph. D. Thesis, California Institute of Technology.

Meads, R. E. and McIldowie, J. E. G. 1960, Proc. Phys. Soc. 75A, 257.

Miller, W. F. and Snow, W. J. 1960, Rev. Sci. Instr. 31, 39.

Mitchell, G. E., Carter, E. B. and Davis, R. H. 1961, Bull. Am. Phys. Soc. 6, 227. 1964, Phys. Rev. 133B, 1434.

Mitchell, I. V. and Ophel, T. R. 1964, Nuclear Physics 58, 529.
1965, ANU/P-330, to be published.

Parker, P. D. M. 1963, Ph. D. Thesis, California Institute of Technology.

Pearson, J. D. 1963, Ph. D. Thesis, California Institute of Technology.

Pearson, J. D. and Spear, R. H. 1964, Nuclear Physics 54, 434.

Radicati, L. A. 1952, Phys. Rev. 87, 521.

Reeves, H. and Salpeter, E. E. 1959, Phys. Rev. 116, 1505.

Reibel, K. and Mann, A. K. 1960, Phys. Rev. 118, 701.

Rose, M. E. 1953, Phys. Rev. 91, 610.

Rose, P. H. 1961, Nuc. Instr. and Meth. 11, 49.

Rose, P. H., Wittkower, A. B., Bastide, R. P. and Gale, A. J. 1961, Rev. of Sci. Instr. 32, 568.

Roth, B. and Wildermuth, K. 1960, Nuclear Physics 20, 10.

Salpeter, E. E. 1957, Phys. Rev. 107, 516.

Schardt, A. W. 1951, Ph. D. Thesis, California Institute of Technology.

Schardt, A. W., Fowler, W. A. and Lauritsen, C. C. 1952, Phys. Rev. 86, 527.

Seeger, P. A. and Kavanagh, R. W. 1963, Nuclear Physics 46, 577.

Shafroth, S. M., Strait, E. N. and Carpenter, R. T. 1958, Nuc. Instr. and Meth. 3, 298.

Sharp, W. T., Kennedy, J. M., Sears, B. J. and Hoyle, M. G. 1959, CRT-556, Atomic Energy of Canada, Ltd.

Sheline, R. K. and Wildermuth, K. 1960, Nuclear Physics 21, 196.

Spear, R. H., Larson, J. D. and Pearson, J. D. 1963, Nuclear Physics 41, 353.

Squires, G. L., Bockelman, C. K. and Buechner, W. W. 1956, Phys. Rev. 104, 413.

Swann, C. P. and Metzger, F. R. 1957, Phys. Rev. 108, 982.

Tanner, N. W. and Mitchell, I. V. 1962, private communication to R. H. Spear.

Thompson, L. C. 1964, Nuc. Instr. and Meth. 25, 333.

Tombrello, T. A. 1964, private communication.

Van de Graaff, R. J. 1960, Nuc. Instr. and Meth. 8, 195.

Walton, R. B., Clement, J. D. and Boreli, F. 1957, Phys. Rev. 107, 1065.

Weisskopf, V. F. 1951, Phys. Rev. 83, 1073.

Whaling, W. 1958, Handbuch der Physik 34, 193; also Dermirlioglu, D. and Whaling, W., private communication.

Wilkinson, D. H. 1953, Phys. Rev. 90, 721.
1953a, Phil. Mag. 44, 450.
1956, Phil. Mag. 1, 127.
1956a, Phil. Mag. 1, 379.
1960, Nuclear Spectroscopy, Part B, ed. by F. Ajzenberg-Selove, Academic Press, New York, Ch V. F.
1964, Physics Letters 11, 243.
1964a, Phys. Rev. Letters 13, 571.

Zerby, C. D. and Moran, H. S. 1961, Nuc. Instr. and Meth. 14, 115.

TABLE I

Legendre Polynomial Coefficients for Experimental Angular Distributions of Ground State Radiation from $C^{12}(\alpha, \gamma)O^{16}$

Coefficients in this table derive from Legendre polynomial fits by least squares analysis of angular distribution data shown in Figure 14. Corrections for anisotropic absorption in the target backing and finite solid angle subtended by the 10.2 cm x 10.2 cm NaI(T1) detector (page 15) have been made. Errors listed with these coefficients are computed from counting statistics only. Listed in the second column is the average differential cross section in microbarns per steradian; the total measured cross section at a given energy is $4\pi a_0$. For additional details see pages 44, 45 and 46.

E_α(MeV)	a_0(μb/sr)	a_1/a_0	a_2/a_0	a_3/a_0	a_4/a_0
7.06	2.8 ± 0.3	0.02 ± 0.04	-1.04 ± 0.07	0.03 ± 0.12	0.01 ± 0.12
7.42	0.3 ± 0.1	-0.04 ± 0.24	-0.58 ± 0.37	-0.16 ± 0.59	0.15 ± 0.62
7.88	2.5 ± 0.3	0.47 ± 0.05	-0.88 ± 0.07	-0.36 ± 0.12	-0.30 ± 0.13
8.00	1.1 ± 0.1	0.28 ± 0.09	-0.70 ± 0.13	-0.37 ± 0.22	-0.12 ± 0.23

TABLE II

Measured Resonance Energies and Widths of O^{16} Levels Using the $C^{12}(\alpha, \gamma)O^{16}$ Reaction

Entries for this table are collected from throughout Part III. Errors in excitation energy are based on the assumed $\pm$ 0.3% absolute energy determination (pages 7 and 8) plus a smaller contribution from uncertainties in locating resonance positions; other effects are insignificant. Errors in total width measurements depend on energy stability rather than absolute precision; this was assumed to be about $\pm$ 0.1% for a continuously conducted excitation sweep over a limited range of energies. Only modest corrections for target thickness were required since the target was relatively thin compared to most of the resonance widths. Total widths listed in this table were used in radiative width determinations unless otherwise indicated in the text. For additional details see pages 55 and 56.

Resonance Energy E_α (MeV)	Excitation Energy E_x (MeV)	Total Width Γ_{CM} (keV)
3.2	9.6	
3.585 $\pm$ 0.013	9.851 $\pm$ 0.010	
4.260 $\pm$ 0.015	10.357 $\pm$ 0.011	27 $\pm$ 4
5.809 $\pm$ 0.018	11.519 $\pm$ 0.014	73 $\pm$ 5
7.05 $\pm$ 0.02	12.45 $\pm$ 0.02	100 $\pm$ 10
7.88 $\pm$ 0.03	13.07 $\pm$ 0.02	135 $\pm$ 20
8.13 $\pm$ 0.03	13.26 $\pm$ 0.02	26 $\pm$ 10

TABLE III

Radiative Widths for Transitions Observed in $C^{12}(\alpha, \gamma)O^{16}$

Individual entries in this table are discussed in Part III. Spins and parities (in parentheses) are from other workers (see Ajzenberg-Selove and Lauritsen 1959). The quantity $|M|^2 = \Gamma_\gamma/\Gamma_{\gamma W}$ represents the ratio of the measured radiative width to that estimated from an extreme single-particle model assuming a nuclear radius $R = 1.2\ A^{1/3} \times 10^{-13}$ cm (pages 61 and 62). Final values for the radiative widths of the states at 13.10 and 13.15 MeV await accurate determination of parameters not measured in the present experiment; pages 51 and 52 of the text should be consulted for a discussion of these uncertainties. For additional details see page 56.

Initial State E_x(MeV)	Final State E(MeV)	Measured Radiative Width Γ_γ(eV)	Multi-polarity	$\lvert M\rvert^2$
9.59 (1^-)	0 (0^+)	0.022 ± 0.005	E1	5.8×10^{-5}
9.85 (2^+)	0 (0^+)	0.0059 ± 0.0006	E2	0.032
9.85 (2^+)	7	0.0012 ± 0.0004		
10.36 (4^+)	6.92 (2^+)	0.046 ± 0.006	E2	49
11.52 (2^+)	0 (0^+)	0.66 ± 0.09	E2	1.6
12.44 (1^-)	0 (0^+)	7 ± 1	E1	0.008
13.10 (1^-)	0 (0^+)	$(9 \pm 1.5)(\Gamma/\Gamma_\alpha)$	E1	$0.009(\Gamma/\Gamma_\alpha)$
13.15 (2^+)	0 (0^+)	$(0.6 \pm 0.2)(\Gamma/\Gamma_\alpha)$	E2	$0.8(\Gamma/\Gamma_\alpha)$

TABLE IV

Sources of Error in Radiative Width Calculations

Listed here are individual sources for the errors quoted in Table III. Transitions from O^{16} states are designated as ground state (g. s.) or cascade (cas.). Calculated, measured or estimated standard deviations of various quantities which contribute significantly to the error in the radiative width measurements are included. Values listed under angular measurements represent the experimental standard deviations of several measurements; individual contributions from statistics, geometry and calculated angular corrections are tabulated for measurements made at one angle only. Each column is totaled by taking the square root of the sum of the squares of separate entries. For additional details see pages 24 and 25.

Resonance energy (MeV) Transition	9.59 g. s.	9.85 g. s.	9.85 cas.	10.36 cas.	11.52 g. s.	12.44 g. s.	13.10 g. s.	13.15 g. s.
Net detection efficiency	10%	10%	10%	10%	10%	10%	10%	
Current integration	1	1	1	1	1	1	1	
Background corrections	10	3	12	3	2	2	2	
Angular measurements	-	4.6	-	3.0	4.5	2.1	-	see page 52
Statistics	3	-	30	-	-	-	1	
Geometry	9	-	-	-	-	-	5	
Angular corrections	5	-	5	-	-	-	5	
Target thickness	15	-	-	8	8	8	8	
Total	23%	11%	34%	14%	14%	14%	15%	30%

TABLE V

Comparison of Radiative Width Measurements

Radiative widths of O^{16} levels measured in the present experiment are compared with results obtained by other workers. References indicated are: (a) Bloom et al. (1957), (b) Black and Treacy (1964), (c) Meads and McIldowie (1960), (d) Gorodetzky et al. (1963), (e) Bishop et al. (1964), (f) Hebbard (1960), (g) Schardt et al. (1952) (see page 51), (h) I. Mitchell and Ophel (1964). For additional details see pages 56 and 57.

Initial State E_x(MeV)	Final State E(MeV)	This Work Γ_γ(eV)	Other Results Γ_γ(eV)	Ref.	Γ_γ(eV)	Ref.
9.59 (1^-)	0 (0^+)	0.022 ± 0.005	$0.006^{+0.006}_{-0.003}$	(a);	$0.008^{+0.016}_{-0.008}$	(b)
9.85 (2^+)	0 (0^+)	0.0059 ± 0.0006	0.02 ± 0.01	(c)		
9.85 (2^+)	7	0.0012 ± 0.0004				
10.36 (4^+)	6.92 (2^+)	0.046 ± 0.006	0.040 ± 0.008	(d)		
10.36 (4^+)	6.13 (3^-)	---	≤ 0.001	(d)		
11.52 (2^+)	0 (0^+)	0.66 ± 0.09	0.9 ± 0.2	(c);	0.86	(e)
12.44 (1^-)	0 (0^+)	7 ± 1	8	(f)		
13.10 (1^-)	0 (0^+)	$(9 \pm 1.5)(\Gamma/\Gamma_\alpha)$	$44(\Gamma/\Gamma_p)$	(g)		
13.10 (1^-)	6.05 (0^+)	---	0.7 ± 0.2	(d)		
13.15 (2^+)	0 (0^+)	$(0.6 \pm 0.2)(\Gamma/\Gamma_\alpha)$	0.6	(h)		

FIGURE 1: Energy Level Diagram of 0^{16}

The central structure in this figure shows excitation energies, spins and parities of excited states in 0^{16}. On each side are indicated schematically numerous nuclear reactions which may lead to these states. The excitation function for $C^{12}(\alpha, \gamma)0^{16}$ displayed to the left of the main diagram comes principally from early data using natural carbon targets (Larson and Spear 1961); this early data, including substantial background presumed to arise from $C^{13} + \alpha$, is displayed later in Figure 9.

This diagram was taken from the compilation of Lauritsen and Ajzenberg-Selove (1962); the notation is standard. Except for direct quotations of experimental results and ambiguous situations involving new states, energies listed on this diagram (in MeV) are used in the text. For additional details see page 1.

FIGURE 1

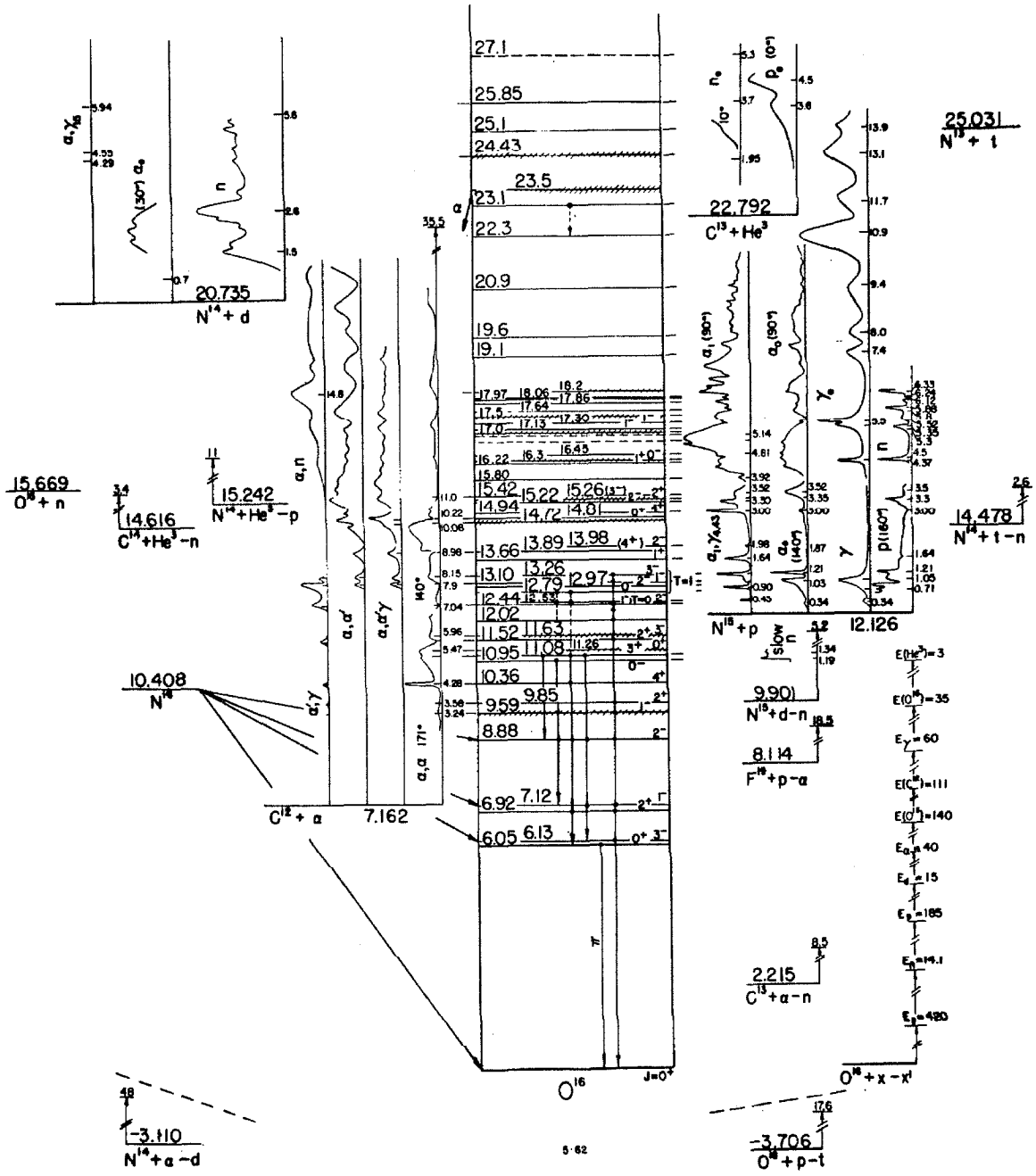
27.1
25.85
25.1
24.43
23.5
23.1
22.3
20.9
19.6
19.1
20.735
N14 + d
22.792
C13 + He3
25.031
N13 + t
15.669
O16 + n
14.616
C14 + He3 - n
15.242
N14 + He3 - p
14.478
N14 + t - n
10.408
N16
C12 + α
7.162
O16
J=0+
N16 + p
12.126
9.901
N15 + d - n
8.114
F18 + p - α
2.215
C13 + α - n
O16 + x - x'
-3.110
N14 + α - d
-3.706
O16 + p - t

FIGURE 2: Radiative Transitions in O^{16}

Figure 2a displays (by vertical arrows) radiative transitions observed in the present experiment using the reaction $C^{12}(\alpha, \gamma)O^{16}$. This energy level diagram for O^{16} is similar to that in Figure 1, but limited to states of particular interest in this experiment. The 2^+ state at 13.15 MeV (pages 47 and 48) is not shown in Figure 1. For additional details see pages 55 and 56.

Figure 2b displays some of the rotational band-like structure of even parity O^{16} states proposed by Borysowicz and Sheline (1964). All known even parity states to 13.15 MeV are included. Designated radiative transitions from the 9.85, 10.36 and 11.52 MeV states were observed in the present experiment. The lifetime of the 6.92 MeV state has been determined by Swann and Metzger (1957); branching ratios for E2 decay of the 6.92 MeV state were recently measured by Gorodetzky et al. (1963). Appropriate values of $|M|^2$ for all these measurements are indicated. Gorodetzky et al. obtain an independent value of Γ_γ corresponding to $|M|^2 = 42$ for the 10.36 to 6.92 MeV transition. (Values of $|M|^2 = \Gamma_\gamma/\Gamma_{\gamma W}$ quoted here are based on a nuclear radius $R = 1.2\ A^{1/3} \times 10^{-13}$ cm, as discussed on pages 61 and 62; Gorodetzky et al. used the radius $R = 1.38\ A^{1/3} \times 10^{-13}$ cm in defining $\Gamma_{\gamma W}$ to obtain somewhat different numerical ratios.) A feature of interest in this figure is the strong enhancement ($|M|^2 \gg 1$) of the E2 transitions observed within the (42), K = 0 band based on the 6.05 MeV state. Further study of radiative transitions within and between these bands appears desirable. For additional details see pages 39 and 66.

FIGURE 2

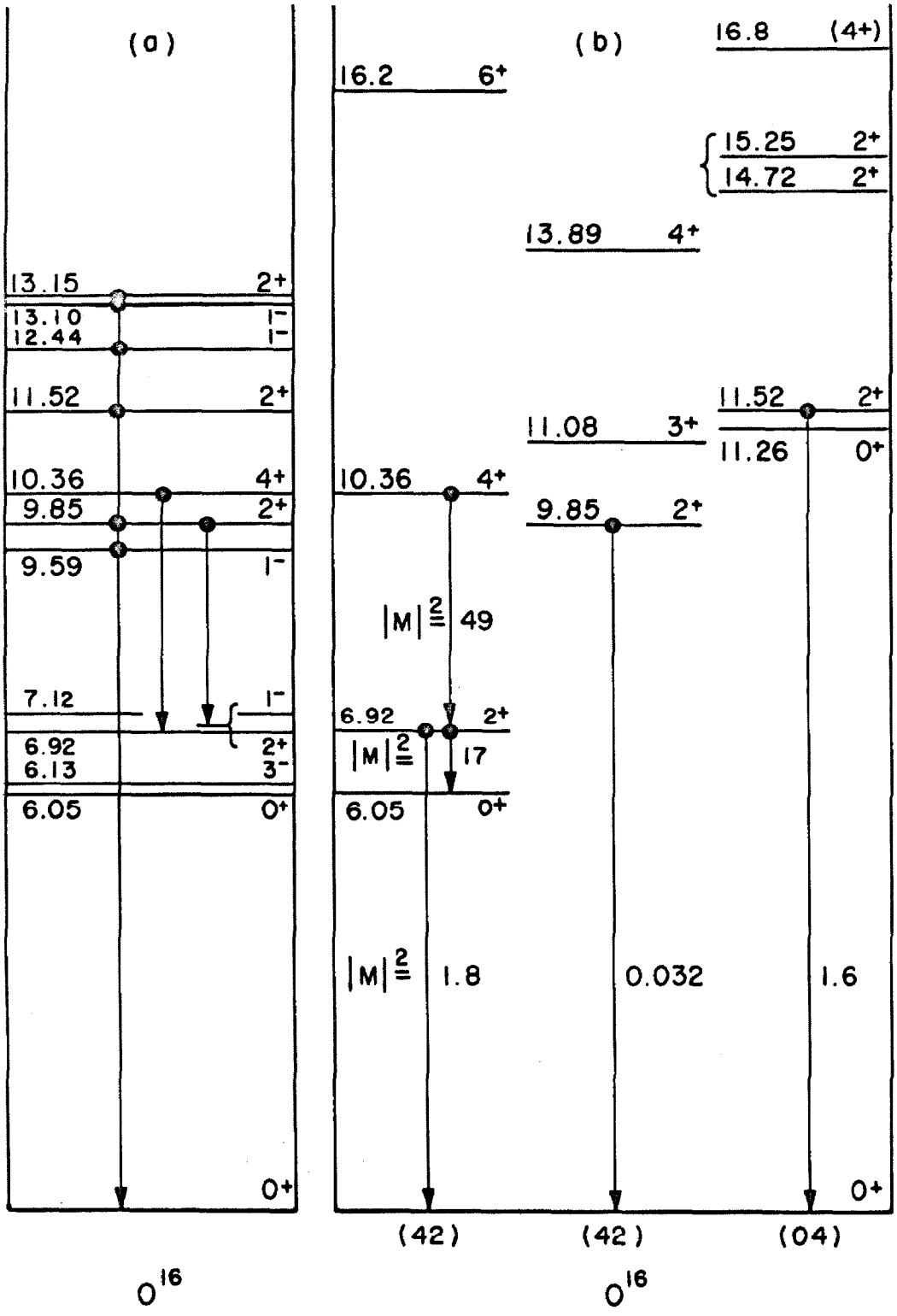
(a)
13.15 2+
13.10 1−
12.44 1−
11.52 2+
10.36 4+
9.85 2+
9.59 1−
7.12 1−
6.92 2+
6.13 3−
6.05 0+
0+
O16
16.2 6+
10.36 4+
|M|² ≡ 49
6.92 2+
|M|² ≡ 17
6.05 0+
|M|² ≡ 1.8
(42)
(b)
16.8 (4+)
15.25 2+
14.72 2+
13.89 4+
11.08 3+
9.85 2+
11.52 2+
11.26 0+
0.032
1.6
(42)
(04)
O16

FIGURE 3: Target Chamber and Auxiliary Pumping

The target chamber used in this experiment was designed to minimize accumulation of natural carbon on the target surface. Communication with the main vacuum system was through a restricted beam transmission tube immersed in liquid nitrogen. Auxiliary pumping of the target chamber was provided by a 9 ℓ/s ion pump; pressures of 2×10^{-8} torr were achieved. This drawing of the target system shows a vertical section taken in the plane of the beam; numbered items are: 1) main vacuum system of tandem accelerator, 2) beam axis, 3) stainless steel in-line cold trap of welded construction, 4) beam transmission tube, 5) liquid nitrogen reservoir, 6) "clean" vacuum side of cold trap, 7) 9 ℓ/s ion pump, 8) pump magnet, 9) concentric magnetic shields 10) glass target chamber, 11) Viton O-rings, 12) glass to metal seal, 13) quartz beam viewer, 14) electron suppressor, 15) target. For additional details see Spear et al. (1963), Pearson (1963) and pages 9 and 10.

FIGURE 3

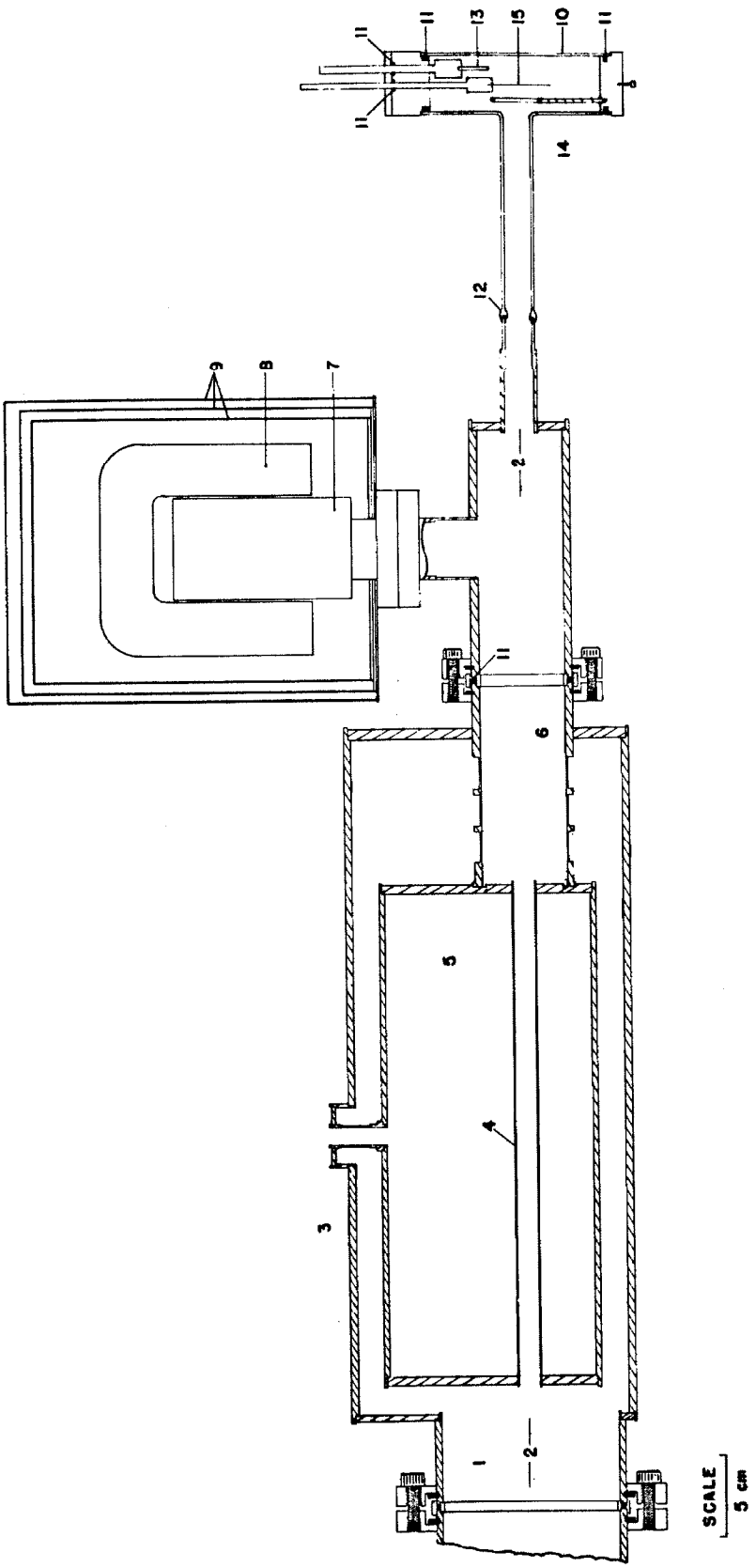

FIGURE 4: Revised Cold Trap

In this design the in-line liquid nitrogen reservoir is attached to a single bulkhead which terminates the conventional vacuum system. This allows the reservoir to be removed axially from its surrounding enclosure for inspection and cleaning. The reservoir and bulkhead assembly are of all welded stainless steel construction. Numbered items in the drawing are: 1) main vacuum system of tandem accelerator, 2) beam axis, 3) support leg on teflon pad, 4) beam transmission tube, 5) liquid nitrogen reservoir, 6) 15-cm standard beam tube, 7) neoprene 0-ring seal, 8) liquid nitrogen inlet, 9) bulkhead, 10) "clean" vacuum side of cold trap, 11) liquid nitrogen overflow vent. For additional details see page 10.

FIGURE 4

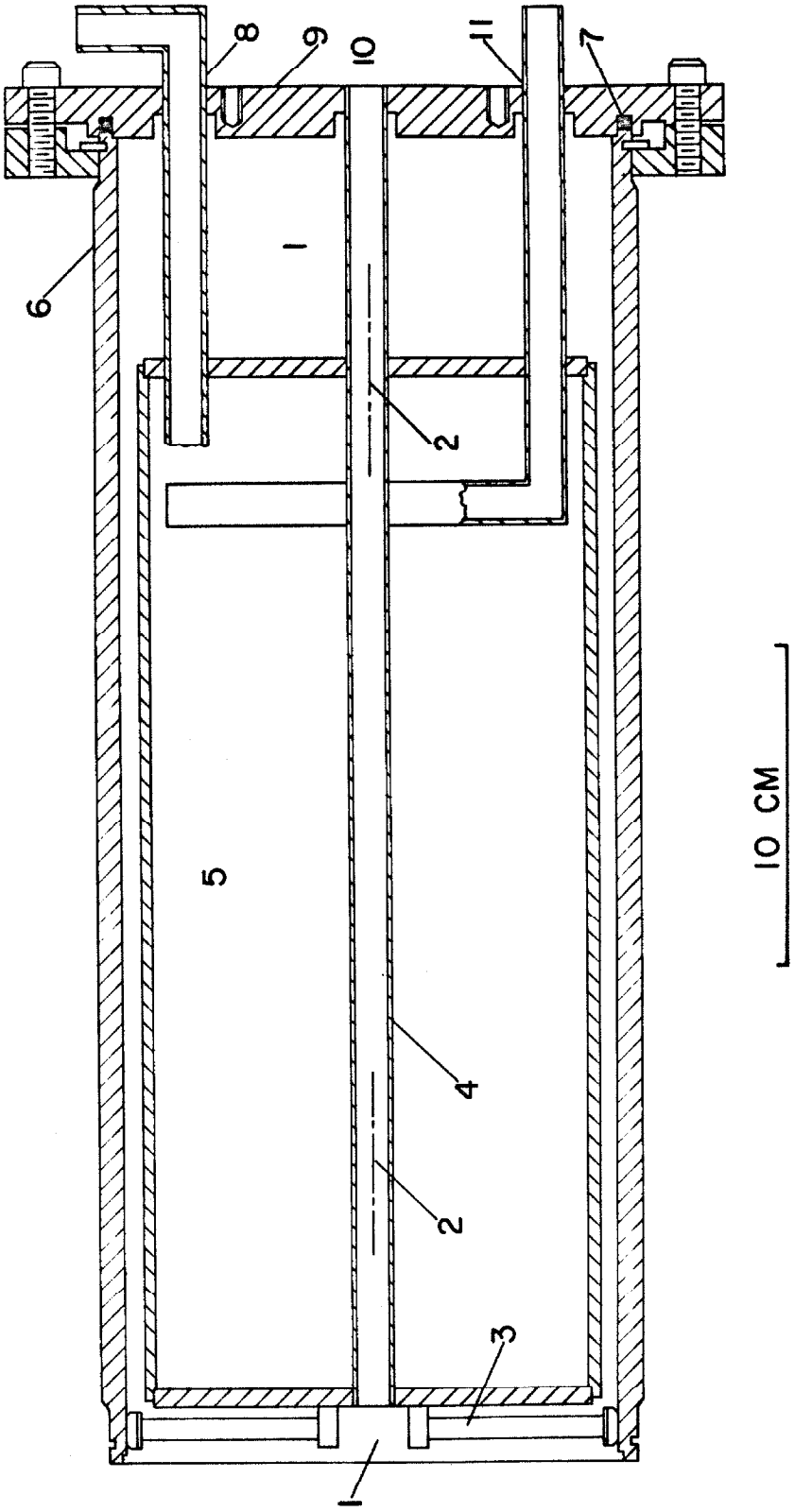

FIGURE 5: Detector Geometry

This drawing shows a horizontal section of the target chamber and 10.2 cm x 10.2 cm NaI(T1) crystal for two geometrical configurations used in this experiment. The arrangement at 0^{o} (with respect to the beam axis) includes the 30.5 cm diameter lead shield which was employed during most of the experiment. Angular measurements were made in the plane of the drawing by rotating the crystal and surrounding shield about the center (vertical axis) of the target chamber. The alpha particle beam intersected this same rotational axis. For measurements at angles greater than 90^{o} the lead shield was removed allowing the unencumbered detector to be placed closer to the target. This drawing shows the unshielded crystal at 135^{o}, the most extreme backward angle at which measurements were made. For each detector geometry illustrated the cylindrical symmetry axis of the NaI(T1) crystal lies in the plane of the drawing and intersects the center of the target. For additional details see pages 12, 13 and 43.

FIGURE 5

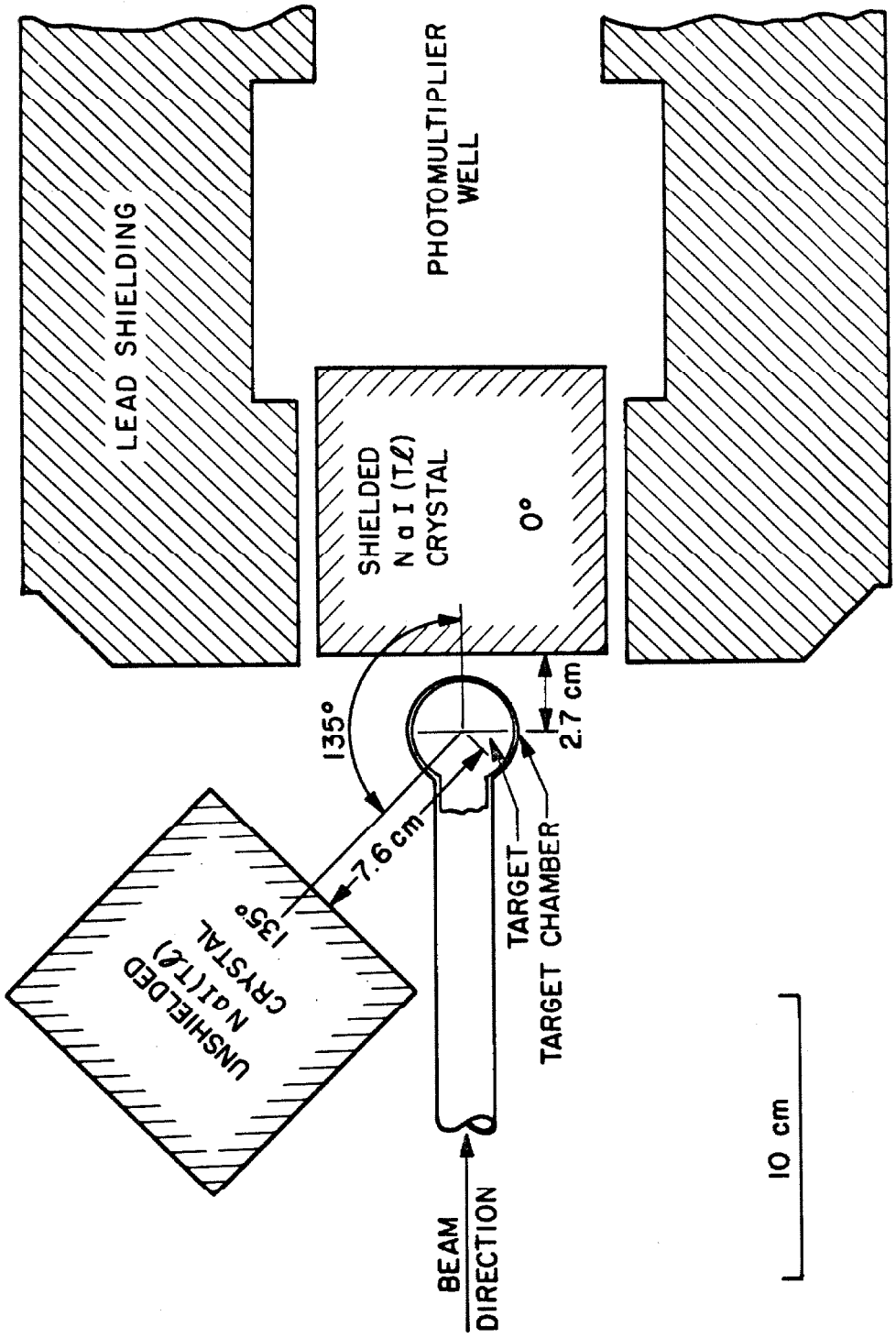
LEAD SHIELDING
PHOTOMULTIPLIER WELL
SHIELDED NaI (Tℓ) CRYSTAL
0°
135°
2.7 cm
7.6 cm
UNSHIELDED NaI(Tℓ) CRYSTAL
135°
TARGET
TARGET CHAMBER
BEAM DIRECTION
10 cm

FIGURE 6: Standard 9.17 MeV Spectrum

This figure shows the response of the 10.2 cm x 10.2 cm NaI(T1) detector to 9.17 MeV gamma radiation from the 1.747 MeV resonance in $C^{13}(p, \gamma)N^{14}$. Numbers of counts are plotted vertically as a function of observed pulse height (channel number). Three vertical arrows above the principal peak indicate the full gamma ray energy, 9.17 MeV, as well as energies corresponding to the loss of one and two annihilation quanta; single quantum (0.511 MeV) losses from the detector evidently are favored at this energy. Background from 6.44 MeV cascade radiation is apparent in channels 90-110; below channel 50 an assortment of lower energy radiation is displayed. The NaI(T1) crystal was placed 2.5 cm from the target and enclosed in the 30.5 cm lead shield (see Figure 5).

The complete spectrum from 9.17 MeV radiation was approximated by continuing the higher energy profile smoothly under the 6.44 MeV background then interpolating linearly from about channel 85 to the calculated analytic intercept at channel zero (solid curve). The interval corresponding to 0.8 - 1.1 E_γ contains 53% of the total 9.17 MeV spectrum thus outlined. The method of horizontal extrapolation, not used for data analysis, is indicated by a dashed curve. For additional details see pages 16-20.

FIGURE 6

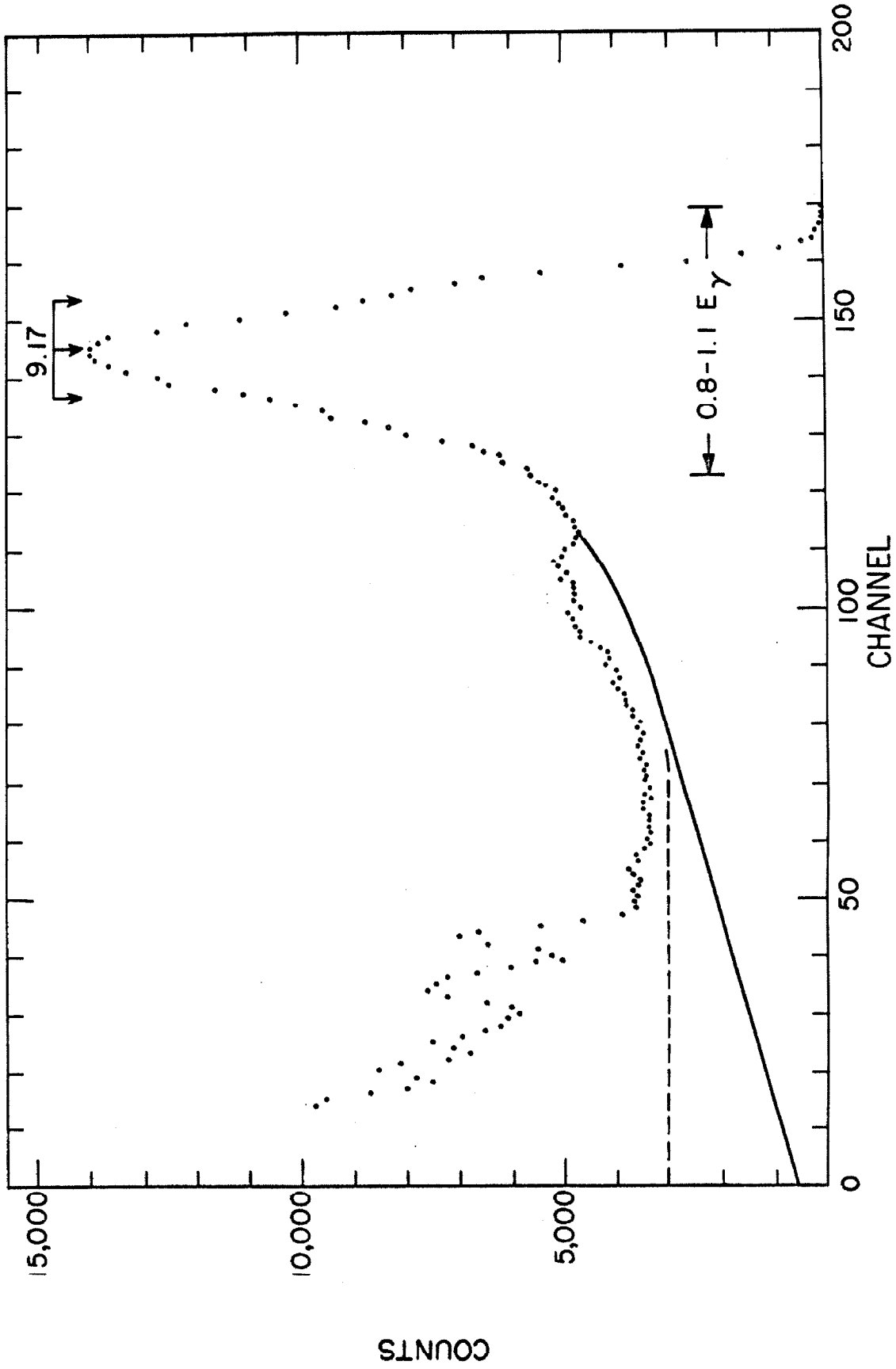
9.17
0.8-1.1 E_γ
COUNTS
15,000
10,000
5,000
0
50
100
150
200
CHANNEL

FIGURE 7: Typical Experimental Spectra

This figure shows typical spectra obtained with the 10.2 cm x 10.2 cm NaI(T1) detector from alpha particle bombardment of an enriched C^{12} target. Crosses indicate averages over ten or more channels in the region of poor statistics. The expected positions of various gamma rays are represented by vertical arrows indicating the full energy and two escape peaks. All curves display an underlying background of pulses decreasing approximately exponentially with energy which is attributed to neutrons from $C^{13}(\alpha, n)O^{16}$ and $C^{13}(\alpha, n\gamma)O^{16}$. At E_α = 6.60 MeV (curve b) the $C^{12}(\alpha, \gamma)O^{16}$ reaction is not resonant but 6.13 MeV radiation from $C^{13}(\alpha, n\gamma)O^{16}$ (Spear et al. 1963) is a prominant feature. At bombarding energies of 7.52 and 7.88 MeV (curves c and d), 13 MeV ground state radiation from $C^{12}(\alpha, \gamma)O^{16}$ is observed along with peaks from $C^{12}(\alpha, n\gamma)O^{16}$ and $C^{12}(\alpha, \alpha'\gamma_{4.43})C^{12}$; also indicated is the summation interval for ground state radiation, 0.8 - 1.1 E_γ, where $E_\gamma = E_x$ = (7.162 MeV + 3/4 E_α). The spectrum observed when E_α = 3.30 MeV (curve a) is reproduced later as Figure 11a and discussed in the caption for that figure. For additional details see pages 26, 27 and 52.

FIGURE 7

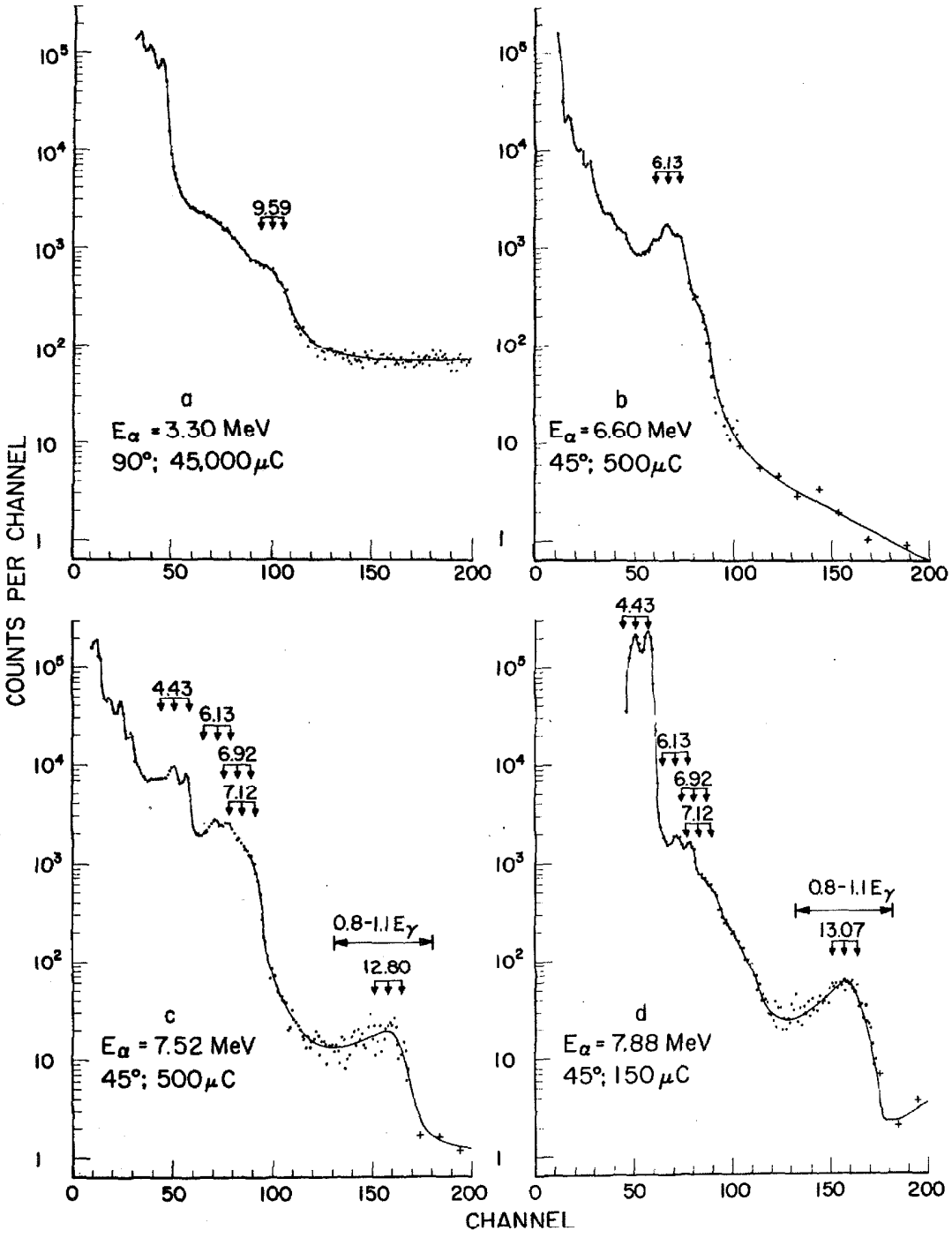
COUNTS PER CHANNEL
CHANNEL
a
E_α = 3.30 MeV
90°; 45,000μC
9.59
b
E_α = 6.60 MeV
45°; 500μC
6.13
c
E_α = 7.52 MeV
45°; 500μC
4.43
6.13
6.92
7.12
0.8-1.1 E_γ
12.80
d
E_α = 7.88 MeV
45°; 150μC
4.43
6.13
6.92
7.12
0.8-1.1 E_γ
13.07

FIGURE 8: Excitation Function for $C^{13}(\alpha, n\gamma)O^{16}$

This figure is taken from Spear et al. (1963). The relative yield of 6 and 7 MeV radiation from $C^{13}(\alpha, n\gamma)O^{16}$ is plotted vertically as a function of alpha particle bombarding energy E_α. Some 22 resonances are found in this interval of excitation. The 10.2 cm x 10.2 cm NaI(T1) detector was located 12.7 cm from an enriched C^{13} target at the designated angles of 0° and 45°. The sharp resonance numbered 5 in this figure appears to be responsible for the step in background found at $E_\alpha = 6.1$ MeV in Figures 9 and 10. For additional details see Spear et al. (1963) and pages 27 and 29.

FIGURE 8

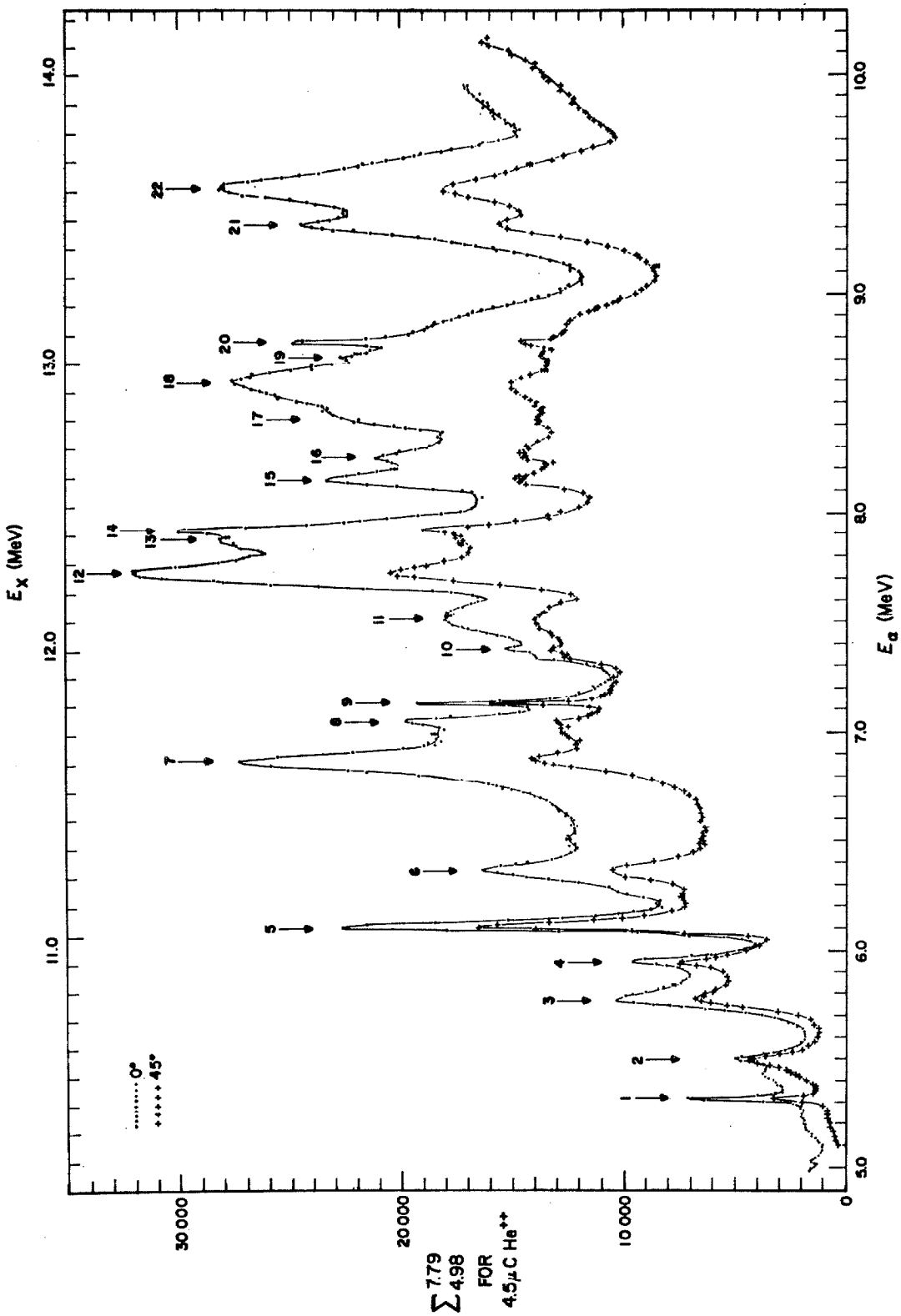
E_x (MeV)
E_α (MeV)
14.0
13.0
12.0
11.0
10.0
9.0
8.0
7.0
6.0
5.0
0
30000
20000
10000
$\sum_{4.98}^{7.79}$
FOR
4.5μC He^{++}
0°
45°
22
21
20
19
18
17
16
15
14
13
12
11
10
9
8
7
6
5
4
3
2
1

FIGURE 9: Results From a Natural Carbon Target

This figure shows results from a preliminary $C^{12}(\alpha, \gamma)O^{16}$ experiment (Larson and Spear 1961) using a natural carbon target. The 10.2 cm x 10.2 cm NaI(T1) detector was placed approximately 2 cm from the target spot at an angle of 45^{o} to the beam. The ordinate N represents the number of counts per 150 μC of He^{+} ions observed in the interval 0.8 - 1.1 E_x. Energy scales indicate the bombarding energy E_α and appropriate excitation energy E_x in O^{16}. Background reduction made possible by the use of enriched C^{12} targets is graphically demonstrated by comparing this data to Figure 10. For additional details see pages 9 and 26.

FIGURE 9

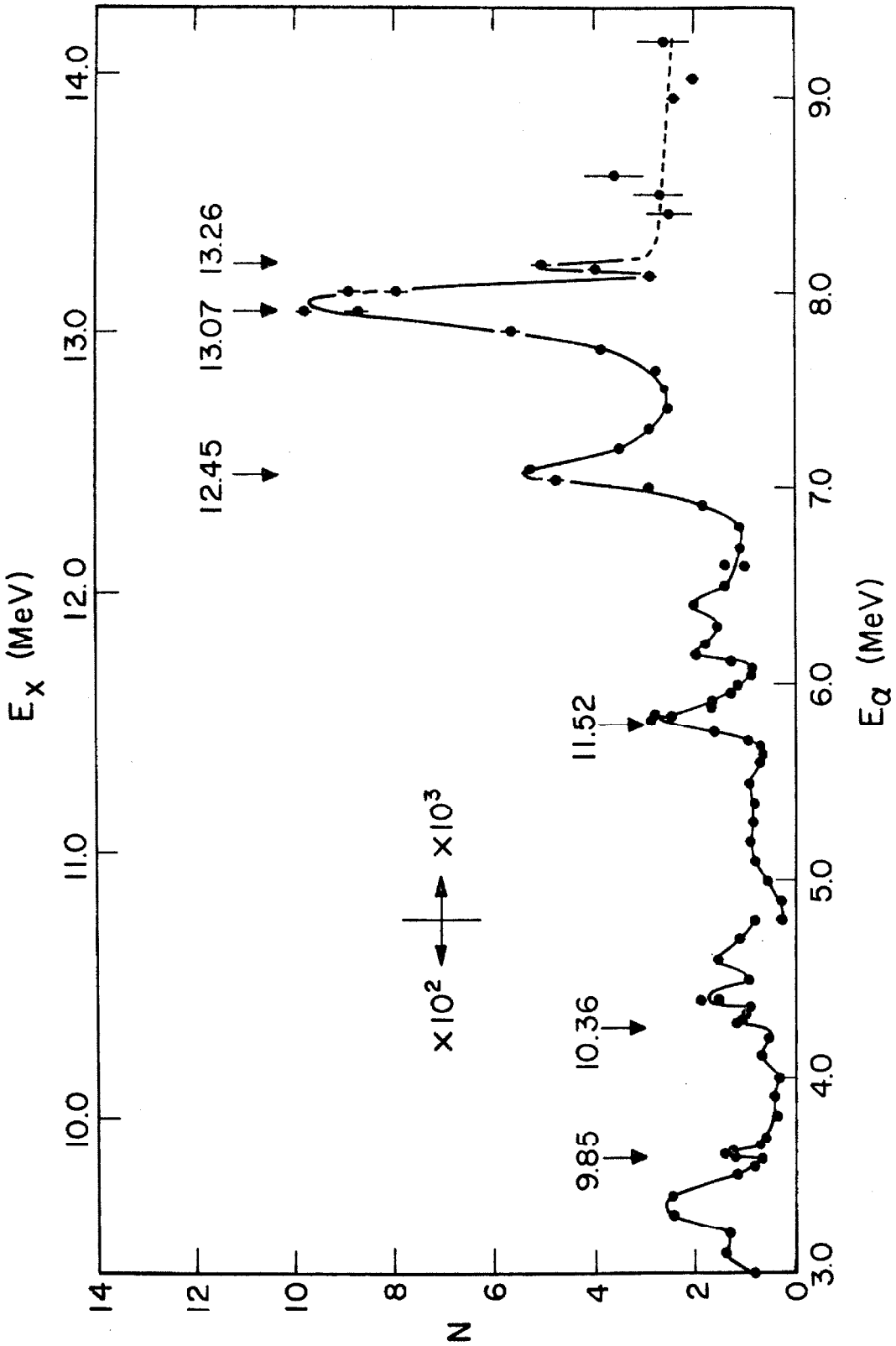
E_x (MeV)
14.0
13.0
12.0
11.0
10.0
13.26
13.07
12.45
11.52
10.36
9.85
×10³
×10²
N
14
12
10
8
6
4
2
0
3.0
4.0
5.0
6.0
7.0
8.0
9.0
E_α (MeV)

FIGURE 10: Excitation Function for $C^{12}(\alpha, \gamma)O^{16}$

The excitation function at 45^{o} for radiation from $C^{12}(\alpha, \gamma)O^{16}$ is shown for alpha particle bombarding energies from 2.8 to 8.3 MeV. Gamma radiation was detected using the 10.2 cm x 10.2 cm NaI(T1) crystal located 2.7 cm from an enriched C^{12} target. The ordinate N represents the number of counts per microcoulomb of He^{+} ions observed within the spectral region 0.8 - 1.1 E_x, where E_x = (7.162 MeV + 3/4 E_α) corresponds to the energy of ground state transitions in O^{16}. Cascade radiation from the 10.36 MeV state is displayed in the inset curve. For additional details see in particular pages 28-30 and also pages 31-56.

FIGURE 10

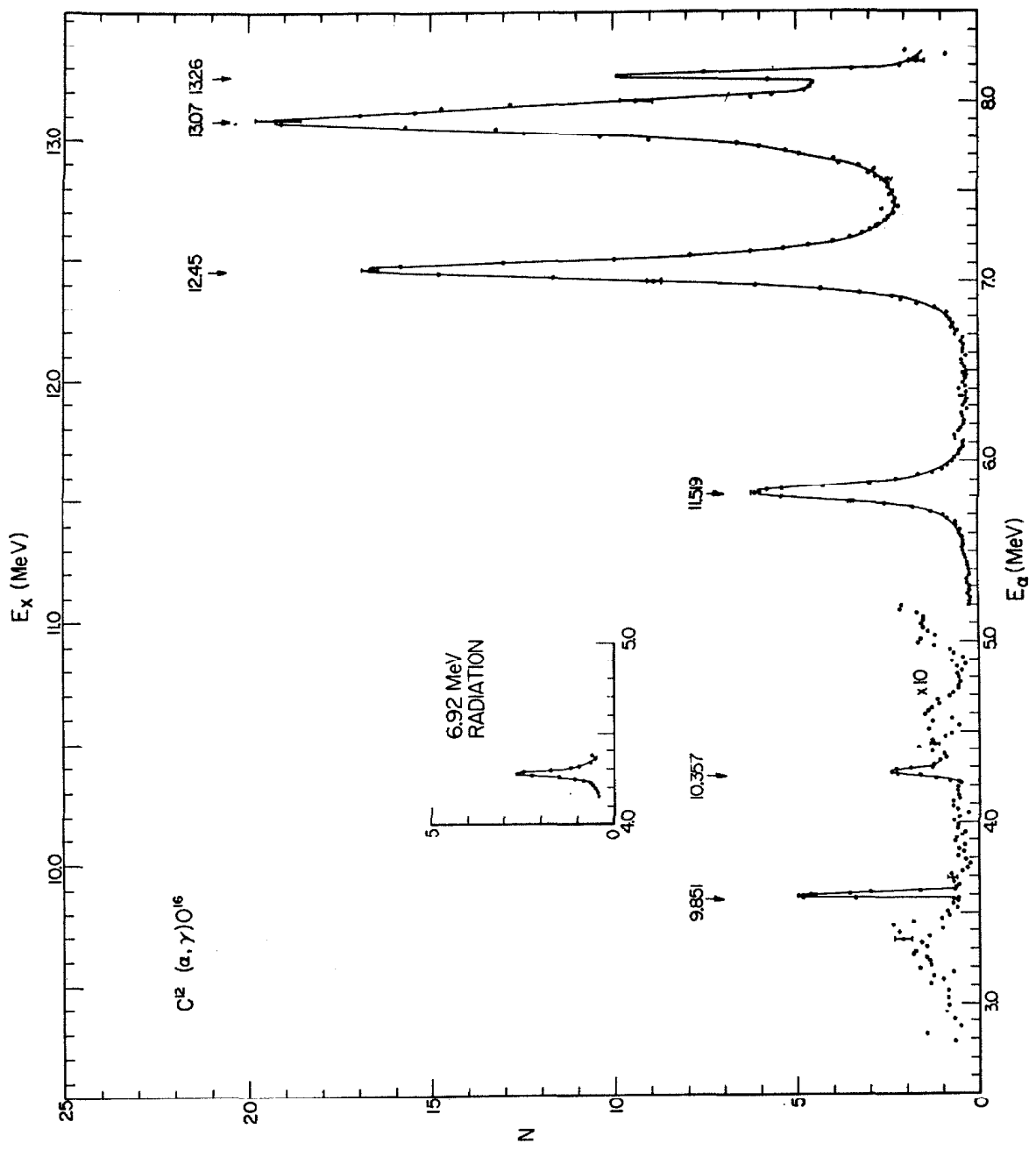
C^{12} $(\alpha, \gamma)O^{16}$
E_x (MeV)
E_α (MeV)
N
1307
1326
1245
11.59
10.357
9.851
6.92 MeV RADIATION
x10

FIGURE 11: Radiation from the 9.59 MeV State

The spectrum in Figure 11a was obtained by bombarding an enriched C^{12} target with 3.3 MeV alpha particles for about 10 hours. The 10.2 cm x 10.2 cm NaI(Tl) detector was 2.7 cm from the beam spot at an angle of 90^{o}. Most of the counts in this spectrum come from $C^{13}(\alpha, n)O^{16}$; cosmic ray room background is responsible for the horizontal extension toward higher energies. The feature at 9.59 MeV is attributed to ground state radiation from $C^{12}(\alpha, \gamma)O^{16}$. Energy calibration at 9.59 MeV is based on comparisons with spectra obtained from the 9.85 MeV resonance.

A spectrum from an enriched (54%) C^{13} target is shown in Figure 11b; the geometry and bombarding energy are unchanged. This background run shows no sign of the feature attributed to 9.59 MeV radiation; instead it closely follows an exponential decrease from channels 80 through 110. Knowledge of this exponential background profile was used in determining the amount of 9.59 MeV radiation contained in Figure 11a. For additional details see pages 31-33.

FIGURE 11

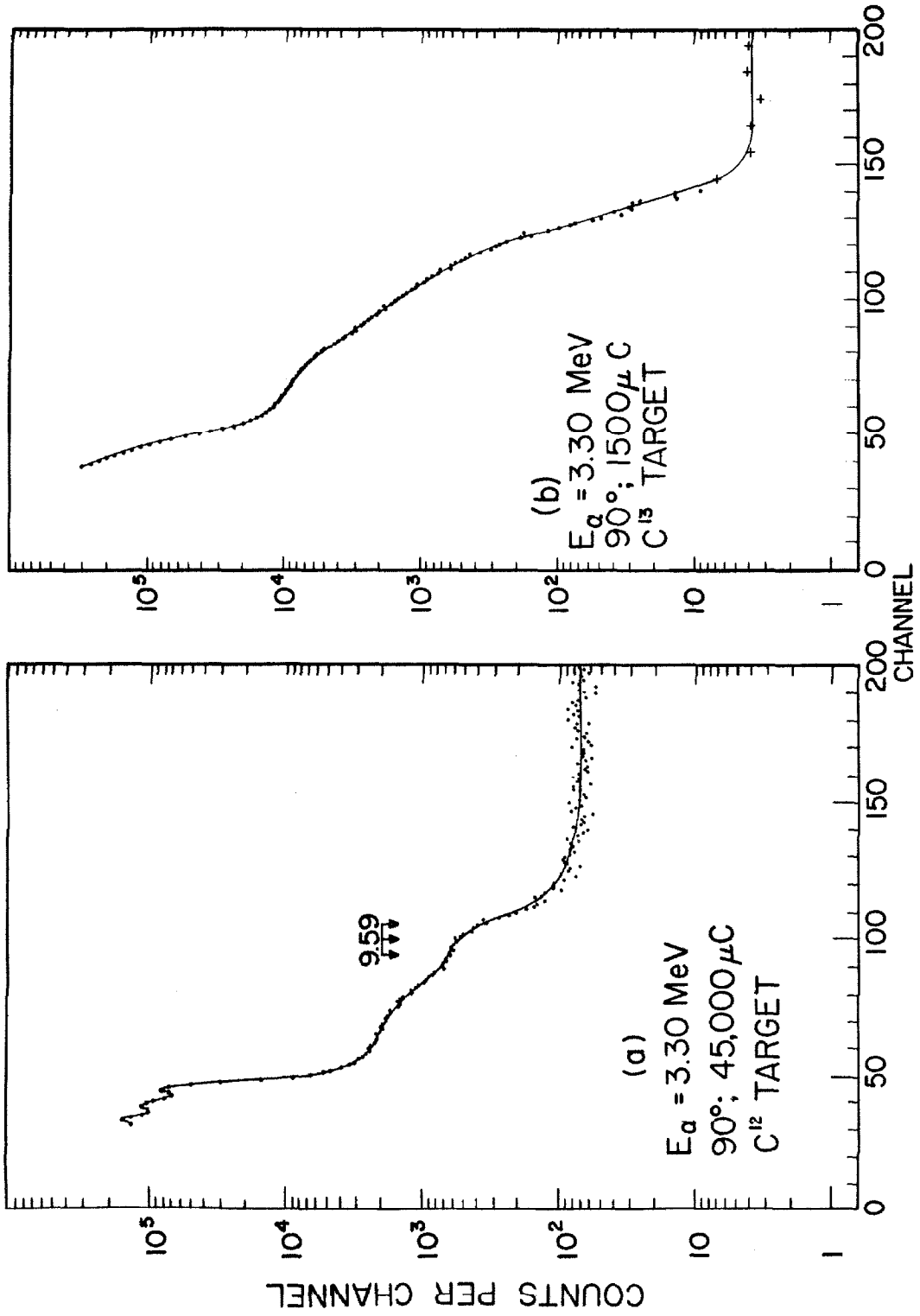
COUNTS PER CHANNEL
CHANNEL
(a)
E_α = 3.30 MeV
90°; 45,000μC
C^{12} TARGET
9.59
(b)
E_α = 3.30 MeV
90°; 1500μC
C^{13} TARGET

FIGURE 12: The 9.85 MeV Resonance

Shown here on a magnified scale is the excitation function for the 9.85 MeV state in O^{16}; these same data appear in Figure 10. Counts per microcoulomb of He^{+} ions, N, are plotted as a function of excitation energy E_{α}; statistical error bars are indicated. This very narrow (0.8 keV) resonance proved convenient for thickness measurements of thin targets. The thickness of the C^{12} target used to obtain this curve was determined from the observed resonance width (at half maximum) of 31 keV. As target thickness is increased the trailing edge of the resonance merges more gradually with background from $C^{13}(\alpha, n)O^{16}$ and this method becomes imprecise. For additional details see pages 25 and 36.

FIGURE 12

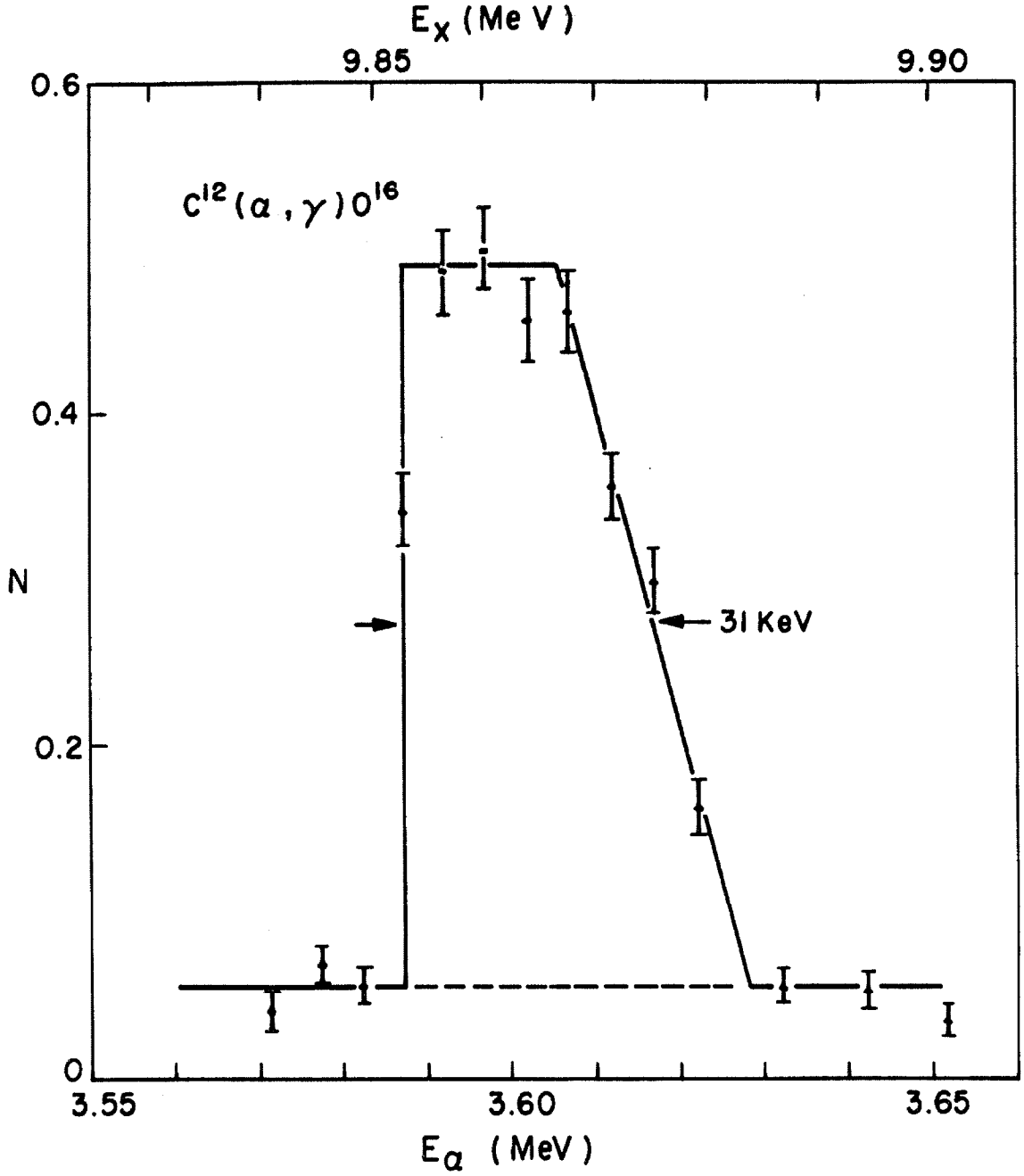
E_x (Me V)
9.85
9.90
0.6
0.4
0.2
0
N
$C^{12}(\alpha,\gamma)O^{16}$
31 KeV
3.55
3.60
3.65
E_α (MeV)

FIGURE 13: $C^{12}(\alpha, \gamma)O^{16}$ at 135^{o}

This excitation function for $C^{12}(\alpha, \gamma)O^{16}$ at 135^{o} (solid curve) was obtained with the unshielded 10.2 cm x 10.2 cm NaI(T1) detector located 7.6 cm from an enriched C^{12} target (see Figure 5). The number of counts N per 450 μC of He^{++} ions are plotted, with statistical error bars, as a function of bombarding energy E_{α}. For comparison, the dashed curve is drawn through data taken with the detector at 7.6 cm and 45^{o}. Asymmetry between the 45^{o} and 135^{o} data is indicative of interference between states of opposite parity near E_{x} = 13.1 MeV. For additional details see pages 43 and 44.

FIGURE 13

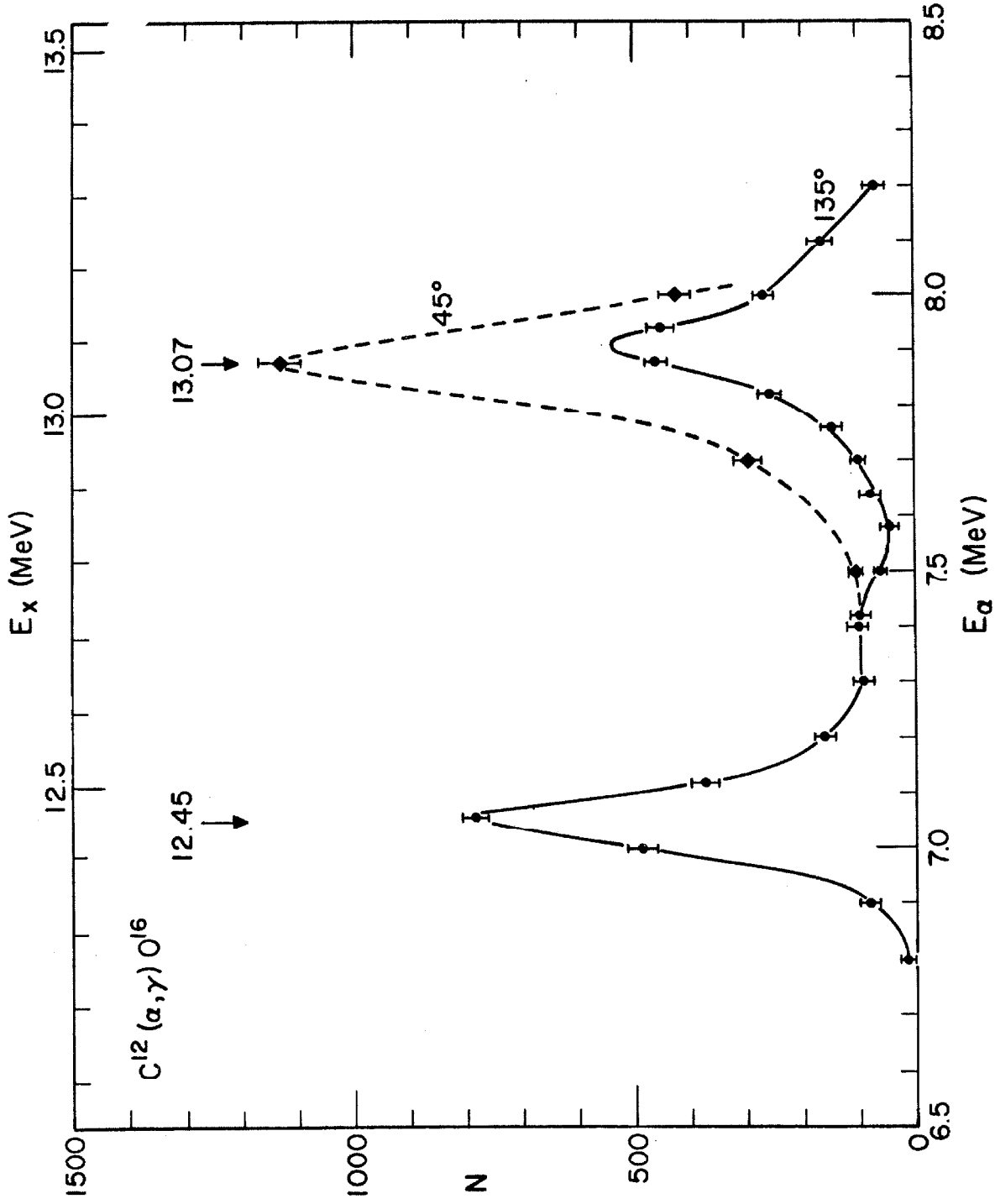
$C^{12}(\alpha,\gamma)O^{16}$
13.07
12.45
45°
135°
E_x (MeV)
E_α (MeV)
N
13.5
13.0
12.5
8.5
8.0
7.5
7.0
6.5
1500
1000
500
0

FIGURE 14: Angular Distribution Measurements

Angular distribution measurements in 22.5° increments from 0° to 135° were made at alpha particle bombarding energies of 7.06, 7.42, 7.88 and 8.00 MeV. Conditions were the same as for Figure 13. The data shown have been corrected for room background, dead-time and anisotropic gamma ray absorption in the target backing. Solid curves represent a least squares fit to the data by Legendre polynomials to fourth order. Coefficients of the polynomial terms are listed in Table I. At E_α = 7.06 MeV the radiation pattern is symmetric about 90° and corresponds to an E1 transition from the 1^- state at 12.44 MeV in 0^{16}. The pattern observed at E_α = 7.88 MeV is asymmetric about 90° revealing interference between 1^- and 2^+ states near 13.1 MeV in 0^{16}. For additional details see pages 43 and 44.

FIGURE 14

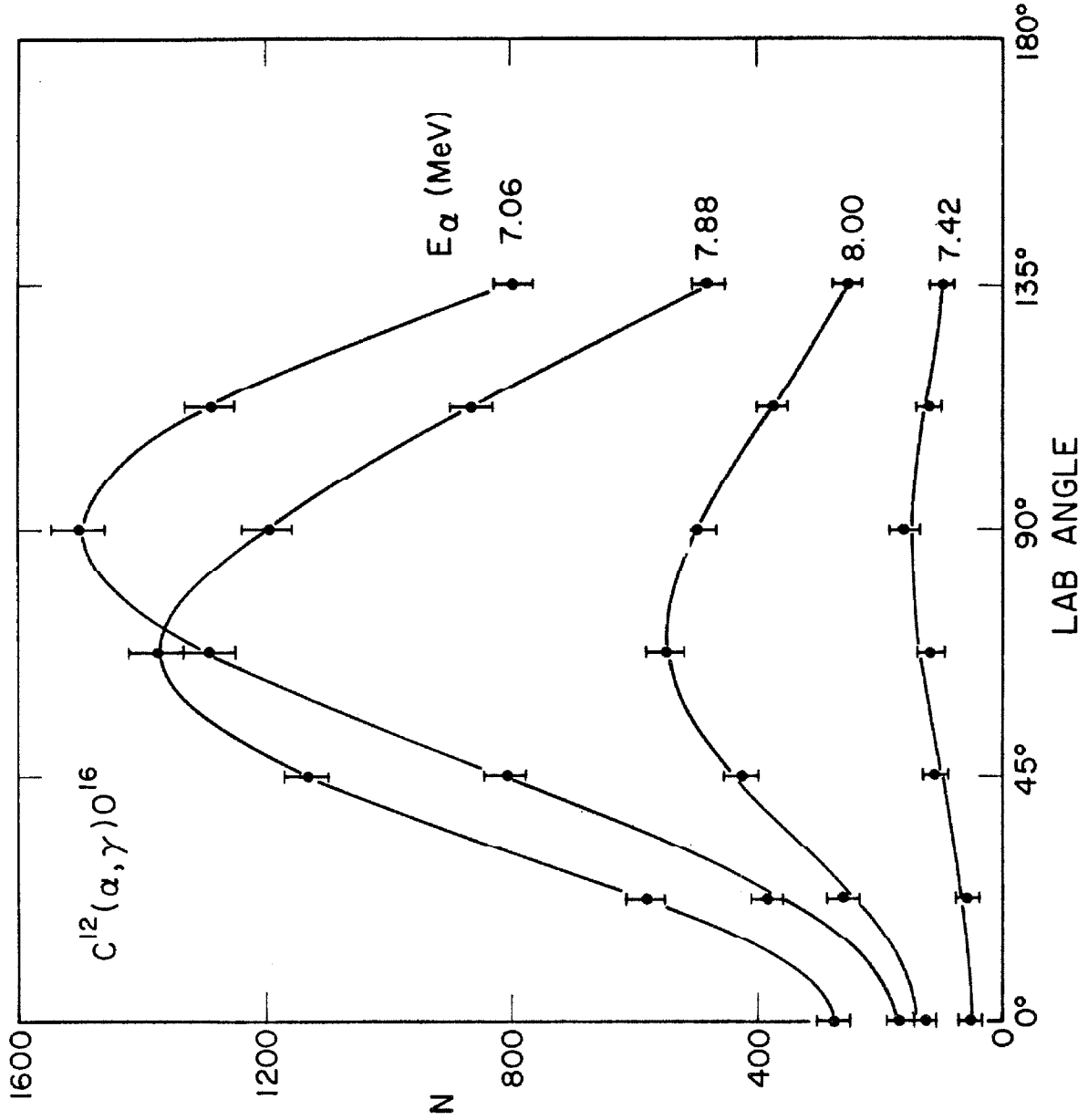
$C^{12}(\alpha,\gamma)O^{16}$
$E\alpha$ (MeV)
7.06
7.88
8.00
7.42
N
1600
1200
800
400
0
0°
45°
90°
135°
180°
LAB ANGLE

FIGURE 15: Excitation Function for $C^{12}(\alpha, \alpha'\gamma)C^{12}$

This figure displays the excitation function of 4.43 MeV radiation obtained from alpha particle bombardment of a natural carbon target. The ordinate N represents the number of pulses observed within a window corresponding to gamma ray energies from 2.91 to 5.20 MeV for a bombardment of 3 μC of He^{++}. Resonances are observed at energies corresponding to E_x = 13.13, 13.27, 13.90, 14.72 (broad) and 14.81 MeV. The resonance at E_x = 13.13 MeV has properties inconsistent with 1^- and 2^+ levels already discovered in this region of O^{16} and is identified as a new 3^- state by I. Mitchel and Ophel (1965). For additional details see pages 54 and 55.

FIGURE 15

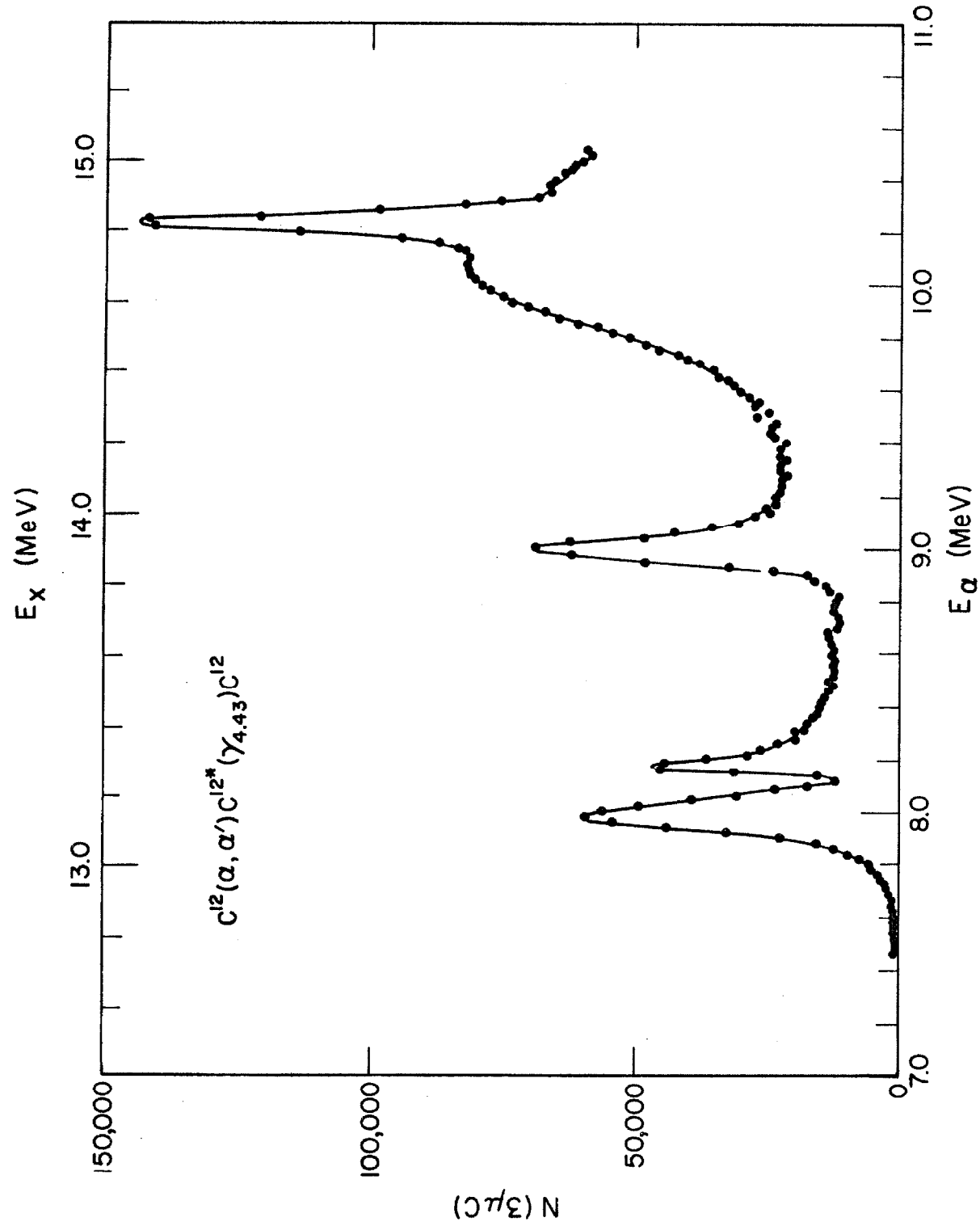
$C^{12}(\alpha, \alpha')C^{12*}(\gamma_{4.43})C^{12}$
E_x (MeV)
15.0
14.0
13.0
E_α (MeV)
11.0
10.0
9.0
8.0
7.0
150,000
100,000
50,000
0
N (3/μC)

FIGURE 16: E1 and E2 Transitions in Light Nuclei

In this figure are histograms taken from a study by Wilkinson (1960). Numbers of E1 and E2 transitions observed in light nuclei are plotted as a function of $|M|^2 = \Gamma_\gamma/\Gamma_{\gamma W}$ (see pages 61 and 62). Dipole transitions which violate the isotopic spin selection rule (page 60) are shaded. Dashed curves outline the results of shell model calculations. Contributions from the present experiment correspond to ground state transitions from states of the designated energies with the exception of an E2 cascade from the 10.36 MeV state. For additional details see Wilkinson (1956, 1960) and pages 62-65.

FIGURE 16

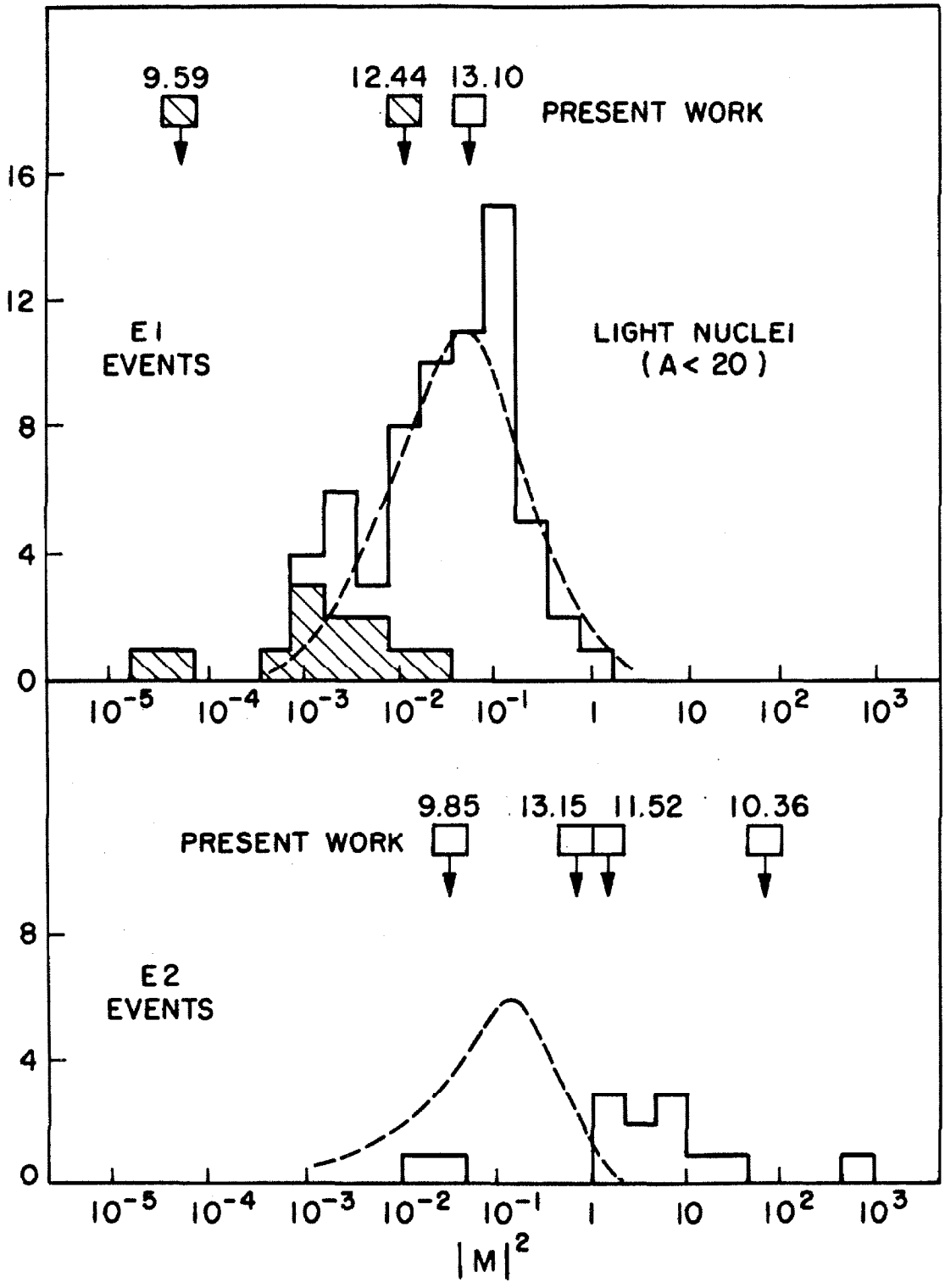
9.59
12.44
13.10
PRESENT WORK
16
12
8
4
0
E1
EVENTS
LIGHT NUCLEI
(A< 20)
10^{-5}
10^{-4}
10^{-3}
10^{-2}
10^{-1}
1
10
10^{2}
10^{3}
9.85
13.15
11.52
10.36
PRESENT WORK
8
4
0
E2
EVENTS
$|M|^2$